Efficient and accurate modeling of wave-driven flooding on coral reef-lined coasts

On the interpolation of parameterized boundary conditions

Vesna Bertoncelj

The resulting effect on the waves is remarkable. To an observer standing on the platform just inside the surf zone, the breakers appear to come crushing down upon him; two sec later, the wave has virtually disappeared, its momentum converted into a noisy surge which rushes up the channels on each side of the platform.

—MUNK AND SAGERENT, 1948

Efficient and accurate modeling
of wave-driven flooding
on coral reef-lined coasts

On the interpolation of parameterized boundary conditions

By

Vesna Bertoncelj

to obtain the degree of Master of Science

at the Delft University of Technology

to be defended publicly on May 12, 2021, at 12:00.

TUDelft   **Deltares**

Preface

The topic of this thesis reflects my passion for the ocean waves and the coastal processes. Despite the challenges that this research has brought, along with the global pandemic changing the course of our lives, I truly enjoyed learning about the hydrodynamic processes on coral reefs and the significance of managing coastal hazards on low-lying islands in the tropics.

I would like to thank my thesis committee for making me feel like the luckiest student on campus. The amount of support I received from you is indescribable, not only in the context of the thesis, but also on the valuable career advises. First, I would like to thank Ap for giving me the opportunity to conduct this research at Deltares. Even though I was only able to visit the company on the starting day of the project, I always felt welcomed and involved in the Department. Ap, thank you for trusting me with this challenging topic and for giving me words of encouragement. I am honoured to be a part of Flat White Hunters. I would like to give special thanks to Tim for always being available for solving my doubts and providing me with me the best Deltares experience I could possibly have (in the considered circumstances). The amount of time you put into giving me the support I needed during this thesis is deeply appreciated. Furthermore, I am thankful for Marion for encouraging me to always think critically about the results and to always search for the physical meanings behind them. Instead of rushing me to provide as much results as possible, I am glad that I was encouraged to focus on the quality of them. At the same time, I appreciate Floortje for keep asking me the 'why?' questions. This furthermore improved the quality of my work. Stuart, I am impressed by your fascination for this topic, it is highly contagious. I am thankful for your advises, especially regarding the EGU conference, and for bringing the smile on my face while reading your comments on my report. Lastly, I would like to thank Jeremy for being a valuable member of this thesis committee. My gratitude goes back in time at the beginning of pandemic when you helped me with the safe return back to Europe.

This thesis project also marks the end of the TU Delft student experience. The entire experience would certainly not be the same without all the study mates. During the last 3 years, we have been through a lot; from long working hours at the faculty, to delicious dinners, dancing and celebrations. Tess, Mayra, Marco, Noor, Fernando, Supriya, Meghan, Chris, Haisam, Ryan, Sjoerd and Felix, I am glad to share this period with you. A special place holds for Daniela; we have shared the entire Dutch experience together and I would not have enjoyed it as much without sharing it with you. The last 11 months have been enjoyable especially because of my precious housemates, who also became my home-base co-workers. Goitze, Julian, Wesley, Tom, Dilayla, Mira and Ian; you made Wednesday my favourite day of the week. The time we spent together was far from monotonous and I am inspired by each one of you. Furthermore, I am expressing my gratitude to Falco, Erin, Tess and Julian for proof-reading the thesis and Wesley for teaching me the designing skills.

I would like to give special thanks to my grandparents and Barbara for unconditionally supporting me with my decisions. To my family and friends from Slovenia; even though we are more than 1 000 km apart, I am keeping you very close to my heart. Last but certainly not the least, I would like to give gratitude to Falco for always being by my side and inspire me. Your support goes far beyond the struggles of this thesis.

Enjoy reading!

Vesna

Summary

Many coral reef islands have low-lying urbanized areas, which in combination with population growth, sea level rise and possibly more frequent extreme weather events is likely to result in increased coastal risk (e.g. Storlazzi et al. (2015)). On smaller scales of O(10 km), wave-driven coastal flooding can be accurately predicted with advanced models such as XBeach (Roelvink et al., 2009), at already high computational costs. For larger scales, larger number of islands, for scenario modelling, and for implementation in early warning systems, computationally faster methods are needed. Reduced physics models, which neglect some of the processes (e.g. non-hydrostatic pressure gradient term and viscosity), are a potential solution. However, their accuracy and the best method to force them has not been established yet.

In this research, a new methodology is developed to model wave-driven flooding on coral reef-lined coasts. A look-up-table (LUT), composed of XBeach model runs, is combined with a reduced-physics model, SFINCS (Leijnse et al., 2021), to achieve high accuracy predictions at limited computational expense. The LUT consists of pre-run 1D XBeach simulations for several reef profiles from Scott et al. (2020), forced with different offshore wave and water level conditions. Wave conditions close to the shore as predicted by the LUT are used to force SFINCS, which then simulates the wave runup, overtopping and flooding. These are forced in SFINCS using random wave timeseries from an interpolated parameterized wave spectrum following Athif (2020).

The accuracy of the method is investigated for 6 distinctive cross-shore profiles from Scott et al. (2020), for two wave scenarios (gentle swell and stormy conditions). Results of complete XBeach simulations are compared to LUT-SFINCS simulations with different boundary forcing locations. The sensitivity analysis shows that the preferred boundary location to initialize the SFINCS model is at a water depth between 0.5 m and 2.5 m, preferably shoreward of the reef edge where the majority of the wave energy is already dissipated. The accuracy of the method is higher for stormy wave scenarios compared to gentle swell scenarios. Also, there is an indication that the accuracy of the method increases with increasing offshore water level. The performance of the method is also better when the waves are more nonlinear at the offshore boundary of SFINCS (determined with the ratio between the wave height of high frequency wave energy and the water depth). In general, predictions of wave-driven flooding are more accurate for dissipative coastlines, i.e. the coastlines that dissipate large amounts of wave energy on long shallow reef flats and/or long gentle fore reef slopes. Despite the differences in the accuracy of the method among different reef profiles, the method can be applied to any arbitrary reef profile.

Interpolation of the forcing conditions at the boundary is investigated with 9 different interpolation methods. Results reveal that the most accurate method to interpolate spectral parameters (the amount of high frequency wave energy, the amount of low frequency wave energy and the frequency peak of high frequency part of the spectrum) and wave setup at the boundary is the Inverse Distance Weighting method with a power of -2. This method also results in the most accurate predictions of wave runup when compared to the runup simulated with SFINCS forced with direct boundary conditions from XBeach. Errors introduced by the method lead to average runup estimation errors of 10-20% depending on the offshore water level and on the reef geometry with the highest errors of up to around 60%. Runup is mostly underestimated. The main source of errors is due to the reduced physics in SFINCS. Simulating wave runup with XBeach LUT – SFINCS couple leads to about 50-times higher computational speed compared to the XBeach model simulating hydrodynamic processes along the entire reef profile.

Follow-up work should first address the application of the methodology to a variety of observed reef profiles in a real-world application. The errors associated with matching of the observed profiles profiles with the representative cluster profiles from Scott et al. (2020)'s database should be investigated. Next steps include the development of the method for 2D modeling of coastal flooding. Different scenarios should be considered (e.g., curved coastline and variable reef profiles along the coast) while the interpolation of the boundary conditions is addressed. Finally, the developed method in 2D can be implemented into flood risk assessment tools such as Delft-FIAT (Slager et al., 2016) and the performance of the resulting model train can be assessed. Additionally, the method can be used as a support to early warning systems or it can be applied to other coastal environments, such as sandy coastlines.

iv

Contents

List of Figures

List of Tables

1

Introduction

1.1 Problem definition

The majority of reef-fronted islands have low-lying urbanized areas and with the combination of population growth, sea-level-rise (SLR) and more frequent extreme weather events due to climate change this can result in more frequent coastal hazards on increasingly exposed areas (e.g. Storlazzi et al. (2015)). As a consequence, the societies living in these areas are facing severe threats, such as the risk to people's lives, damage of infrastructure and increased risk of salt water contamination of the fresh water lenses (Winter et al., 2020). Communities living in these areas can either relocate or implement coastal adaptation strategies. The latter is preferred as relocation can potentially cause significant cultural and societal impacts. However, coastal adaptation strategies require time for thorough planning and adaptation to build resilience. With this in mind, the demand for accurate and efficient flood risk assessments on a global scale is high.

Coastal inundation is a consequence of several flooding mechanisms that can either occur separately, or concurrently which can make the flooding even more severe. These mechanisms are flooding from river (fluvial), due to excess rain (pluvial), and flooding from the sea (tidal, wind-, and wave-driven). Especially wave-driven processes are highly complex, but certainly a crucial factor for flooding of coral reef-lined coasts (e.g. Hench et al. (2008), Quataert et al. (2015), Cheriton et al. (2016)). A well-known example of its importance, witnessed by the locals, is the case study of a tsunami-like wave that attacked the city of Hernani, Philippines, explained by Roeber and Bricker (2015). In their study they show that the setup, generated by the breaking of waves, oscillated with the incidence of long and small wave groups, and steepened into a tsunami-like wave that caused extreme damage and causalities.

From the study by Roeber and Bricker (2015) it is evident that wave-driven processes on coral reefs cannot be simply simulated with phase-averaged wave models, but that they need phase-resolving wave models as they resolve individual waves and its transformation on the coral reefs. For small scale projects the modeling of coastal inundation can be accurately predicted with advanced models such as XBeach with acceptable computational costs. However, in order to conduct flood risk assessments on a global scale, faster methods are needed.

An important step to increase computational efficiency while keeping the accuracy relatively high was the development of Bayesian Estimator for Wave Attack in Reef Environments (BEWARE) by Pearson et al. (2017). BEWARE consists of a large synthetic database, created with a process-based wave-resolving hydrodynamic model (XBeach Non-Hydrostatic+). The next version of BEWARE, which is currently under development, will include a large number of offshore wave conditions and coral reef profiles, however, it will still only predict runup. On the other hand, flood risk assessment requires 2-dimensional water depth maps in order to predict damage from future climate change scenarios. In order to perform flood risk assessments, overtopping and flooding need to be simulated.

1.2   Proposed solution

Wave runup and overtopping are very complex processes on reef-lined coasts and consequently no parametric formulation is yet available. A model that will capture the accurate runup and overtopping for a specific reef profile and at the same time keep the computational costs low is needed. This can be accomplished with the use of a reduced-physics model such as SFINCS (Leijnse et al., 2021). Reduced-physics modeling limits the computational expense by solving the simplified shallow water equations, while allowing the user to apply the relevant processes that play a role in wave-driven flooding. However, the application of the model is not straightforward, as the reduced-physics models come with a cost of lowering the accuracy of the inundation modeling. Since SFINCS is based on simplified shallow water equations, the highest accuracy is achieved when the model is applied to shallow water. In order to accomplish that, another more advanced model is required to simulate the propagation of waves from the deep water to the shallow water depths, i.e. another model needs to provide the boundary conditions for forcing SFINCS. The question is: *How can this be achieved in a computationally efficient way?*

The proposed solution is schematically presented in Figure 1.1. A process-based phase-resolving numerical wave model XBeach non-hydrostatic+ (XB-NH+, de Ridder et al. (2021)) is used to obtain boundary conditions for forcing SFINCS. Since XB-NH+ is a computationally demanding model, a look-up-table (LUT) consisting of pre-run simulations with XB-NH+ is built (XB-NH+ LUT). XB-NH+ LUT consists of a limited number of offshore wave and water level conditions and a limited number of observed bathymetric reef profiles from Scott et al. (2020)'s database. To simulate flooding for arbitrary offshore conditions, interpolation of the boundary conditions needs to be preformed. Interpolated boundary conditions are used to provide the water level time series at the certain location along the reef to force SFINCS. Finally, SFINCS can simulate runup and overtopping.

Interpolation will be performed over parameterized boundary conditions, following Athif (2020). Wave spectrum at the boundary can be described with the TMA+GAUSS function using three parameters: the amount of low frequency (LF) wave energy, the amount of high frequency (HF) wave energy and the frequency peak of HF part of the spectrum. The TMA function consists of two parts. TMA determines the HF part of the spectrum with the TMA shape of the spectrum (Bouws et al., 1985). GAUSS determines the LF part of the spectrum with the Gaussian function. A more elaborated description of parameterization is included in Section 3.5.2.

The proposed methodology consists of finding the optimal boundary location for forcing SFINCS and developing an accurate interpolation in order to apply the method to arbitrary offshore wave conditions. Validation is performed with the use of the process-based hydrodynamic model (XBeach).
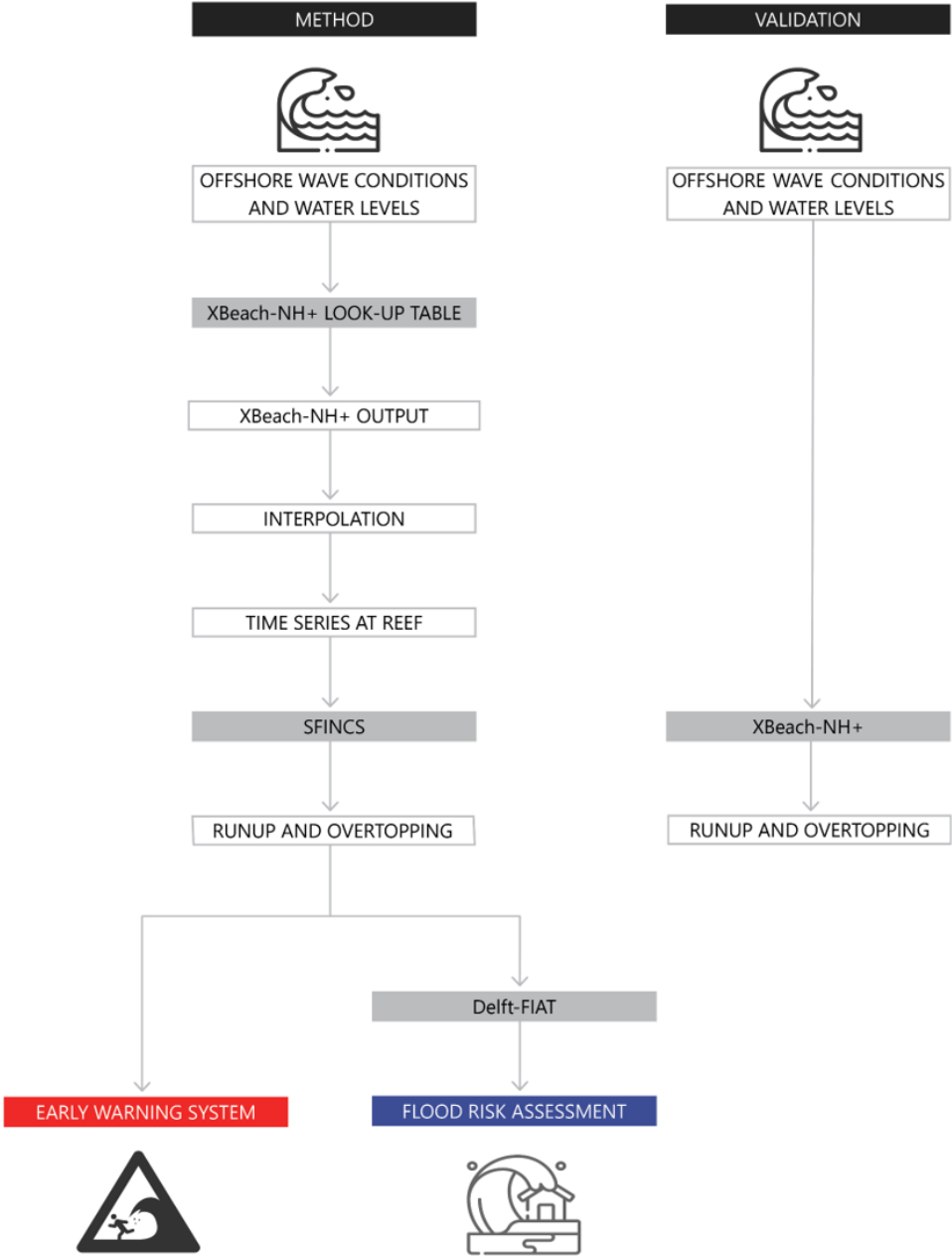
Figure 1.1: Simplified scheme of proposed solution that is developed throughout the research project.

1.3   Objectives and research questions

The main objective of the research is to develop a methodology for efficient and accurate modeling of wave-driven flooding on coral reef-lined coasts with the use of a reduced-physics model, which can be implemented in flood risk assessment tools and Early Warning Systems (EWS). The main research question follows directly from this objective:

> **How can wave-driven flooding on coral reef-lined coasts be modeled in a computationally efficient and accurate way without the need for nesting of several numerical models?**

The proposed solution is to develop a methodology to combine a look-up-table (LUT) consisting of simulations of the process-based phase-resolving numerical wave model XBeach Non-Hydrostatic+ (XB-NH+ LUT) with a reduced-physics model SFINCS to simulate 1-dimensional (1D) coastal inundation in an accurate and computationally efficient way. In order to answer the main research question, the following sub-questions need to be addressed:

> (1.)   How can the output of process-based phase-resolving numerical wave models be used as an input wave boundary condition close to the shore for forcing a reduced-physics numerical model?

Research performed by Athif (2020) proposed the application of the TMA+GAUSS function for parameterizing the wave spectrum at the boundary. Consequences of using the simplified parameterized spectra at the boundary and generating new random phased water level time series for forcing SFINCS will be addressed in the sensitivity analysis (Chapter 4). Analyses will be performed for five different boundary locations in order to find the boundary locations that result in the highest accuracy.

> (2.)   What interpolation method is the most appropriate to calculate the desired water level time series from the given offshore conditions with the use of discretized runs from XB-NH+ LUT?

XB-NH+ LUT is limited to a finite a number of offshore wave and water level conditions. Consequently, it cannot be used directly to simulate an arbitrary offshore conditions. Interpolation of the boundary conditions needs to be applied. In Chapter 5, chosen interpolation methods will be tested on conceptual cases and the interpolation method that results in the least error will be selected.

> (3.)   Can the methodology be generalized to all types of reef geometries and hydrodynamic regimes?

Analysis will be performed on conceptual cases on 6 distinctive cross-shore profiles and two offshore wave scenarios. A design of conceptual cases will be based on the literature review (Chapter 2) where bathymetric complexity of coral reefs and wave transformation across the reef profiles will be studied. Conceptual cases will be designed in a way to test the method to different hydrodynamic regimes on various coral reef profiles.

> (4.)   What are the performance and computational efficiency of the developed methodology?

The efficiency and accuracy of the developed method will be assessed by comparing the model results and the model run-time with the simulations performed with the physics-based model XB-NH+.

1.4   Thesis outline

1	**INTRODUCTION**
	objectives and research questions

2	**THEORETICAL BACKGROUND**
	bathymetric complexity of coral reefs
	cross-shore hydrodynamic processes
	modeling wave-induced flooding

3	**METHODOLOGY**
	approaching the problem
	design of conceptual cases

4	**SENSITIVITY ANALYSIS**
	parameterized boundary conditions
	performance of SFINCS
	the optimal forcing location
	computational demand

5	**INTERPOLATION METHODS**
	interpolated spectral parameters
	interpolated wave setup
	errors of predicted runup
	sensitivity of interpolated parameters
	discussion

6	**DISCUSSION**
	critical view on the approach
	constrains of the method

7	**CONCLUSION**
	key findings
	advances
	recommendations
	possible applications

Figure 1.2: Thesis outline with chapter numbers on the right side of the highlighted boxes.

2

Theoretical background

Coral reefs are a unique ecosystem, providing an important habitat structure for high-diverse marine communities (Richmond, 1993). Living reef structures do not only provide sand that forms tropical beaches, but also form bathymetric features around the coastline. These features are beneficial for protection of coasts by attenuation of wave energy propagating across the reef platforms. On typical coastlines surrounded by coral reef platforms an average of 97 % of wave energy can be dissipated (Ferrario et al., 2014). This leads to high reduction of coastal hazards. However, the typical coasts surrounded by coral reefs are low-lying. In certain circumstances when the water levels become too high, the flooding can still occur. Moreover, the threats to coastal safety are increasing with increasing sea-level rise (SLR) (Storlazzi et al., 2015) and more extensive coral degradation. With this in mind, the following questions appear: (1) *How and to what extent are the coral reefs successful at attenuating the wave energy and thus reducing the coastal hazards? (2) How can we capture these high-complexity wave transformation processes with the use of existing computational modeling tools?*

In order to understand the beneficial effects coral reefs have on reduction of coastal hazards, first the bathymetric complexity of coral reefs is described in Section 2.1. After understanding the main coral reef features, the hydrodynamic processes are reviewed in Section 2.2. Cross-shore wave transformation is presented, as this is the focus of the thesis. After an overview of main hydrodynamic processes that contribute to coastal flooding, the computational modeling is presented in Section 2.3. Physics-based model XBeach and physics-reduced model SFINCS are introduced and compared, as these two models are the basis of the developed methodology in this thesis.

2.1   Bathymetric complexity of coral reefs

Three main types of coral reefs exist, classified as: fringing reefs, barrier reefs and coral atolls (Heemsoth, 2014a). The most common ones are **fringing reefs** that colonize near the shoreline of continents and islands. They do not contain any lagoon, therefore they are directly connected to the land. **Barrier reefs** are placed further offshore than fringing reefs while still being placed parallel to the shore. In-between the barrier reefs and the land is the lagoon. One of the most famous examples is the Great Barrier Reef in Australia. An **atoll** is an oval, circular or horseshoe-shaped coral reef, formed from volcanoes. An atoll, at least partially, surrounds a lagoon and contains a coral rim where the islands are formed.

Figure 2.1: Three main types of coral reefs (from left to right): fringing reefs, barrier reefs and coral atolls (Heemsoth, 2014a).

The reef zonation of fringing reefs is described in Section 2.1.1, as these are the most common types of reefs. Atolls and barrier reefs both hold similar characteristics as fringing reefs, if lagoons are excluded. Therefore, their zonation is not studied further. In Section 2.1.2 a database consisting the 1-dimensional (1D) cross-shore reef profiles, as used further in the thesis as a part of methodology, is described in detail.

2.1.1   Geomorphic zonation of fringing reefs

Four different geomorphic zones of fringing reefs are identified (depicted in Figure 2.2): fore reef, reef crest, reef flat and shoreline (Heemsoth, 2014b).

The fore reef extends from the reef crest to the shelf break or deep basin (Lugo-Fernández and Roberts, 2011). Usually, this occurs between the depths of 20 m and 50 m. Fore reef is the downward sloping reef section that normally ends in a sediment apron. The slope of the fore reef is highly variable between the reefs, but generally increases from fringing reefs, to barrier reefs, to atolls (Gourlay, 1996). Spurs and grooves that form vertical relief between 2–20 m frequently occur here as well (Roberts and Suhayda, 1983). While spurs are areas with parallel ridges of corals, grooves separate these ridges and contain eroded sediment from the spurs.

The reef crest is the usually the highest point of the reef, placed between the fore reef and the reef flat (Heemsoth, 2014b). It is a narrow zone where wave breaking mostly occurs (surf zone). During the low tide it can be exposed to air. Due to frequent air and light exposure and high wave energy, the corals living on reef crests must have strong structures.

The reef flat is usually the shallowest part of the reef structures (Blanchon, 2011). They are intertidal platforms that can be as narrow as hundred's of meters or as wide as several kilometers. Their slope is usually negligible, however if the reef flats contain gradient, it slopes back from the shoreline towards the reef crest. Two common subzones were recognized in open reef flats by Hopley (1982): an outer living zone that contains corals and an inner sand zone that contains sediment eroded from coral structures.

In-between the reef flat and shoreline is the **beach toe**, which is a location at the mean sea level.
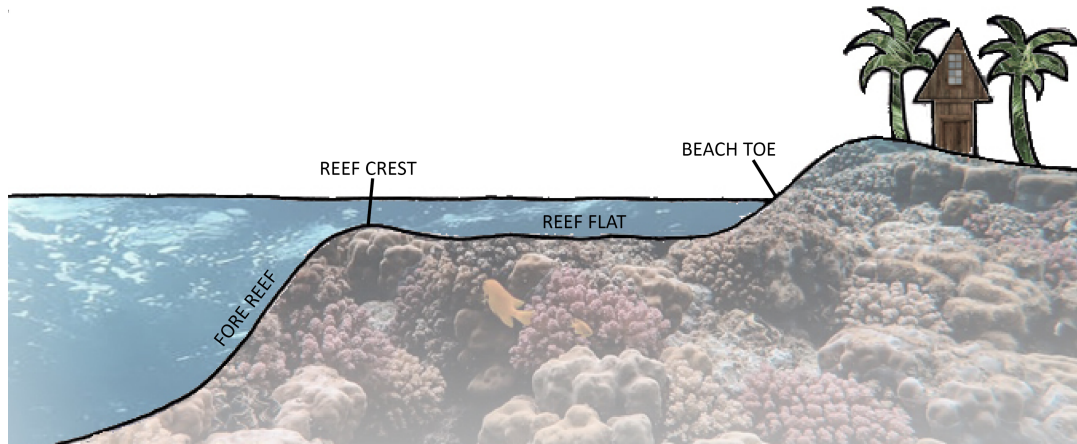
Figure 2.2: A schematic representation of a fringing reef with its main characteristics.

2.1.2 Representative cluster profiles

A wide range of coral reef morphologies exist, each exposed to a number of different hydrodynamic conditions. However, it is expected that reef profiles with similar bathymetric characteristics would result in similar hydrodynamic response. With this in mind, Scott et al. (2020) developed a methodology to cluster profiles with similar characteristics (both morphologic and hydrodynamic) in groups.

Scott et al. (2020)'s methodology is build with dataset of 30,166 measured coral reef topobathymetric 1D cross-shore profiles obtained by Storlazzi et al. (2019). The reef profiles were measured between 2001 and 2016 from seven regions from the Pacific Ocean, Atlantic Ocean and Caribbean Sea. Before processing the reef profiles further by classifying them, the adjustment was made to the original reef profiles. The 0 m elevation contour with respect to mean sea level is taken as a shoreline reference point (beach toe). The land was defined as the most seaward part of the profile with an elevation greater than or equal to 0.2 m above mean sea level (depicted in Figure 2.3). Therefore, the lagoons are not taken into the account. Grid spacing of the profiles is 2 m. Moreover, reef profiles that had too wide reef flat to be accurately modelled with process-based model XBeach Non-hydrostatic, were discarded from the dataset.
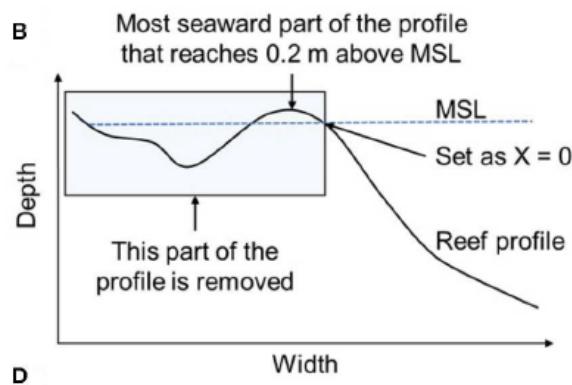
Figure 2.3: Defined part of the reef profiles that are included in the Scott et al. (2020)'s database. The 0 m elevation contour with respect to mean sea level is taken as a shoreline reference point (beach toe) and the part landward from the beach toe is removed.

From a full dataset of reef profiles, a set of 50-312 representative cluster profiles (RCPs) are obtained (Scott et al., 2020). This is performed with a use of unsupervised cluster analysis techniques. First step of large data reduction is performed using reef morphology and wave celerity with unsupervised machine learning (cluster analysis). The chosen method that performed with the largest accuracy was K-means clustering algorithm with the cityblock distance metric. Since wave celerity is more sensitive to changes in shallow water depths, its inverse was used as a non-linear weighting component in the clustering algorithm. Wave celerity was calculated using

linear wave theory. With this step, 500 initial RCPs (iRCPs) were selected.

The second stage of cluster analysis was performed with hydrodynamic response of reef profiles to typical storm wave conditions (Scott et al., 2020). Four wave conditions (wind wave and swell conditions) were applied to each of 500 iRCPs using the XBeach Nonhydrostatic model. The aim was to group profiles based on their hydrodynamic response from a wide range of conditions. Additionally, semi-infinite beach slope was added to reef profiles in order to simulate and compare the wave runup. The objective of RCPs is to forecast wave runup, therefore the wave runup values with different forcing conditions played an important role in reducing the iRCPs to a smaller set of RCPs. In fact, to reduce the amount of RCPs, 50% weight was decided for hydrodynamic response (equally divided among the three components: 2% wave runup, setup at the shoreline and IG and SS components of swash) and 50% weight was decided for reef morphology. In this step, agglomerative hierarchical clustering was applied (Day and Edelsbrunner, 1984).

Finally, the five groups of RCPs were obtained with the five thresholds to limit the dissimilarities of joined observations (Scott et al., 2020). The numbers of RCPs with each applied thresholds are: 312, 201, 149, 109 and 50 RCPs. When using the highest number of RCPs (312 RCPs), the accuracy of forecasting the runup is the greatest (mean relative difference of 9.7%) while using the lowest number of RCPs (50 RCPs) results in the lowest accuracy (mean relative difference of 13.1%). Each RCP in a cluster group has its own representative profile, derived from a set of similar profiles that was the closest to the mean in terms of 2% wave runup values. An example of RCPs with cluster group of 149 RCPs is depicted in Figure 2.4.

For more detailed description of the methodology to define the RCPs, refer to Scott et al. (2020).
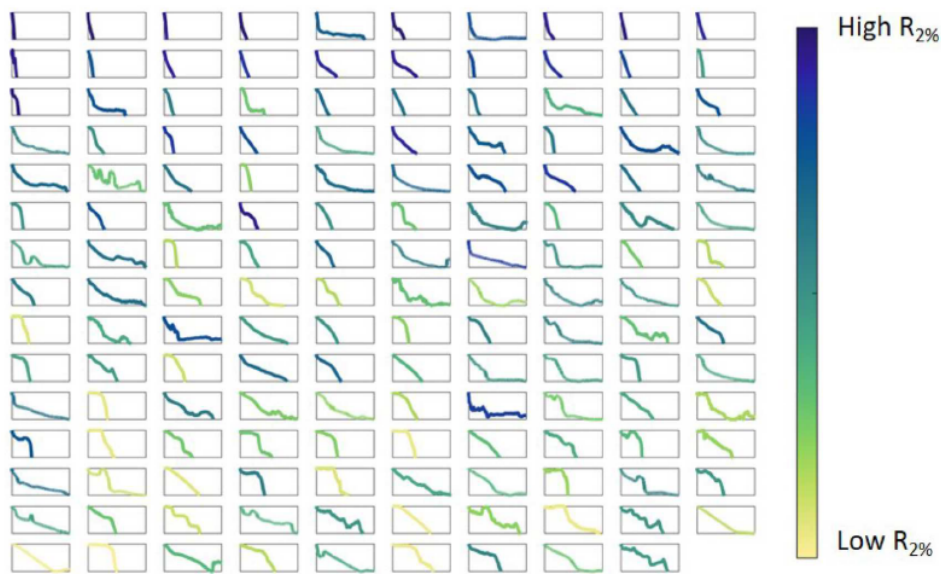
Figure 2.4: Adopted from Scott et al. (2020): 'The RCPs for the case of 149 cluster groups, colored based on their relative wave runup rank, and sorted based on their average slope from 0 to 15 m depth. The x-axis is the profile width set at a constant range of 0 to 3,068 m, and the y-axis is the profile depth from MSL set at a constant range of 30 to 0m.'

2.2 Cross-shore hydrodynamic processes

The following sections will lead the reader through some of the most important hydrodynamic processes occurring on fringing coral reefs, starting from the typical wave conditions originating offshore, going all the way to the shore while describing the typical wave transformation processes. The focus is on the cross-shore wave processes, because the thesis is based on 1D cross-shore modeling of wave-driven flooding. Figure 2.5 depicts the division of topics that this section approaches, as well as the reference of the subsections where each topic can be found. Each subsection describing the hydrodynamic processes includes the process-descriptive part (normal text) and frequency-domain part (text in gray background boxes). Frequency domain part explains the evolution of waves with the changes occurring in wave spectra.
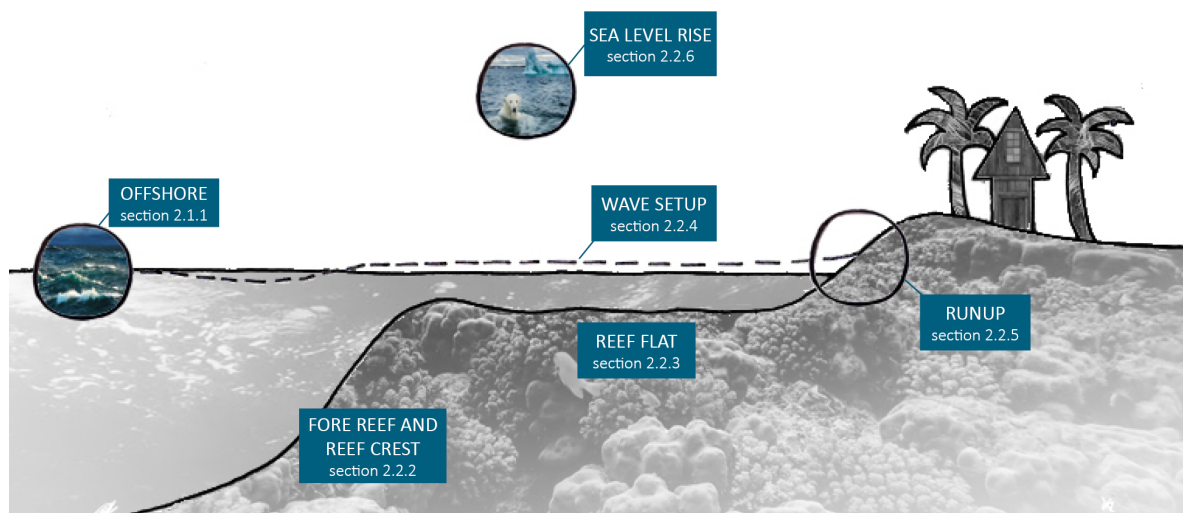
Figure 2.5: Topics that are included in Section 2.2 are depicted in this scheme together with the sections numbers where each topic can be found.

Terminology in frequency domain

Table 2.1: Definition of abbreviations of terminology in frequency domain, as used in this thesis.

Abbreviation	Explanation
HF	high frequency; usually referring to high frequency waves with typical frequencies between 0.04 and 1 Hz, sometimes referred to as sea-swell
IG	infra gravity; usually referring to infra gravity waves with typical frequencies between 0.004 and 0.04 Hz
VLF	very low frequency; usually referring to very low frequency motions with frequencies lower than 0.004 Hz
LF	low frequency; in this thesis LF describes both IG and VLF motions

The concept of the following sketches of spectra is partially adapted from Pearson and Tissier (2018).

2.2.1 Offshore wave conditions

Islands and mainland surrounded by coral reefs are found in the tropical areas around the globe. Flooding hazards threatening those areas are generated offshore by atmospheric and oceanographic processes (Ford et al., 2018). These processes include typhoon-driven storm waves and far-field generated swell. Tsunamis are a subject of different forcing conditions (e.g. tectonic) and are not considered in this study.

Typhoon-driven storm waves are generated during typhoons and tropical storms. Typhoons (i.e. tropical cyclones) occur as intense areas of low pressure with a central eye and a circular wind system (Gentry, 1968). The low pressure locally raises the sea level within the storm (Talley, 2011). Moreover, the winds in the storm generate large irregular waves. Those winds also push the water towards the land, thus resulting in an increase in water level called the storm surge.

Far-field generated swell is a field of waves generated from a distant storm (e.g. Barber and Ursell (1948)). During a severe storm above the ocean, the strongest winds are generating the waves for a limited time, typically in order of 12-24 hours. The swell field has a lifetime of a few weeks due to its propagation across the ocean basins more than 20,000 km from their source (Munk et al., 1963). Due to dispersion relation, the irregular waves generated at a distant storm disintegrate into fields of more regular waves (Holthuijsen, 2010). Low frequency waves are leading while high frequency waves are lagging behind.

Translation to frequency domain:

Typhoon-driven storm waves and far-field generated swell both occur due to high velocity winds mixing the surface of ocean water. While storm waves occur close to the land and thus remain irregular, the swell waves due to the dispersion relation and propagation across the ocean become regular waves. Therefore, the energy spectra of storm waves and swell differ. In deep water, swell has its distinctive narrow spectrum usually in lower part of the frequency domain. On the other hand, storm waves have wider spectrum, usually very well estimated with the JONSWAP spectrum (Hasselmann et al., 1973). The shape of the JONSWAP spectral tail of waves in a deep water is f^{-5}-shape (f stands for frequency; shape of a spectral tail is indeed a function of frequency.).

Both spectra are depicted in Figure 2.6 and Figure 2.7. Even though the frequency peak of both spectra differ (swell usually has a lower value of the frequency peak than storm waves), they both contain energy in the HF band.
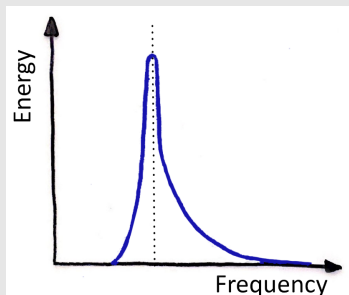
Figure 2.6: The JONSWAP spectrum.
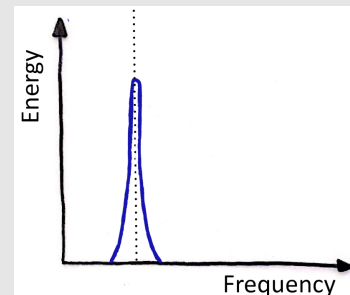
Figure 2.7: The spectrum of the swell.

In the following sections, no distinction between the storm waves and the swell is made. All offshore waves, either storm waves or swell, are now denoted as *sea-swell*.

2.2.2 Towards the fore reef and the reef crest

Incident waves coming from the offshore start *feeling the bottom* at the lower slope of the fore reef (Lugo-Fernández and Roberts, 2011). Wave-reef interactions start at water depths of up to 50 m for most energetic waves with wave periods higher than ≈ 8 s. Due to interactions the waves start shoaling while propagating across the fore reef towards the reef crest.

Sea-swell waves are primarily dissipated due to breaking (Péquignet et al., 2014). In case of steep fore reef, the breaking generally occurs in breaking zone near the reef crest, however this is highly dependent on the water depth and the intensity of offshore wave conditions. According to meta-analysis performed by Ferrario et al. (2014), reef crest can on average dissipate 86% of the incident wave energy.

Wave breaking leads to wave setup, a phenomenon described in detail in Section 2.2.4. Besides that, in the zone of wave breaking the energy from the HF band is also transferred to lower wave frequencies. Two mechanisms are responsible for that due to (1) release of bound long waves and (2) breakpoint forcing.

Bound long waves with frequencies in IG frequency band are phase locked to the primary HF waves (Masselink, 1995). This occurs because of the grouping of natural random waves. As theoretically demonstrated by Longuet-Higgins and Stewart (1964) with radiation stresses, high waves have larger mass transport than low waves which results in difference in the momentum flux. This difference causes fluid to move from groups of high waves to groups of low waves. As a result, set-down and set-up waves develop with the same wave period as the incident wave groups. The period of this wave is in IG frequency band and the wave is called the bound long wave. The phase difference between the bound long wave and the the incident wave group is $180°$. When the incident waves shoal, a phase lag between the incident wave group and the bound long wave develops (Masselink, 1995). The phase shift is increasing with decreasing distance from the shore and decreasing water depth (the increase in phase shift is from $0°$ to $90°$ at the breaking, as shown by Elgar and Guza (1985)). Concurrently, a transfer of wave energy from HF wave energy towards IG wave energy is proceeding until the incident (sea-swell) waves break and the bound long waves are freed into free IG waves (demonstrated by Battjes et al. (2004)).

Breakpoint forcing results due to variation of high and low waves traveling from the offshore towards the fore reef and the reef crest (Symonds et al., 1982). Due to variation of wave amplitudes, the waves break at slightly different locations along the reef. This variation results in time-varying setup due to time-varying radiation stress gradients (Longuet-Higgins and Stewart, 1964). The frequency of this time-varying setup is in IG frequency band, therefore these waves are categorized as IG waves.

Translation to frequency domain:

When waves are propagating from deep water to shallow water, the f^{-5}-shape of a spectra slowly transforms into f^{-3}-shape (Holthuijsen, 2010). As an alternative to JONSWAP spectrum (which can only be used in deep water applications), Bouws et al. (1985) proposed a more generalized spectrum that can be applied to arbitrary water depths. The so-called **TMA spectrum** was verified by Bouws et al. (1985) on three datasets Texel (The Netherlands), Marsen (North Sea) and Arsole (Atlantic Ocean), thus the name TMA spectrum. The TMA spectrum differs from the JONSWAP spectrum through the transformation function $\phi(f, d)$. TMA spectrum is based on the hypothesis of Kitaigordskii et al. (1975) which states that the wave number (k) is better at describing the evolution of waves of a young sea state than the wave frequency (f). How different the TMA spectrum is from the JONSWAP spectrum is depicted in Figure 2.8.
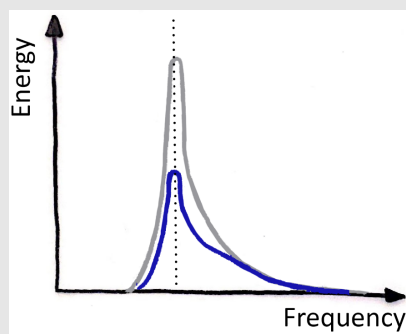
Figure 2.8: The TMA spectrum (blue) and the JONSWAP spectrum (gray).

As explained above, while sea-swell propagates across the fore reef and the reef crest, the wave energy is transformed from HF wave energy to IG wave energy. This nonlinear interaction is in frequency domain depicted in Figure 2.9.
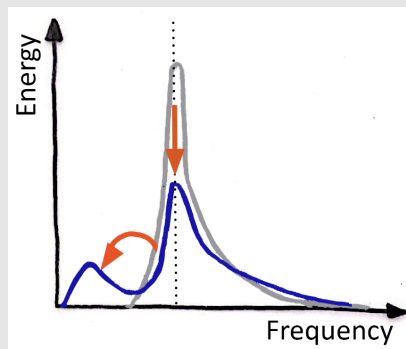
Figure 2.9: A transfer of wave energy from sea-swell (e.g. JONSWAP spectrum in gray) to IG waves (blue).

2.2.3 Reef flat

Although majority of the wave energy is dissipated prior to the reef flat, a large part of remaining wave energy is dissipated on the reef flat. According to Ferrario et al. (2014), 65% of the remaining wave energy is dissipated here, mostly in the first parts of the reef flat (i.e. 150 m closest to the reef crest).

Due to dissipation of sea-swell waves and generation of IG waves at the fore reef and reef crest, oscillations at IG wave periods are dominating the reef flat (Nwogu and Demirbilek, 2010). While IG wave energy is initially increasing shoreward during the propagation of waves across the reef flat, a few mechanisms are responsible for decrease if its energy in the nearshore, namely:

  – bottom friction dissipation;
  – shoreline breaking; and
  – nonlinear transfer to higher frequencies due to undulation of propagating turbulent bore.

HF waves are dampened due to **bottom friction dissipation** more extensively than LF wave (Pomeroy et al., 2012). The extent of bottom friction dissipation is governed by characteristics of the reef flat (water depth, width of the reef flat and roughness) and the shape of the incoming waves (Péquignet et al. (2009), Pomeroy et al. (2012)). Complex canopy of the reef is responsible for the wave dissipation through the wave friction factor f_w which was found to be up to 1.80±0.07 on a healthy reef like the one of Palmyra Atoll (Monismith et al., 2015). Authors thus argue that healthy reefs have higher potential for the coastal protection than degraded reefs.

Another interesting phenomenon occurring on reef flats is the generation of **undular bores**. When the waves (both IG waves and sea-swell contribute to this phenomenon, as experimentally shown by Dekkers (2018)) are breaking on the reef flat, they propagate across the reef as a turbulent bore (Pearson and Tissier, 2018). Once the breaking stops, the undulation in the form of wiggles is generated at the crest of the turbulent bore. The wave energy of the breaking wave at that moment transfers into higher frequencies, thus increasing the amplitude of the wiggles. A photography of captured undular bore is depicted in Figure 2.10.

Undular bore formation leads to significant modification of wave field across the reef flat (Dekkers (2018), Tissier et al. (2018)). While undulations are formed, the height of the leading bore increases as well. Energy transfer from lower to higher frequencies is independent on incident wave height (Grue et al., 2008). However, it is highly dependent on the bottom topography. When the reef flat is wide enough for a full development of undular bore, the initial long wave splits into a set of solitary waves. This effect can have a large influence on the wave runup. Due to its nonlinear properties, the formation of growth and propagation can only be properly accounted for in numerical modeling with models based on non-linear shallow water equations including the non-hydrostatic pressure term (Dekkers, 2018).

Figure 2.10: Undular bore formation, captured by Gallagher (1972).

Under certain circumstances when the period of the incoming IG waves has the same period as the natural period of the seiche in the reef flat, a **resonant response** can occur (e.g. Cheriton et al. (2016), Gawehn et al. (2016), Pearson et al. (2017)). Natural period of reef basin can be calculated as:

$$T_\circ = \frac{4l}{(2n+1)\sqrt{gh}}; \quad (n = 0, 1, 2 \cdots)$$ (2.1)

where l is the width of the reef flat, h is still water level (depicted in Figure 2.11), g is gravitational acceleration and n is mode number.
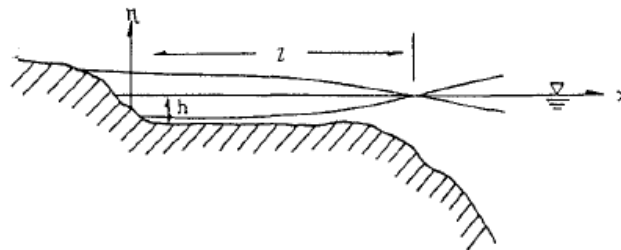
Figure 2.11: A scheme of the first mode of resonant motion on the reef basin (Munk and Sargent, 1948).

Due to dissipative nature of reef flats (reef flats are usually very wide and shallow), IG wave resonance predominantly occurs for the longest fundamental mode ($n = 0$ in Equation (2.1)) (Gawehn et al., 2016). In that case a water level node is near the reef crest and an antinode at the shoreline. It occurs when $\frac{1}{4}L = l$ and L is a wavelength of the incoming wave (Lugo-Fernandez et al., 1998). The consequences of a resonant response can be substantial due to its ubrupt excitement of amplitude of the incoming waves, as discovered during field observations by Nakaza et al. (1990), Péquignet et al. (2009), Roeber and Bricker (2015) and Tajima et al. (2016).

Translation to frequency domain:

When waves are dissipated due to bottom friction, they are losing their energy. In terms of spectral representation of waves across the reef, that means that with decreasing distance from the shore, the variance density spectrum is decreasing. On the other hand, when resonance occurs, the energy at the frequency of the resonance increases. The two situations (dissipation and resonance) are depicted in Figure 2.12 and Figure 2.13.
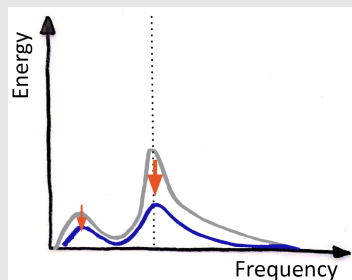
Figure 2.12: Dissipation due to breaking.
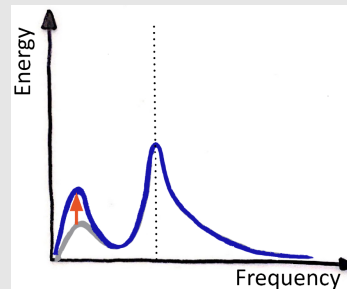
Figure 2.13: Resonance of IG wave.

Breaking of waves across the reef results in cross-spectral transfer of energy from the peak frequencies to the lower and higher frequencies (Nwogu and Demirbilek, 2010). Due to complex transformation of energy across the reef and many different phenomena happening concurrently (breaking, friction dissipation, undular bore, resonance), the interpretation of spectrum at a certain location along the reef flat is difficult. In order to better understand the wave evolution across the reef, computing other wave parameters is needed. An example is to study the wave shape evolution across the reef by computing the skewness and asymmetry.

2.2.4   Wave setup

Breaking of waves on the reef induces a force on the water column which is balanced by a pressure gradient (Longuet-Higgins and Stewart, 1964). As a consequence, water level rises, i.e. wave setup is induced. Wave setup on the coral reefs was first observed and described by Munk and Sargent (1948), during their field observations at Bikini Atoll in the Pacific Ocean. They observed a wave setup between 0.45 m and 0.6 m, much higher than usually observed on sandy coastlines.

The amount of wave setup is highly dependent on bathymetric characteristics of the reef. It increases with increasing fore reef slope due to breaking of waves in a more confined shallower area (Quataert et al., 2015). This consequently results in a higher pressure response in the cross-shore momentum balance. Moreover, in the laboratory study by Seelig (1983), they observed that the setup increased as the water level over the reef flat decreased. Consequently, setup is time-varying due to influences of tides (Becker et al., 2014), which can be partially explained due to incomplete breaking. Similarly, sea level rise has a potential to decrease the amount of wave setup while increasing the amount of runup due to higher amounts of wave energy propagating across the reef flat and towards the shore (Beck et al. (2018) and Quataert et al. (2015)).

The amount of wave setup is also a function of wave parameters. With increasing incoming wave height, the radiation stress gradients increase which results in increased wave runup (e.g. Seelig (1983), Vetter et al. (2010), Quataert et al. (2015)). Consequently, mean water level, wave height at a shoreline and wave runup all increase approximately linearly with increasing incoming wave height (Quataert et al., 2015). Incoming wave period also plays an important role in the amount of wave setup. In fact, setup increases with increasing wave period (Gourlay, 1996).

2.2.5   Runup and overtopping

The most common parameter for forecasting wave-driven flooding is the wave runup at the beach. Wave runup is defined as the maximum water level in the foreshore with respect to still water level (Hunt, 1959). It is composed of mean water level increase due to wave setup and of swash, i.e. fluctuations above the setup level (Guza and Thornton, 1982). Overtopping occurs when the wave runup exceeds the crest of the beach. This event potentially leads to flooding of the area behind the beach. The 2% exceedence value of the wave runup (denoted as R2%) is widely used measure for engineering applications (Holman, 1986). The impact of severe storms on coastlines are scaled up primarily with R% values (e.g. Stockdon et al. (2006)).

The amount of wave runup and overtopping is strongly correlated to the morphology of the reef and the offshore wave conditions (Scott et al., 2020), the same parameters that are controlling the evolution of waves

across the reef, as explained in the previous sections. **Generally, reefs with narrow reef flats, large water depths and steep beach slopes result is larger wave runup compared to reefs with wide shallow reef flats and gentle beach slopes** (Quataert et al. (2015), Pearson et al. (2017)). Differences between the runup characteristics of regular and irregular waves was first studied by Seelig (1983) in laboratory settings. During the observations of regular waves a larger wave setup was measured, whereas during the observation of irregular waves the maximum values of wave runup were much higher due to strong LF wave evolution and propagation along the reef profile.

Several wave-induced runup parameterizations have been formed in the past, however most of them are applied to sandy coastline (e.g. Stockdon et al. (2006)). Due to complex evolution of waves along the reef, reliably estimating the wave runup with wave parameters and reef profile characteristics is challenging. In their study, Medellín et al. (2016) emphasized that a site-specific runup parameterizations should be developed, based on the field observations. However, field observations usually do not include extreme wave conditions, since measurements are more difficult during these events. One of the well known empirical formulations for extreme runup, applied for use on sandy coastlines over a wide range of conditions, is from the research performed by Stockdon et al. (2006). Throughout the research, the following formulation of runup was derived:

$$R_{2\%} = 1.1 \cdot [< \eta > + \frac{S}{2}] \tag{2.2}$$

where $< \eta >$ is mean wave setup and S is swash, which is furthermore divided into incident and infragravity swash. Both, mean setup and swash, are parameterized in this study and for both constituents it was found that they are functions of beach slope and a square root of the offshore wave height H_0 and offshore wave length L_0. These findings are in line with the site-specific parameterization of wave runup, derived by Medellín et al. (2016) for the barrier island in Yucatan, Mexico. They concluded that both, wave-induced runup and setup are functions of offshore wave height H_0 and offshore water level η_0.

2.2.6 Impact of sea level rise to reef hydrodynamics

Data from observations and projections of sea level reveals that by the end of the 21st century eustatic sea level rise (SLR) could exceed 2 m above 2000 levels (Jevrejeva et al. (2009), Kopp et al. (2014)). Projections (Slangen et al., 2014) also suggest that SLR will be higher in the tropical areas where most low-lying atoll islands are present. A study by Storlazzi et al. (2015) reveals that SLR and the associated intensified wave-driven flooding will force the islanders of tropical atolls to relocate by the mid-21st century.

The impacts of wave-driven flooding on coastlines surrounded by coral reefs is intensified due to SLR. Baldock et al. (2014) conducted a study with 1D model to assess the consequences of SLR to reef hydrodynamics for barrier reefs with lagoons. They showed that with SLR the wave height increases, however wave induced velocities are way more complex and their response varies for every reef profile. Moreover, their research suggests that wave periods of the waves propagating across the reef platforms will generally increase with SLR. Wave period was found to be relatively constant on fore reef under SLR, but increases almost everywhere else. Furthermore, SLR enables longer period waves to propagate over the reef. According to the research by Quataert et al. (2015) SLR causes increase in wave runup.

Although these projections are pessimistic, Masselink et al. (2020) gives a more optimistic view on the situation. In their research, Masselink et al. (2020) performed numerical modeling simulations of reef islands composed of gravel material. Their results suggest that these islands can evolve under SLR by accreting vertically. The mechanisms behind these results can be explained by wave-driven overtopping processes that are transferring sediment from the beachface to the island surface. The study suggests that climate-related assessment of future of these islands should be performed with models that include morphodynamic processes.

2.3   Modeling wave-induced flooding

Flooding can essentially be simulated with three different approaches: simple flood models (e.g. with static bathtub type approach, e.g. Vousdoukas et al. (2016)), reduced-physics models (e.g. SFINCS, Leijnse et al. (2021)) and full-physics process-based models (e.g. SWASH, Zijlema et al. (2011) and XBeach-Nonhydrostatic, Roelvink et al. (2018)). A decision to use either of them is governed by the balance between the desired accuracy and the computational demand. While simple flood models require low computational costs for a price of low accuracy, full-physics process-based models can be computationally demanding but can simulate wave-driven flooding with high accuracy (see Figure 2.14). Reduced-physics models aim to be as accurate as possible with as low as possible computational demand (Leijnse et al., 2021).
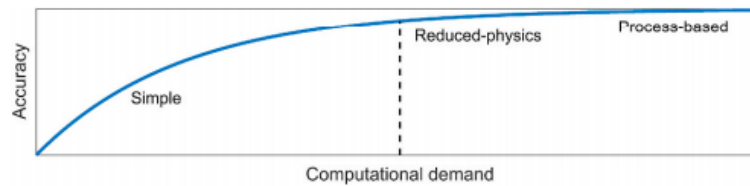
Figure 2.14: Graph showing how the balance between the accuracy and the computational demand is tackled in different approaches to model flooding (Leijnse et al., 2021).

In this thesis reduced-physics model SFINCS (Leijnse et al., 2021) is used as the featured model, whereas process-based model XBeach with nonhydrostatic+ mode (de Ridder et al., 2021) is used as: (1) look-up-table, used for boundary conditions input for SFINCS, and (2) to validate the performance of the developed methodology. It is therefore important to understand the similarities and differences between the two models in order to be able to interpret the results, obtained in the research. First, the models XBeach and SFINCS are described in Section 2.3.1 and Section 2.3.2, respectively. Then, the two models are compared in Section 2.3.3. Look-up-table consisting of XBeach runs is outlined in Section 3.2.2.

2.3.1   Process-based model XBeach

XBeach (eXtreme Beach behaviour, Roelvink et al. (2009)) is an open-source program, initially developed to model the nearshore response to hurricane impacts. It can account for alongshore variability in the coast due to e.g. man-made coastal protections and natural features such as variations in dune heights, rip currents and shoals. Essentially it is a 2-dimensional model that includes all the relevant physical processes to simulate morphological changes (e.g. dune erosion and avalanching) and propagation of waves till shore. To what extend can the model accurately simulate waves till shore is dependent on the mode the user implies. Based on the time-scales with which the model is able to resolve hydrodynamic processes in the nearshore, three modes of XBeach are currently available:

 – stationary mode (solves wave-averaged equations, neglects IG waves);
 – surfbeat mode (solves short wave variations on the group scale and long waves associated with them);
 – non-hydrostatic mode (solves propagation and decay of individual waves) with an option for 2 horizontal layers (non-hydrostatic+ mode).

To model wave-driven flooding on coral reef-lined coasts, all contributions to wave runup need to be accounted for accurately. This includes resolving individual waves, including sea-swell (Quataert et al., 2020). Therefore, non-hydrostatic pressure term needs to be included in the model. XBeach non-hydrostatic (following XB-NH) model solves propagation and decay of individual waves. However in the complex environments such as the coral reefs, XB-NH fails to correctly simulate the individual contributions of setup, IG and incident-band swash to the wave runup (Roelvink et al., 2018). Therefore, the use of non-hydrostatic+ mode (XB-NH+) is needed as this option accounts for simulation of individual waves in intermediate and shallow waters (de Ridder et al., 2021). This option is therefore further explained below. For description of the stationary mode and the surfbeat mode, the reader is referred to Roelvink et al. (2009).

XBeach Non-hydrostatic +

XBeach Non-hydrostatic + (following XB-NH+) is a 2-layer model as opposed to all other XBeach modes which only have 1 horizontal layer (de Ridder et al., 2021). With additional layer approximation, the model is able to better account for dispersion relation in intermediate water depths for kh[1] up to 4, compared to 1-layer model that is only applicable in shallow waters (kh less than 1). Nevertheless, if the model would account on full 2-layer description, the model would be effective for up to kh of 5-6. However, the intended application domain of an approximate 2-layer model is in relatively shallow water with small kh.

XB-NH+ is governed by Nonlinear Shallow Water Equations (NSWE) including the non-hydrostatic pressure (de Ridder et al., 2021). 2-layer model of the flow is applied based on Cui et al. (2014). The water column is divided into two layers that are defined with a layer distribution parameter α. Horizontal flow velocities are along the centres of the layers whereas vertical velocities and the non-hydrostatic pressure are at the cell face. The 2-layer approximation can only be applicable with the assumption that the velocity difference Δu between top and bottom layers is small, i.e. $\Delta u/U \ll 1$ where U is depth averaged velocity. Non-hydrostatic pressure is assumed accordingly as $\Delta q/q \ll 1$ where q is the pressure at the centre interface (between the two layers) and Δq is the difference between q in the centre and at the bottom. This approximation assumes that a constant non-hydrostatic pressure distribution is present in the lower layer. Thus the improved capturing of dispersive behaviour is performed without much additional computational cost. However, with this approximation, the application of the model is limited to nearshore shallow water. Consequently, the dispersive behaviour is incorrect for some wave frequencies which in shallow water does not result in large deviation. Nevertheless, the results are still better than with 1-layer model.

Breaking of waves is captured with hydrostatic front approximation, just like in Smit et al. (2014). With this approach, the model is reduced locally to shallow water model with strict momentum conservation. This ensures the good representation of bulk energy dissipation.

Validation with the analytical solutions were performed (de Ridder et al., 2021) and the 2-layer model (XB-NH+) was compared to 1-layer model (XB-NH). 2-layer model showed a good performance of dispersive characteristics of the group velocity, wave celerity and the radial frequency for cases up to $kh = 5$, whereas 1-layer model was only valid for up to $kh = 1$. Due to incorrect representation of dispersive relation in deep water, waves in deep water travel too fast in the 2-layer model and too slow in the 1-layer model. Validation of linear shoaling showed that the 2-layer model accurately simulates shoaling of waves, as opposed to the 1-layer model that incorrectly simulates shoaling behaviour of the shorter waves and thus underestimates wave heights.

Validation using laboratory data was performed for three cases with different hydrodynamic conditions (de Ridder et al., 2021). (1) Validation of bichromatic waves over a plane beach showed that the 2-layer model accurately captures the energy transfer of the primary waves to the sub-harmonic and the shape of the sub-harmonic. Moreover, the dissipation and reflection of the sub-harmonic at the shoreline is captured well. (2) Validation of irregular waves over a barred beach showed a good performance of the 2-layer model to capture the bulk wave statistics and spectral properties. The validation of the second order statistics (by means of the skewness and asymmetry) showed that the 2-layer model overestimates the asymmetry close to the shoreline when spilling/plunging type of breakers are present. This is due to hydrostatic front approximation that is based on the energy dissipation of a bore with a steep bore face, which is not the case for the spilling/plunging type of breakers. (3) Irregular waves over a fringing reef were captured with the 2-layer model with good accuracy. The bulk wave properties and spectral properties were both captured with good accuracy. The second order statistics were also captured with good accuracy, however the asymmetry on the reef crest was was slightly overestimated for all tests. Due to the hydrostatic front approximation, the slightly lower radiation stress gradients were simulated, resulting in slight underestimation of the setup.

2.3.2 Reduced-physics model SFINCS

SFINCS (Super-Fast INundation of CoastS) is a reduced-physics model developed by Maarten Van Ormondt (Deltares). It includes relevant processes to compute compound flooding in coastal systems in computationally efficient way (Leijnse et al., 2021). Compound flooding events that can be simulated with SFINCS can include wind- and wave-driven processes as well as fluvial (riverine processes), pluvial (precipitation) and tidal processes.

---

[1]k is the wave number and h is the water depth.

In addition, spatially varying friction, infiltration and precipitation can be included in the model.

Model description

SFINCS is governed by equations that are based on LISFLOOD-FP model (Bates et al., 2010). Primarily, the model is based on Local Inertial Equations (LIE) that are simplifications of the full Saint-Venant equations including local acceleration (Leijnse et al., 2021). Advection, Coriolis and viscosity are neglected. This option of SFINCS is called SFINCS-LIE. It is possible to include advection in the model and thus the LIE equations turn into Simplified Shallow Water Equations (SSWE). This option is called SFINCS-SSWE. Due to simplified shallow water equations, non-hydrostatic pressure term is neglected in SFINCS. Additionally, SFINCS differs from the full-physics process-based models in the lack of atmospheric forcing, Coriolis and viscosity.

The computational mesh is composed of rectangular, equidistant, staggered grid, with bed levels and water depths in cell centers (Arakawa C-grid, based on Arakawa and Lamb (1977)) and fluxes in velocity points (Leijnse et al., 2021). Momentum fluxes are calculated using explicit scheme (1st order accurate in space and time and conditionally stable). Spatial smoothing of the fluxes from the previous time steps is applied with Lax-scheme to improve the stability of numerical solution. This effect is controlled by factor θ which extends from 0 to 1 with a default of $\theta = 0.9$. Continuity equation is discretized with 1st order explicit time stepping with 1st order central differences approximation of spatial derivatives (i.e. BTCS scheme). Moreover, SFINCS includes an option to apply an absorbing-generating weakly-reflective boundary in order to absorb reflected long waves.

Input for SFINCS is currently as a text file with parameters (grid spacing, simulation time, etc.), depth file, mask file, time series at the boundary and other input files such as point discharges, spatially varying roughness, infiltration rates and meteorological forcing (Leijnse et al., 2021). With mask file the user determines which cells in computational grid active and inactive and which cells serves as boundary cor forcing the model with e.g. water level time series. Time series at the boundary consist of two separate input files:
  – slowly-varying water level time series (input name: `bzs`): water level elevations due to tide, storm surge, wave setup; and
  – rapidly-varying water level time series (input name: `bzi`): sea-swell, IG waves, VLF waves.

How important is advection term?

Whether the user includes advection in the model or not (SFINCS-LIE or SFINCS-SSWE), depends on the application of the model and the desired accuracy. The importance of including advection term in the model for simulating wave-driven flooding on coral reef-lined coasts is shown with the test cases performed by Leijnse et al. (2021). The model was applied to simulate the wave driven flooding on Hernani (Phillipines) during Typhoon Haiyan in 2013 (Roeber and Bricker, 2015) where large IG waves (Hs = 18 m and Tp = 16 s) were generated over fringing reef and causing substantial flooding. Comparison was performed between SFINCS-LIE, SFINCS-SSWE and XB-NH+. SFINCS (for both LIE and SSWE options) was forced landward from reef flat with alongshore resolution of 10 m and cross-shore resolution of 5 m.

Results showed that without the advection term the simulated wave fronts remain too steep in the direction of the shore while flow velocities are underestimated (Leijnse et al., 2021). As a consequence, SFINCS-SSWE (including advection) performed with good accuracy, while SFINCS-LIE (without advection) resulted in overestimation of the wave heights. By comparing the output results of SFINCS-SSWE to XB-NH+, SFINCS-SSWE mostly under-predicted max water depths with relative bias of -2%. These underestimations mainly occurred along the seaward boundary where the waves are steep. On the other hand, maximum water depths closer to the shore were better predicted. Largest differences were observed in mean water depths with relative bias of -20%. With XB-NH+ waves remained steeper and higher on average, while penetrating further into the domain. Total flooded volume simulated with SFINCS-SSWE was underestimated with relative bias of -5.9%. However, runtime with SFINCS-SSWE was at least 300 times lower compared to runtime with XB-NH+.

Overall, it is shown that SFINCS-SSWE can model wave runup in a physically correct way. However, adding advection increased the runtime by 21% (Leijnse et al., 2021).

Limitations of a physics-reduced model

Atmospheric pressure, Coriolis and viscosity are not included in either version of SFINCS, however theoretically these three terms should not have a large impact on simulation of coastal flooding (Leijnse et al., 2021). However, morphological changes are not included in the model either. Therefore, sediment dynamics and morphological changes such as dune erosion and breaching of barrier islands cannot be modelled with SFINCS. This limits the application of the model to locations where abrupt changes in morphological features are expected.

Non-hydrostatic pressure correction term is not solved with SFINCS. This term is important for resolving incident waves correctly (Roelvink et al., 2018). Consequently, dispersive behaviour of the waves is not captured and waves cannot be correctly predicted with SFINCS. However, in shallow water the kd values are usually low. Thus, the errors associated with the lack of non-hydrostatic pressure correction term are not expected to be high.

From a case study of Hernani (Leijnse et al., 2021), it was shown that with advection the wave runup on coral reef-lined coast is predicted with relatively high accuracy when SFINCS is forced landward from reef flat. Including advection thus significantly improves the modeling of the waves, but it results in 15-85% increase in computational demand (compared to SFINCS without advection term).

A case study of Hernani (Leijnse et al., 2021) also showed that SFINCS performs best when forced landward from the reef flat. The water level and wave conditions are therefore needed at the location of the SFINCS boundary. These boundary conditions can be obtained with the use of computationally demanding models such as XB-NH+, but to what extent is this process feasible? By using computationally demanding model to force SFINCS, the runtime of the model train increases drastically. There is therefore still an open question: *how can the boundary conditions be obtained to force SFINCS without the use of computationally demanding models such as XB-NH+?*[2]

2.3.3 Comparison between XB-NH+ and SFINCS

XB-NH+ and SFINCS-SSWE are used in this thesis to develop a method to model wave-driven flooding in computationally efficient way. It is therefore important to understand the differences between the models. Comparison of important properties is outlined in Table 2.2.

---

[2]Hint: the method that is developed throughout this thesis aims to provide an answer to this question.

Table 2.2: Comparison between physics-based model XB-NH+ and reduced-physics model SFINCS.

Property	XB-NH+	SFINCS
Computational mesh	Curvilinear, non-equidistant, staggered grid	Rectangular, equidistant, staggered grid
Number of layers	2	1
Governing equations	Full nonlinear Shallow Water Equations (NSWE)	Simplified Saint-Venant equations, two options: – Local Inertial Equations (LIE) - no advection; – Simplified Shallow Water Equations (SSWE) - advection included
↪ Non-hydrostatic pressure gradient term	Included	Neglected
Wave resolving	Wave resolving model	Wave resolving model
Coriolis	Neglected by default, can be turned on	Neglected by default, can be turned on
Viscosity	Included	Neglected
Atmospheric pressure gradients	Neglected	Neglected by default, can be turned on
Numerical scheme	Default: implicit finite-difference scheme (Beam and Warming, 1976)	First-order explicit backward in time with a first-order central difference approximation of the spatial derivatives (BTCS-scheme)
Wind drag	Included	Included, but not used in this thesis
Advection	Included	Not included in LIE, but included in SSWE (included in this thesis)
Flow boundary conditions	Weakly reflective absorbing-generating boundary condition	1D weakly reflective absorbing-generating boundary condition
Bed shear stress	Several options, dimensional friction coefficient (cf coefficient) used in this thesis	Manning

3
Methodology

Development of efficient and accurate methodology for modeling wave-driven flooding on coral reefs requires thorough understanding of the model outputs, identification of the possible methods and sensitivity testing of the methods. A detailed description of the steps taken throughout the research is included in Section 3.1. Model set-up and description of the look-up-table (XB-NH+ LUT) are included in Section 3.2. Examples of input parameter files for SFINCS and XB-NH+ are can be found in Appendix A.

In general, the research is divided into two parts: (1) sensitivity analysis and (2) development of interpolation method at the boundary. Methodology of each part is described in Section 3.4 and Section 3.5, respectively. Both parts are applied to conceptual cases on six reef profiles and two offshore wave and water level scenarios, described in Section 3.3.

3.1   General approach to the problem

The main idea that defines the flow of the thesis project is to use the **physics-reduced model SFINCS** to simulate wave-driven flooding on coral reef-lined coasts. Since SFINCS is based on simplified shallow water equations (see Section 2.3.2 for a description of the model), it performs with higher accuracy when it is forced in shallow water. Therefore, another model, preferably a process-based phase-resolving numerical model, is needed to obtain the boundary conditions for forcing SFINCS. For this purpose, a **look-up-table (LUT) consisting of pre-run simulations with physics-based model XB-NH+** (Section 3.2.2) is used to obtain boundary conditions for forcing SFINCS. A schematic representation of the proposed methodology is shown in Figure 1.1. The following two main questions need to be addressed first: *How can the XB-NH+ LUT be used to obtain boundary conditions for SFINCS, and how generalized can the developed method be?*

Theory showed that bathymetry plays a major role in the evolution of waves till shore (refer back to Section 2.2). For example, long shallow reef flats promote wave breaking, generation of IG waves and generation of undulations by turbulent bore propagation. To develop a method that can be applicable on a large number of possible cases, the approach is to test the method for different offshore conditions and different coral reef topobathymetric profiles. Therefore, the first step in the analysis is a **design of conceptual cases** (described in Section 3.3). These conceptual cases are used in all steps of the analysis. They are designed in a way to test the method to different hydrodynamic regimes.

The second step is the **sensitivity analysis** (Section 3.4 and Chapter 4). From the research performed by Athif (2020) it was shown that the TMA+GAUSS function for parameterizing the spectra at the boundary is a good strategy, therefore the TMA+GAUSS function is used in this thesis. The purpose of the sensitivity analysis is to understand what are the consequences of using the simplified parameterized spectra at the boundary and generating new random phased water level time series for forcing SFINCS. For this purpose, the boundary conditions from parameterized spectra are compared to the exact boundary conditions. Furthermore, the evolution of waves with SFINCS forced with different boundary conditions is studied. Detailed analysis is performed on one test case (selected and described in Section 4.1.1). Finally, the best suitable boundary location for forcing SFINCS is identified. The set-up for testing interpolation methods is designed based on the outcome of the senitivity analysis.

The third step is the **design and testing of interpolation methods** (Section 3.5 and Chapter 5). Interpolation of boundary conditions is needed because XB-NH+ LUT is limited to only a number of offshore wave and water level conditions and therefore cannot be used directly to simulate arbitrary offshore conditions. Chosen interpolation methods are tested on conceptual cases. TMA+GAUSS spectral parameters and wave setup are interpolated. First, the performance of interpolation methods is evaluated at the boundary: interpolated parameters at the boundary are compared to the exact parameters. Next, the values of wave runup, simulated with interpolated boundary conditions, are compared to (a) the wave runup simulated with exact boundary conditions and (b) the correct wave runup simulated with the full XB-NH+ model. The influence of each interpolated parameter to the final runup is investigated as well. Finally, the most accurate interpolation method is identified.

> **Important note: Measure for assessing the performance of the methods**
>
> The chosen measure to assess the performance of the tested methods throughout the thesis is the 2% exceedence value of the wave runup (R2%). This measure was chosen because (a) it is the most common parameter for forecasting wave-driven flooding and (b) it can be easily connected with the severity of coastal flooding. This parameters is widely used for engineering applications, therefore the results of this thesis are comparable with other studies.
>
> Note that along the entire thesis report when referring to the runup, the calculated runup is R2%.

3.2 Model set-up and look-up-table

Here, input parameters for physics-reduced model SFINCS (Section 3.2.1) are outlined. Moreover, look-up-table of physics-based model XB-NH+ runs (shortly XB-NH+ LUT) is described in Section 3.2.2. Examples of input parameter files for SFINCS and XB-NH+ are can be found in Appendix A.

3.2.1 SFINCS input

The highlighted model is reduced-physics model SFINCS, described in detail in Section 2.3.2. Because wave-driven processes are crucial on coral reefs, the model needs to solve them accordingly. Therefore, advection term is included in the model, i.e. the version SFINCS-SSWE based on simplified shallow water equations, is used throughout the entire research.

As already known from Section 2.3.2, two input files are needed that form the boundary conditions for forcing SFINCS: slowly-varying and rapidly-varying water level time series. Slowly varying time series (`bzs` input in SFINCS) are calculated as the sum of offshore water level and the wave setup. The wave setup is calculated with the following equation:

$$\eta_{\text{w. setup}} = \overline{\eta} - \eta_{\text{offshore}} \tag{3.1}$$

where $\overline{\eta}$ is the mean of the water level time series at the chosen boundary location obtained from XB-NH+ output and η_{offshore} is the offshore mean water level. Rapidly-varying water level time series (`bzi` input in SFINCS) are the instantaneous water level oscillations, i.e. the waves. They are obtained from the XB-NH+ output as the water level time series minus the calculated wave setup $\eta_{\text{w. setup}}$.

SFINCS is run with the input parameters that were chosen based on the experiences from the previous work by van Engelen (2016), Leijnse et al. (2021) and Athif (2020). With these parameters the stability of the model is assured. The values of the main parameters that are applied to all simulations with SFINCS are listed in Table 3.1. An example of an input file for SFINCS is included in Appendix A.1.

Table 3.1: The values of the main input parameters that are applied to all simulations with SFINCS to assure the stability and the good performance of the model, followed by the motivation behind the chosen values.

Input parameter	Value	Motivation
Model grid resolution (dx)	0.5 m	Followed by research done by Athif (2020)
Simulation time	3600 s	The model is able to resolve low frequency waves; Spin up time is surpassed
Mannings roughness coefficient	0.03 s/m$^{1/3}$	Followed by research by Athif (2020); Different values were additionally tested, with nearly the same results obtained
Stability of numerical solution θ	0.9	Followed by research by Athif (2020); If $\theta = 1.0$, numerical instabilities develop For $\theta = 0.9$, solution is stable, but HF waves are dissipated
Advection	yes	Modeling wave-driven flooding must involve advection (Leijnse et al., 2021)
Minimum flow depth limiter	0.005	To be consistent with the output of the model XB-NH+ in XB-NH+ LUT

3.2.2   XB-NH+ look-up-table

XB-NH+ look-up table (referred in text to as XB-NH+ LUT) is used for (1) obtaining boundary conditions for forcing SFINCS and (2) for validating the performance of developed method. XB-NH+ LUT serves as a short-cut for using advanced model output without running it every time. It consists of pre-run 1-dimensional simulations with XB-NH+ model for a limited number of reef profile and a limited number of offshore wave conditions.

XB-NH+ LUT is part of the development of BEWARE (version 2). It was initially developed on simplified reef profiles for development of Bayesian Estimator for Wave Attack in Reef Environments (BEWARE) by Pearson et al. (2017) to forecast wave runup on coral reefs. A second version of BEWARE is currently under the development. This version is applied to 216 reef profiles, derived from database of representative cluster profiles (RCPs), designed by Scott et al. (2020) (see Section 2.1.2 for a detailed description of RCPs). Each reef profile has three different values of the beach slope of $tan(\beta_{beach}) = 0.05, 0.1$ and 0.2.

> **Intermezzo: Overlay between BEWARE (verison 2) and this thesis project**
>
> Similarities between this thesis project and BEWARE (version 2) lie in the same database that both projects use. This is the database of the pre-run XB-NH+ simulations, in this thesis called the XB-NH+ LUT. The focus of BEWARE (version 2) is in computing the probability distribution of the wave runup for a certain location along the coast based on the offshore wave conditions. This will serve as an Early Warning Systems. Similarly, interpolation needs to be applied in order to obtain the probability distribution of runup from the desired offshore conditions. However, the interpolation is performed on the runup values obtained directly from XB-NH+ LUT. No other numerical model is applied. On the other hand, this thesis aims to develop a method that can provide the flooding maps for a chosen location. It can also provide the runup values, however that is not the main application. The interpolation needs to be applied on the optimal boundary location along the reef in order to obtain the input boundary conditions for forcing SFINCS (and not on the final runup values).

The offshore wave conditions that are currently[1] being simulated and stored in XB-NH+ LUT are:

- offshore significant wave height $H_s = \{1, 3, 5, 7, 9, 11\}$ m
- offshore peak wave period $T_p = \{6, 8, 10, 14, 18, 22\}$ s
- offshore mean water level $\eta_0 = \{0, 1, 2, 3, 4\}$ m.

Moreover, the XB-NH+ LUT has a limited number of output options, in order use less storage space. Variance, mean, maximum and minimum water level values at each computed cell are stored as a global output for 5 pre-determined time-steps. Additionally, 25 point output location are included with full water level time series. These are defined with the water depths based on the zero water level (when the offshore water level is $\eta_0 = 0$ m):

- offshore end of the profile
- beachtoe
- first depth points of $\{15, 10, 2.5, 0.5\}$ m
- last depth point of 0.5 m
- mid reef, defined as the middle between the first and the last depth point of 0.5 m
- overtopping points at heights of $\{1, 2, 3, 4, 5, 6, 7, 8, 9, 10, 11, 12, 14, 16, 18, 20\}$ m.

The split between the incoming and outgoing waves is calculated for each point output location. XB-NH+ LUT also contains swash time series which are used for computing the wave runup. 2% exceedence values of the wave runup (R%) are calculated from XB-NH+ LUT simulations. These values serve to validate the performance of developed methodology with XB-NH+ LUT – SFINCS model train. An example of an input file for XB-NH+ from the XB-NH+ LUT is included in Appendix A.2.

---

[1]This was the case in 2020 when the majority of the analysis was conducted. At the beginning of 2021, the XB-NH+ LUT has extended by implementing more offshore wave conditions to the LUT.

3.3 Design of conceptual cases

Conceptual cases are applied to the entire analysis performed during this thesis project. These are 1-dimensional hypothetical cases on which the designed methods are tested. They are designed in a way to assess the broadness of the designed methodology by selecting the variety of different reef topobathymetric profiles (Section 3.3.1) and two different offshore wave conditions (Section 3.3.2). Consequently, different hydrodynamic conditions are tested. Based on knowledge of hydrodynamic processes occurring on coral reef platforms (Section 2.2), they can result in different scenarios that can potentially lead to coastal flooding.
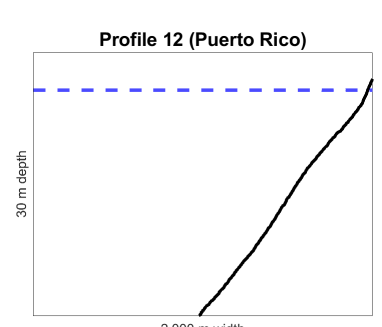
3.3.1 Topobathymetric cross-shore profiles

Six topobathymetric 1-dimensional cross-shore reef profiles are chosen for the conceptual analysis performed. The selected reef profiles are depicted in Table 3.2. Distinctive bathymetric characteristics and hypotheses of wave processes over the reef profiles are included in the table as well. Hypotheses are derived from the theoretical knowledge of hydrodynamic processes across the reef platforms, described in Section 2.2. The profiles, derived from the datasets, do not contain the topographic part, therefore the beach slope of $tan(\beta_{beach}) = 0.1$ was added. The slope is *semi-infinite*, i.e. it is very long and consequently runup does not reach the end of the domain.
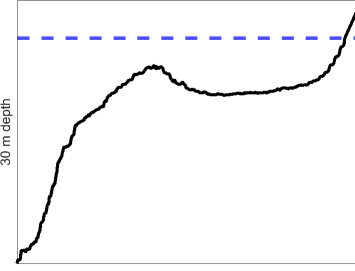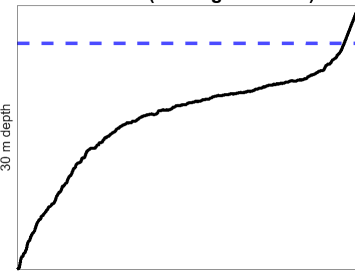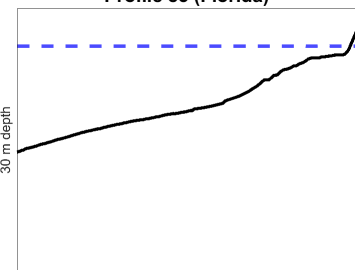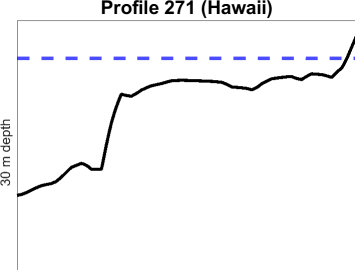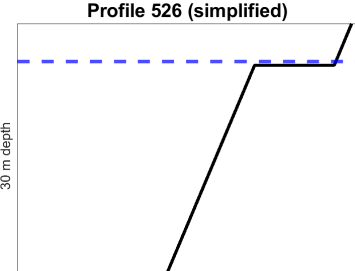
Five bathymetric reef profiles (Profiles 12, 24, 38, 83 and 271) are taken from 49 representative cluster profiles (RCPs), designed by Scott et al. (2020) and described in detail in Section 2.1.2. The selection is made based on theoretical knowledge on wave generation and transformation over the reefs. The aim is to select the profiles with varying hydrodynamic characteristics. That was achieved by selecting profiles with different fore reef and reef flat characteristics. With this selection the aim is to test if the method is valid for different coastal types and hydrodynamic regimes. The reef profiles come from five different locations in Puerto Rico (2x), US Virgin Islands, Florida and Hawaii.

Additionally, one bathymetric reef profile (Profile 526) was chosen from the set of idealized reef profiles from the research of Pearson et al. (2017). The aim of comparing this profile with the other profiles is to see whether idealized profiles deviate considerably from realistic profiles. The performance of SFINCS on idealized and observed reef profiles is assessed and the accuracy of interpolated parameters at the boundary for idealized and observed reef profiles is compared.

Table 3.2: Selected reef profiles, their distinctive characteristics and the hypotheses of the wave evolution across the reefs (derived from the theoretical knowledge of the reef hydrodynamics, included in Section 2.2). Five reef profiles (Profiles 12, 24, 38, 83 and 271) are measured 1D transects, selected from 49 representative cluster profiles (RCPs), designed by Scott et al. (2020) and described in detail in Section 2.1.2. One simplified reef profile (Profile 526) is selected from the set of idealized reef profiles from the research of Pearson et al. (2017).

Profile	Distinctive characteristics	Hypothesis
Profile 12 (Puerto Rico); 30 m depth; 2 000 m width	Steep profile, no reef flat; similar to sandy coastline	Energy dissipation mainly due to wave breaking; predicted high runup as wave breaking occurs in a narrow area and no reef flat is present for strong frictional dissipation

(The table continues on the next page.)

Profile	Distinctive characteristics	Hypothesis
Profile 24 (Puerto Rico)	Steep reef front, distinctive reef crest, with deeper reef flat behind the reef crest, followed by steeper beach slope	During intense offshore wave conditions a majority of wave energy dissipation is expected to occur at reef crest; reef flat can promote IG wave generation; frictional dissipation expected on the reef flat
Profile 38 (US Virgin Islands)	Steep reef front, reef flat slope, steep beach slope	Breaking is expected to continue towards the shore because of reef flat slope, which results in gradual reduction of short wave energy and therefore lower setup
Profile 83 (Florida)	Long reef profile with mild slope; narrow and shallow reef flat	Shoaling waves are expected to be dominant due to mild slope; breaking is expected to initiate far from the shore and continue towards the shore, which results in gradual reduction of short wave energy and therefore lower setup; strong frictional dissipation expected near the shore
Profile 271 (Hawaii)	Relatively complex bathymetry with deeper reef crest offshore (not seen in this figure), followed by the shallower reef crest nearshore and a wide reef flat	Wave dissipation expected due to breaking close to the reef crest, a majority of frictional dissipation expected to occur on the shallow reef flat, where IG wave generation is possible; under certain circumstances reef flat can promote resonant motions
Profile 526 (simplified)	The simplified reef profile with relatively long reef flat (depth of 0.5 m); simplified version of Profile 271	A majority of wave energy dissipation due to wave breaking close to reef crest (moving breakpoint expected depending on the offshore wave conditions), strong frictional dissipation expected on reef flat; under certain circumstances reef flat can promote resonant motions

3.3.2 Offshore wave scenarios and nearest XB-NH+ LUT sea-states for the interpolation method

Two characteristic offshore wave scenarios are considered for testing the proposed method on conceptual cases. These two scenarios are considered in order to represent two distinguishing wave climates that can result in coastal flooding. Ford et al. (2018) analyzed the hydrodynamic data of the Majuro Atoll (The Republic of the Marshall Islands) and found several driving mechanisms that resulted in flooding of Majuro Atoll in the past. Two more pronounced conditions are considered in conceptual cases: (a) far-field swell events and (b) tropical storms and typhoons. Inspired by Bosserelle et al. (2015), the following values of the offshore wave conditions for these two target scenarios are considered:

- swell: significant offshore wave height H_s = 1.6 m, offshore peak wave period T_p = 9.7 s, offshore mean water level η_0 = 0.7 m;
- stormy conditions: significant offshore wave height H_s = 3.5 m, offshore peak wave period T_p = 16 s, offshore mean water level η_0 = 0.7 m.

The gentle swell and *the stormy conditions* are the target scenarios. XB-NH+ LUT does not include the values of their offshore wave and water level conditions. For that reason, the interpolation of the nearest simulations from the XB-NH+ LUT needs to be performed. Each scenario corresponds to 8 neighbouring simulations from the XB-NH+ LUT. The neighbouring conditions are defined as the simulations that contain the closest higher and lower values of H_s, T_p and η_0 as the target scenario (thus 2x H_s, 2x T_p and 2x η_0 result in 8 unique combinations of these parameters). The scenarios and the corresponding offshore wave conditions are listed in Table 3.3. These combinations are currently (July 2020) available in the XB-NH+ LUT. Note that the last column represents the simulation numbers (1-4 swell, 5-8 storm), as it is enumerated in the report. The enumerating does not account for the offshore water level, thus this information is always stated separately throughout the report.

The two target scenarios together results in 16 unique simulations from the XB-NH+. In the sensitivity analysis (Section 3.4 and Chapter 4), all 16 conditions are analysed for each reef profile separately. In the analysis of interpolation methods only the two scenarios (gentle swell and stormy conditions) are applied, but the interpolation is performed over the 8 nearest offshore wave conditions for each scenario.

Table 3.3: Two offshore wave scenarios are chosen (gentle swell and stormy conditions). The neighbouring simulations from XB-NH+ LUT are listed in columns 3-5 (significant wave height H_s, peak wave period T_p and offshore water level η_0). The last column represents the simulation number, as it is referred in the report (1-4 swell, 5-8 storm).

Target scenario	Offshore conditions	H_s (LUT) [m]	T_p (LUT) [s]	η_0 (LUT) [m]	Sim. number
Swell	Hs = 1.6 m Tp = 9.7 s η_0 = 0.7 m	1	8	0	**1** with $\eta_0 = 0$ m
		1	10	0	**2** with $\eta_0 = 0$ m
		3	8	0	**3** with $\eta_0 = 0$ m
		3	10	0	**4** with $\eta_0 = 0$ m
		1	8	1	**1** with $\eta_0 = 1$ m
		1	10	1	**2** with $\eta_0 = 1$ m
		3	8	1	**3** with $\eta_0 = 1$ m
		3	10	1	**4** with $\eta_0 = 1$ m
Storm	Hs = 3.5 m Tp = 16 s η_0 = 0.7 m	3	14	0	**5** with $\eta_0 = 0$ m
		3	18	0	**6** with $\eta_0 = 0$ m
		5	14	0	**7** with $\eta_0 = 0$ m
		5	18	0	**8** with $\eta_0 = 0$ m
		3	14	1	**5** with $\eta_0 = 1$ m
		3	18	1	**6** with $\eta_0 = 1$ m
		5	14	1	**7** with $\eta_0 = 1$ m
		5	18	1	**8** with $\eta_0 = 1$ m

3.4   Sensitivity analysis

Sensitivity analysis is performed to understand the performance of the reduced-physics model SFINCS when the model is forced with the parameterized boundary conditions. Based on results from research by Athif (2020), the wave spectrum at the boundary will be parameterized with the TMA+GAUSS function. The consequences of generating random water level time series from simplified wave spectra at the boundary will be assessed. Three boundary type methods (following: BT methods) are compared, as further described in Section 3.4.1.

Another intention of the sensitivity analysis is to find the optimal boundary location for forcing SFINCS. The optimal boundary location is the location with the lowest error in the predicted runup. For that purpose five different boundary locations are tested, as described further in Section 3.4.2.

3.4.1   Boundary type methods

Parameterizating boundary conditions for forcing SFINCS is essential because interpolation of boundary conditions cannot be directly performed on water level time series. A convenient method to interpolate conditions at the boundary consists of a low number of discrete values that describe conditions at the boundary. In this thesis, parameterized wave spectra will be used to describe conditions at the boundary.

Based on results from the research by Athif (2020), parameterizing wave spectrum with three parameters with the TMA+GAUSS function works with good accuracy. In the sensitivity analysis, parameterization of wave spectra with the TMA+GAUSS function is assessed. Generating new water level time series from parameterized wave spectra is implemented with a random phase, therefore the wave phase information is lacking. The consequences of random-phased water level time series for forcing SFINCS are assessed. With that in mind, three different types of methods to generate input time series at the boundary are designed, called the *boundary type methods* (following: BT methods). All three BT methods generate water level time series that are used as a `bzi` input to SFINCS (rapidly-varying water level time series). Slowly-varying water level time series (`bzs` input) consist of discrete values of wave setup, therefore parameterization for this case is not needed.

Figure 3.1 schematically illustrates designed BT methods. All three methods use water level time series output from XB-NH+ LUT at the tested boundary locations. The difference between BT methods lies in the method to obtain water level time series that are then used as an input for SFINCS. Following is the detailed explanation of each BT method.

BT method 1: direct method

BT method 1 is the most straightforward method. The water level time series are directly obtained from XB-NH+ LUT. Because of the nature of SFINCS input (Section 3.2.1), the water level time series need to be split into two input files for SFINCS:

  – slowly-varying time series, calculated as the mean of the water level time series; and
  – rapidly-varying time series, calculated as the water level time series subtracted by the mean water level time series.

Since no other processes are involved in this method, the wave characteristics (heights, periods and nonlinear wave shapes) from the original XB-NH+ LUT are not affected. Consequently, no information at the boundary is lost with this method. The method therefore serves for comparison with the other two methods where the boundary conditions are altered. With this comparison the consequences of simplified boundary conditions due to parameterization and lack of phase information can be identified. Additionally, this method serves to assess the performance of SFINCS on coral reef-lined coasts and the correct evolution of waves across the reef. Note that this is not the target method, as the raw water level time series cannot be used for interpolation of the boundary conditions.
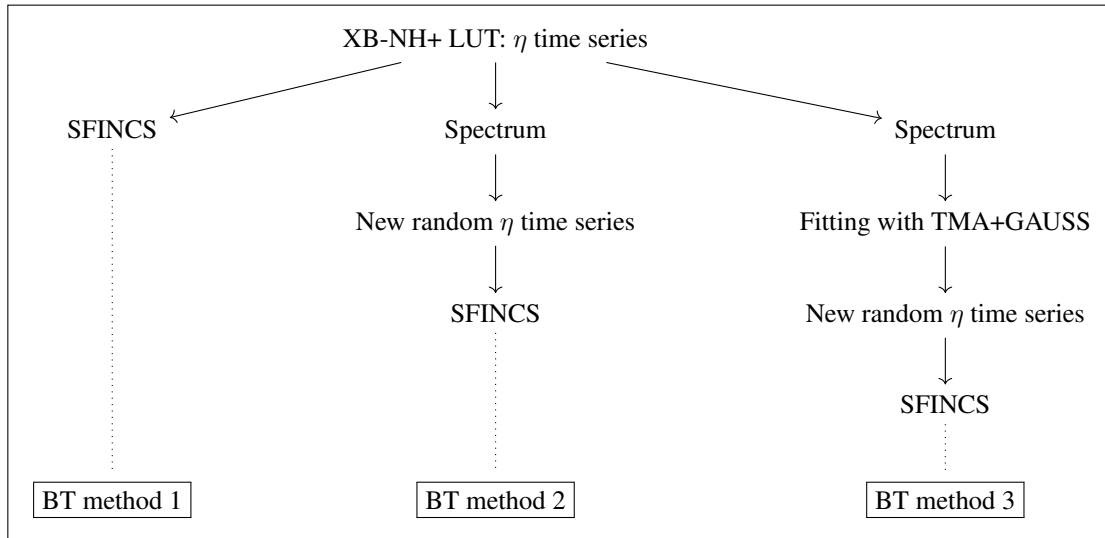
Figure 3.1: Schematic illustration of boundary type methods (BT methods) that are compared in sensitivity analysis (Chapter 4). BT method 3 (parameterized method) is the target method as it can be used for interpolation of boundary conditions.

BT method 2: spectral method

In BT method 2, spectral analysis is applied in order to generate new random water level time series which are used as an input for SFINCS. The first step in the method is the same as in BT method 1: water level time series are split into the slowly-varying time series and rapidly-varying time series. Slowly-varying time series (i.e. mean water level and setup or setdown) are directly used as `bzs` input for SFINCS. Rapidly-varying time series are further processed in the following order:

1. Fast Fourier transform is performed on time series and the associated wave spectrum is obtained;

2. random water level time series are generated from the obtained spectrum, which are then used as `bzi` input for SFINCS.

   In this method new water level time series have the correct amount of wave energy, but are lacking the wave phase information. Therefore, this method serves to evaluate the effect the lack of phase information has on wave evolution with SFINCS and the resulting runup. Note that this method is still not the target method for further analysis on interpolation of boundary conditions. The full spectrum obtained with Fast Fourier transform is not convenient for interpolation because it does not consist of a small number of discrete values.

BT method 3: parameterized spectral method

BT method 3 involves parameterization of spectrum in order to generate new water level time series that are used as an input for SFINCS. First step in the method is again the same as in BT method 1 and 2: water level time series are split into the slowly-varying time series and rapidly-varying time series. Slowly-varying time series (i.e. mean water level and setup or setdown) are directly used as `bzs` input for SFINCS. Rapidly-varying time series are further processed in the following order:

1. Fast Fourier transform is performed on time series and the associated wave spectrum is obtained;

2. parameterizing spectrum with TMA+GAUSS function is performed, as proposed by Athif (2020);

3. the random time series are generated from the obtained fitted spectrum and they are used as `bzi` input for SFINCS.

   Parameterizing spectrum with the TMA+GAUSS function consists of splitting of spectrum between LF and HF part of the spectrum. Cut-off frequency between IG and HF waves is 0.04 Hz, based on a research by Quataert et al. (2015). TMA+GAUSS function consists of Gaussian fitted curve for LF part of the spectrum and TMA fitted curve for HF part of the spectrum. An example of parameterized spectrum with TMA+GAUSS

function is depicted in Figure 3.2.

Gaussian shape of spectrum is defined with the variance of the LF part of the spectrum. The frequency peak is pre-defined at the frequency of 0.02 Hz (the middle of the LF part of the spectrum). Shape of the spectrum is calculated with the Gaussian function as:

$$E_{\text{GAUSS}} = a \exp\left(-\frac{(f-b)^2}{2c^2}\right) \tag{3.2}$$

where a is the scaled variance of the LF part of the spectrum, f are the frequency components of LF part of the spectrum, b is the location of the peak (fixed at 0.02 Hz) and c is the width of the Gaussian curve (0.04 Hz based on cut-off frequency between LF and HF part of the spectrum) (Athif, 2020).

TMA shape of spectrum is defined with two parameters from the original spectrum: variance of the HF part and the peak period of the HF part of the spectrum. The shape of the spectrum is the TMA spectrum. It is a wave spectrum shape that can be applied to arbitrary water depths (described in Section 2.2.2).

BT method 3 is the target method for the further analysis. With TMA+GAUSS function, the wave spectrum at any given location can be simplified with only three discrete parameters: variance of LF part of the spectrum, variance of HF part of the spectrum and frequency peak of HF part of the spectrum. With the sensitivity analysis the performance of simplified wave spectrum is assessed. At the same time, the fitting of spectra is examined.
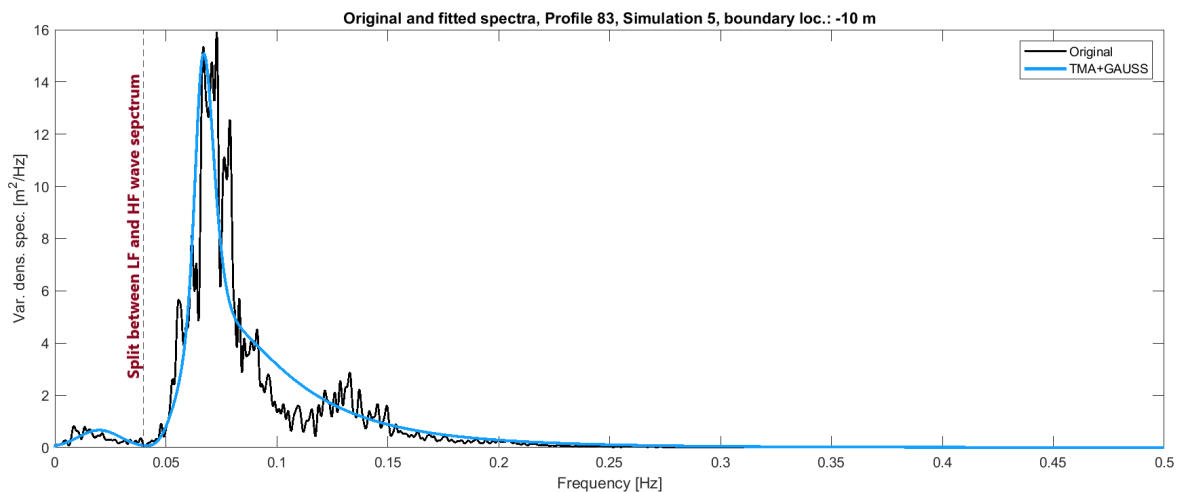
Figure 3.2: Parameterizing spectrum with the TMA+GAUSS function, as applied in BT method 3. Example is applied on reef Profile 83 (Table 3.2) with simulation 5 (H_s = 3 m, T_p = 14 s, η_0 = 0 m; Table 3.3), with the boundary location at a depth of -10 m. Black line depicts original wave spectrum and blue line depicted parameterized wave spectrum. Dashed vertical line at frequency of 0.04 Hz shows frequency cut-off between LF and HF part of the spectrum.

3.4.2   Tested boundary locations

Five different boundary locations are chosen from 26 available model outputs from XB-NH+ LUT (all options are listed in Section 3.2.2). Boundary locations are defined with the water depth with respect to offshore water level of 0 m. Therefore, the considered boundary locations all have different cross-shore distance from the coast and different lengths of the SFINCS domain.

The chosen boundary locations are at depths of: -10 m, -5 m, -2.5 m, -0.5 m and at the beachtoe (where still water is 0 m with regards to offshore water level of 0 m). An example of boundary locations for Profile 83 is depicted in Figure 3.3. These five boundary locations were chosen because they are the five boundary locations from the XB-NH+ LUT options that are the closest to the coastline (while still being at sea). The closest locations were chosen because (a) SFINCS is based on simplified shallow water equations and thus it should be implemented to shallow waters, and (b) forcing SFINCS close to the shore results in less computational grid cells.

Computational efficiency increases with decreasing distance from the shore. At the same time, accuracy is being tested.
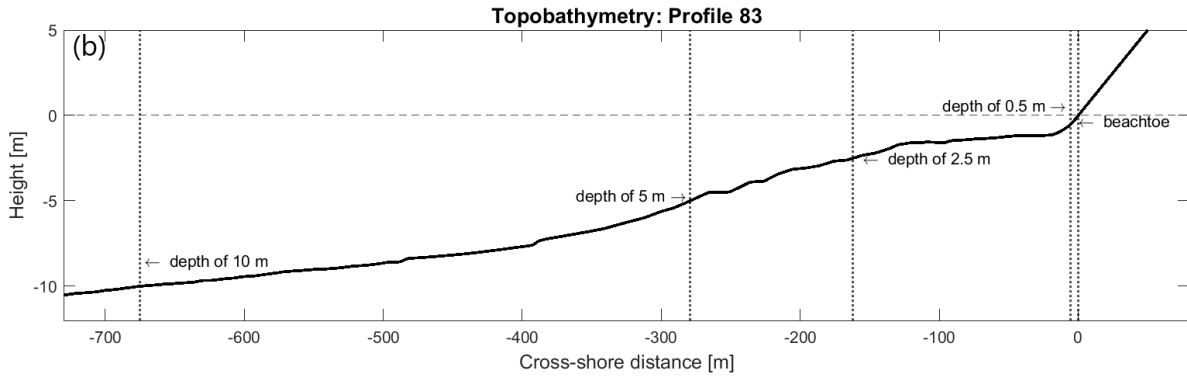
Figure 3.3: Five chosen boundary locations marked on example Profile 83 that are tested in the sensitivity analysis (Chapter 4). Boundary locations are defined with the water depth with respect to offshore water level of 0 m.

3.5 Analysis of interpolation methods

Analysis of interpolation methods is performed after the sensitivity analysis. Based on the sensitivity analysis, boundary location(s) for forcing SFINCS are determined and the performance of parameterized wave spectrum with the TMA+GAUSS function is understood. These two aspects determine the flow of the following analysis on interpolating the boundary conditions.

The aim is to find a method that will be applicable to arbitrary offshore wave conditions. Because XB-NH+ LUT consists of a limited number of offshore wave and water level scenarios, its output cannot be directly used for forcing SFINCS. A solution is to interpolate the parameters that describe the wave spectrum and the wave setup at the boundary. The wave parameters describing the TMA+GAUSS function and the wave setup are interpolated over the three offshore parameters X_i, also known as multivariate vectors:

$$X_i = \{H_{s,i}, T_{p,i}, \eta_{0,i}\}; \quad i = 1, \ldots, N \tag{3.3}$$

where N is the number of combinations. In our case N equals 8, since there are 8 neighbouring simulations for each target scenario, found in XB-NH+ LUT. They are a combination of 2 neighbouring values of each offshore parameter: 2X significant wave height, 2X peak wave period and 2X offshore water level (see Table 3.3 for a full list of combinations).

Interpolation over the offshore multivariate vectors provides weights of each neighbouring simulation from XB-NH+ LUT. The weights are determined based on how close are the values of multivariate vectors to the chosen (arbitrary) offshore wave conditions. These weights are then applied to wave parameters describing the TMA+GAUSS function at the chosen location along the reef (i.e. the boundary location). The wave spectral parameters that serve as an estimate of the real wave spectral parameters are calculated based on these weights. The question is: *How can the weights be determined to provide the most accurate estimation of wave spectral parameters, while being computationally efficient?*

Sensitivity testing of different approaches is performed. First, the simplest two methods are tested: the mean and the median of the 8 neighbouring simulations. No weighting of the multivariate vectors is applied, i.e. all 8 neighbors have the same amount of influence on the final calculated boundary conditions. The aim of this step is to compare it to the more advanced interpolation methods and assess how important is the weighting between the neighbouring simulations. Next, three different interpolations methods are tested: linear interpolation, nearest neighbour (NN) interpolation and inverse distance weighting (IDW) interpolation. These are described in detail in Section 3.5.2. Interpolation methods are applied with two different distance metrics, i.e. two different definitions of the distances between the multivariate vectors. These are Euclidean distance and geometric mean distance. They are described in detail in Section 3.5.1. All tested methods with chosen combination of interpolation

methods and distance metrics are listed in Section 3.5.3. Note that these methods are all computationally efficient as opposed to more advanced methods such as kriging. In Chapter 5 (results) it is clear that these methods provide satisfactory results, therefore more advanced methods are not applied in this thesis.

The accuracy of the interpolation method is determined with (a) the ability to accurately predict the TMA+GAUSS spectral parameters and wave setup at the boundary (Section 5.1 and Section 5.2) and (b) the ability to accurately simulate wave runup with the interpolated boundary conditions (Section 5.3).

3.5.1   Definition of distance metrics

Distance metrics determine the distances between the target (arbitrary) and the available (from XB-NH+ LUT) offshore wave and water level parameters. They define the weight of the neighbouring simulations that are applied in the algorithms of interpolation methods (Section 3.5.2).

The first step is to normalize the vector components so they can be evenly weighted when the distances are calculated. This step has to be taken because the interpolation is applied through three different offshore parameters (H_s, T_p and η_0) with different mean values and different units (seconds and meters). The scalar variables are normalized by scaling the variable values between 0 and 1 with a simple linear transformation between the minimum and maximum values of multivariate vectors X_i.

Two distance metrics are chosen for the analysis. Euclidean distance metrics are chosen because they are straightforward and easy to interpret. Geometric mean distance metrics are chosen because they are commonly applicable to cases when interpolation is performed over multivariate vectors with different mean values and units.[2]

Euclidean distance

The Euclidean distance is the length of a line segment between the two points in Euclidean space. It is defined with the following equation:

$$d_{\text{Eucl}}(X, Y) = \sqrt{\sum_{j=1}^{M} (Y_j - X_j)^2} \tag{3.4}$$

where Y_j are the values of the normalized target offshore wave conditions, X_j are the the normalized nearest neighbours and $j = 1, ..., M$ are the dimensions of the multivariate vectors Y_j and X_j. In our case M=3, because we have three dimensions: offshore wave period, wave height and water level. The distance has to be calculated for each neighbour separately, as each distance serves as a weight for each neighbouring simulation from XB-NH+ LUT.

Geometric mean distance

Geometric mean indicates the typical value of a set of numbers by using the product of their values. The geometric mean distance is defined as:

$$d_{\text{GM}}(X, Y) = \left[\prod_{j=1}^{M} (1 - |Y_j - X_j|) \right]^{\frac{1}{M}} \tag{3.5}$$

with the parameters of Y_j, X_j, j and M which are the same as in Euclidean distances.

3.5.2   Interpolation methods

Interpolation methods connect the offshore parameters (and thus the weights) with the TMA+GAUSS spectral parameters and the wave setup at the chosen boundary location for forcing SFINCS along the reef. The final outcomes are the predicted TMA+GAUSS spectral parameters and the wave setup at that location that are as close

---

[2]Geometric mean distance metrics are also currently applied to the BEWARE (version 2) system.

to the exact values as possible. Errors associated with the predicted parameters compared to the correct parameters determine the accuracy of the interpolation method (results are included in Section 5.1 and Section 5.2).

Three interpolation methods are tested: linear interpolation, nearest neighbour (NN) interpolation and inverse distance weighting (IDW) interpolation. A detailed description of each method is included below. Distance metrics are applied to all three tested interpolation methods. Chosen combination of interpolation methods and distance metrics is listed in Section 3.5.3.

Nearest Neighbour interpolation

With the Nearest Neighbour (NN) interpolation, the TMA+GAUSS parameters and the wave setup are selected as the values that correspond to the nearest simulation from XB-NH+ LUT. The nearest neighbour is determined as the XB-NH+ LUT simulation with the smallest value of distance metrics. In the current analysis only Euclidean distance is considered.

Linear interpolation

With the linear interpolation method, the distances (both Euclidean and geometric mean distances) are applied as the linear weights in order to derive the interpolated TMA+GAUSS spectral parameters and wave setup. The mathematical formula that describes the method is:

$$\hat{z}(X_0) = \begin{cases} z(X_0) & \text{if } X_0 \in \{x_1, \ldots, x_N\} \\ \frac{\sum_{i=1}^{n} w_i \cdot z(X_i)}{\left(\sum_{i=1}^{N} w_i\right)} & \text{else} \end{cases} \tag{3.6}$$

where X_0 are target offshore parameters, $\hat{z}(X_0)$ the target TMA+GAUSS parameter, X_i the nearest offshore parameters and $w_i = d(X_0, X_i)$ the interpolation weights, defined as the distances between the multivariate vectors.

Inverse Distance Weighting interpolation

The inverse distance weighting (IDW) interpolation method is applied with the same equation as in linear interpolation (Equation (3.6)). The difference lies in definition of the weight w_i. In IDW interpolation method the weight is defined as:

$$w_i = d(X_0, X_i)^p \tag{3.7}$$

where $d(X_0, X_i)$ is the distance metrics and $p < 0$ is the power. The power p determines how much weight is put into the closer neighbours. The higher the power indicates the higher the influence of the closest neighbours is to the interpolated values.

Different values of power p will be applied, since they are an important factor in the methodology. The following values are chosen: $p = [-1, -2, -3]$ for Euclidean distance metrics and $p = -2$ for geometric mean distance metrics.

3.5.3   An overview of tested methods

9 different cases are designed for sensitivity test of interpolation methods. These are listed in Table 3.4. Two control cases are performed to compare the interpolation to the cases without interpolation:

- full XB-NH+ case: for each scenario and each profile a full XB-NH+ simulation is performed. This case serves to compare the interpolated spectral parameters and wave setup at the considered boundary locations to the correct values and to calculate the errors of predicted runup.
- IM-0 case: the XB-NH+ LUT – SFINCS model train is applied with parameterized boundary conditions (BT method 3 in Section 3.4.1) with the correct values of TMA+GAUSS spectral parameters and correct values of wave setup that are derived from full XB-NH+ case. This case serves for comparison with cases with interpolation to assess the additional errors that are introduced by the interpolation process.

Based on the results of this sensitivity test, an optimal method for interpolation at the boundary is selected.

Table 3.4: Designed cases for testing the interpolation methods. Two control cases are performed to compare the interpolation to the cases without interpolation (full XB-NH+ and IM-0). BT method 3 is the parameterized spectral method for obtaining the boundary conditions for forcing SFINCS (described in Section 3.4.1).

Name	Interpolation method	Distance	BT Method
full XB-NH+	*only XB-NH+ used, serves as 'reality'*		
IM-0	*no interpolation, true boundary conditions*		3
IM-1	mean	-	3
IM-2	median	-	3
IM-3	Nearest Neighbour (NN)	Euclidean	3
IM-4	Linear	Euclidean	3
IM-5	Inverse Distance Weighting, p = -1 (IDW)	Euclidean	3
IM-6	Inverse Distance Weighting , p = -2 (IDW)	Euclidean	3
IM-7	Inverse Distance Weighting, p = -3 (IDW)	Euclidean	3
IM-8	Linear	geometric mean	3
IM-9	Inverse Distance Weighting, p = -2 (IDW)	geometric mean	3

4

Sensitivity of parameterization and the forcing location

A sensitivity analysis is performed to find an accurate method that can combine the look up table built with advanced model (XB-NH+ LUT) with reduced-physics model (SFINCS). XB-NH+ LUT is used to provide the wave and water level characteristics at a certain location along the 1D reef profile, which are then used for generating boundary conditions for forcing SFINCS. SFINCS is used to simulate waves till shore. Consequences of using the simplified parameterized spectra at the boundary and generating new random phased water level time series for forcing SFINCS will be addressed in this chapter. Interpolation of the boundary conditions from the LUT is discussed extensively in Chapter 5.

A deeper analysis of water level time series is performed in order to understand (a) how the application of different boundary type methods (BT methods) influences the input boundary conditions for SFINCS (Section 4.1); and (b) how the important hydrodynamic processes are captured with SFINCS across the reef depending on the input boundary conditions (Section 4.2). The most appropriate boundary locations and the associated errors of runup are described in Section 4.3. Finally, computational time of the tested methods is analysed in Section 4.4.

4.1   Generating boundary conditions for SFINCS

Boundary conditions for forcing SFINCS are generated from the information obtained with the use of advanced model XB-NH+. For the purpose of sensitivity analysis, the output from XB-NH+ model, as it is stored in XB-NH+ LUT database, is used. No interpolation of boundary conditions is applied yet (this analysis is shown in Chapter 5). Three methods for generating boundary conditions for forcing SFINCS with instantaneous time series (`bzi` input in SFINCS) are tested, as described in Section 3.4.1. These are:

- BT method 1 (direct method): using the original water level time series;
- BT method 2 (spectral method): computing wave spectrum from the original water level time series and generating new random water level time series from the spectrum;
- BT method 3 (parameterized spectral method): computing wave spectrum from the original water level time series, parameterizing the spectrum with the TMA+GAUSS function with three parameters, and generating new random water level time series from the parameterized spectrum.

The analysis is performed on one test case, described in detail in Section 4.1.1. The water level time series before and after applying the BT methods are compared in Section 4.1.2, in order to understand how the application of different BT methods influences the input boundary conditions for forcing SFINCS. Moreover, the original and the parameterized wave spectra are compared for the considered boundary locations.

4.1.1   Characteristics of the test case

Analysis is performed on one test case on Profile 83, Simulation 5. The chosen reef profile is a long cross-sectional profile with mild slope ($\tan \beta \approx 0.01$) and a narrow (≈ 110 m) and shallow (between 1 m and 1.5 m deep) reef flat. A topobathymetric profile together with considered boundary locations is included in Figure 4.1 (b). Simulation 5 has a significant wave height Hs = 3 m, peak wave period Tp = 14 s and an offshore water level $\eta_0 = 0$ m. The resulting runup, calculated with the reference model XB-NH+, is 1.43 m. This reef profile is chosen because it represents a more general shape of reef profile that is often found along the coasts of low-lying islands. Moreover, the stormy offshore wave scenario was chosen because these conditions are more relevant for modeling of coastal inundation.

Relative errors of runup for the test case when SFINCS is forced at 5 different boundary locations are depicted in Figure 4.1 for each BT method. SFINCS performed with good accuracy regardless of applied BT method with relative errors of runup up to 20%, but mainly lower. The error of the estimated runup for the boundary location that performed with the highest accuracy is between 1-4 % compared to the simulation performed fully with XB-NH+ model.
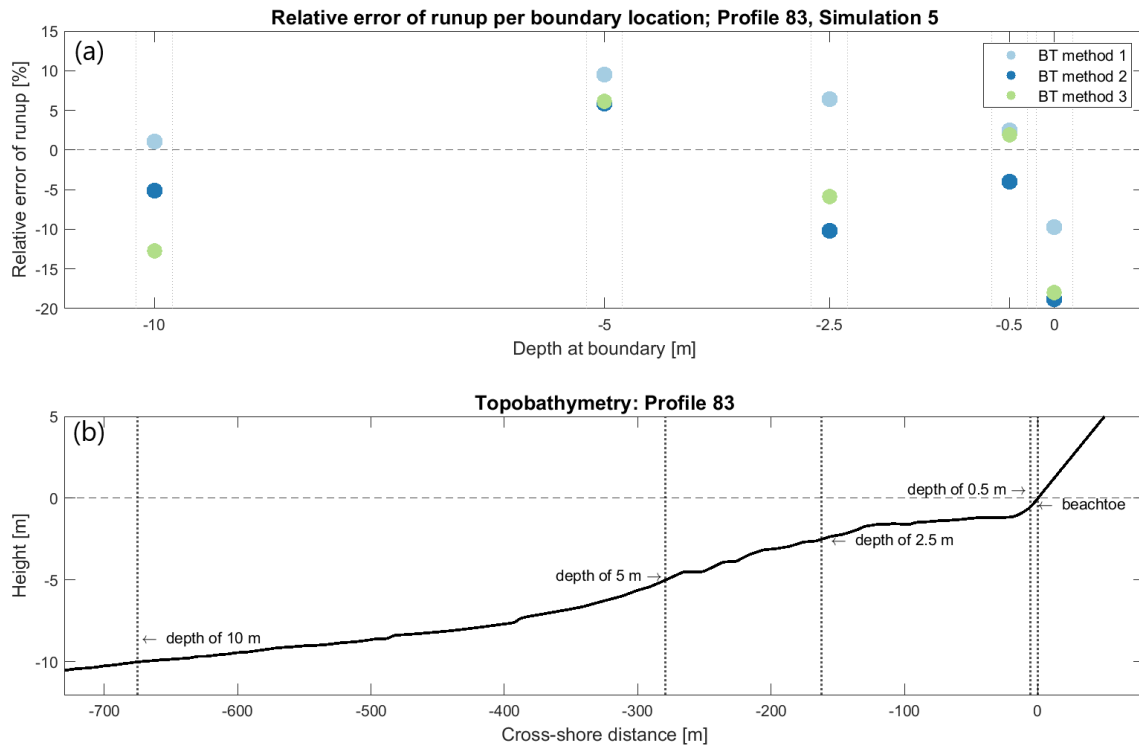
Figure 4.1: (a) Relative errors of runup per boundary location for the test case for Profile 38, Simulation 5 (significant wave height Hs = 3 m, peak wave period Tp = 14 s and an offshore water level $\eta_0 = 0$ m). Three different BT methods are compared, each depicted with different colour. The columns represent depths at the offshore boundary location for forcing SFINCS. (b) Topobathymetry of Profile 83 with marked boundary locations are at depths of -10 m, -5 m, -2.5 m, -0.5 m and at the beachtoe (0 m depth).

For the test case the most direct nesting method, BT method 1, performs with the highest accuracy when SFINCS is forced at the boundary at a depth of -10 m. However, it performs with high accuracy also for the boundary location at a depth of -0.5 m. Methods that involve additional steps for generating the boundary conditions, BT methods 2 and 3, both preferred boundary location at a depth of -0.5 m. No trend is observed between the BT method applied, the relative errors of runup and the boundary location, by only observing the test case. Therefore, to solidify the results further, the relative errors of runup for all 8 simulations for Profile 83 are compared. Results are depicted in Figure 4.2.
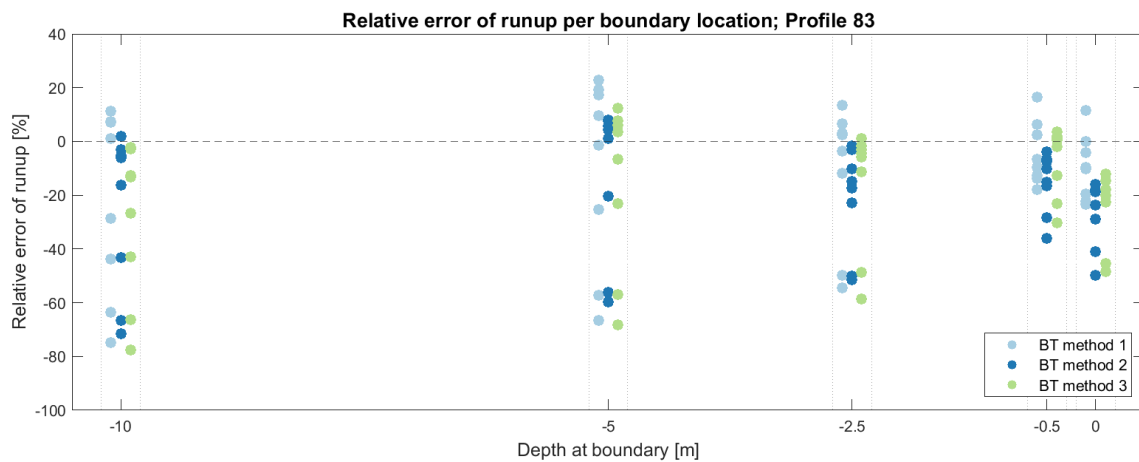
Figure 4.2: Relative errors of runup per boundary location for reef Profile 38, for all 8 simulations (see Table 3.3 for their offshore wave conditions) and offshore water level $\eta_0 = 0$ m. Three different BT methods (Section 3.4.1) are compared, each depicted with different colour in separate column. The columns represent depths at the offshore boundary location for forcing SFINCS.

The range between the relative errors of runup decreases with decreasing distance of the forcing boundary location from the shore. Large negative errors of runup (between 50% and 80%) for the boundary locations at depths of -10 m, -5 m an -2.5 m are observed for all three BT methods. These high errors are linked to Simulations 1 and 2: swell with the most gentle conditions. Observed accuracy of runup prediction increases with increasing intensity of offshore wave conditions.

The accuracy of predicted runup also increases with decreasing distance of the forcing boundary location from the shore from the boundary location at a depth of -10 m till a depth of -0.5 m. The results are summarized in Table 4.1, where relative errors of runup are averaged over the 8 simulations for each boundary location and each BT method separately. The aim in the next sections is to find the possible reasons for this behaviour by comparing the influence of BT methods at the boundaries (Section 4.1.2) and comparing the evolution of waves across the shore (Section 4.2). Three boundary locations at depths of -10 m, -2.5 m and -0.5 m are considered for further analysis.

Table 4.1: Averaged relative errors of runup (R2%) depending on the applied BT method (rows, see Section 3.4.1) and on the offshore boundary location for forcing SFINCS (columns, see Figure 4.1 (b) for the marked locations on the topobathymetric profile) for Profile 83 for all 8 simulations together (see Table 3.3 for the list of simulations with offshore water level $\eta_0 = 0$ m).

Depth at boundary	Averaged relative error of runup [%] (absolute values)				
	-10 m	**-5 m**	**-2.5 m**	**-0.5 m**	**beachtoe**
BT method 1	29.7	27.5	18.1	10.7	12.6
BT method 2	26.7	20.4	21.4	15.5	26.8
BT method 3	30.6	23.0	16.8	9.4	24.9

4.1.2 Comparison of BT methods at the boundary

At the offshore boundary location for forcing SFINCS, the three BT methods result in different boundary conditions which are used as an input for forcing SFINCS. With BT method 3 (parameterized spectral method), the TMA+GAUSS function is applied to parameterize wave spectrum with three spectral parameters (see Section 3.4.1). To understand the consequences of applying the TMA+GAUSS function, the parameterization of the spectrum is first analyzed. Next, the water level time series, generated from the parameterized spectrum, are compared with the water level time series generated with BT methods 1 and 2.

Parameterization of spectrum with TMA+GAUSS function

Spectral analysis is performed on the five studied boundary locations and the results for the test case are depicted in Figure 4.3. The black line on the figure represents spectra from the original XB-NH+ LUT time series, which are used to generate new water level times series for forcing SFINCS with BT method 2. The blue line represents spectra parameterized with the TMA+GAUSS function, which are used to generate new water level times series for forcing SFINCS with BT method 3. Clear evolution of waves over the reef is observed. High levels of HF wave energy are present at the larger depths, which are dissipated across the shore and transformed to lower frequencies. Closer to the shore LF wave energy dominates. An order of magnitude larger variance density spectrum is observed at a depth of -10 m compared to shallower depths, meaning that closer to the shore a majority of wave energy is dissipated. The evolution of wave spectra across the reef is in line with the theoretical predictions, described in gray text boxes in Section 2.2.

Due to characteristics of the TMA+GAUSS function, the parameterized spectra at depths of -10 m and -5 m ignore the second peak of the HF part of the spectrum at the frequency of 0.13 Hz while overestimating the amount of wave energy at the primary frequency peak. This difference is even larger at a depth of -2.5 m where relatively large amounts of energy are stored at frequencies between 0.13 Hz and 0.40 Hz due to wave breaking and transformation of wave energy partially to higher frequencies. As a consequence, a large difference between the energy stored at the frequency peak of HF wave energy of original and parameterized spectra is observed.

Peak infragravity wave frequency is not estimated correctly close to the shore at depths of -0.5 m and at the beachtoe because the TMA+GAUSS function assumes that the peak infragravity wave frequency is at 0.02 Hz. This value is pre-defined and it assumes that there is only one frequency peak at the LF part of the spectrum, associated with the IG wave energy. However, very-low frequency waves are present on the reef platforms as well, especially close to the shore. They are ignored with parameterization and their energy is transformed to IG wave energy. Consequently, the original and the parameterized wave spectra deviate from each other while the total amount of energy is roughly the same for both spectra.
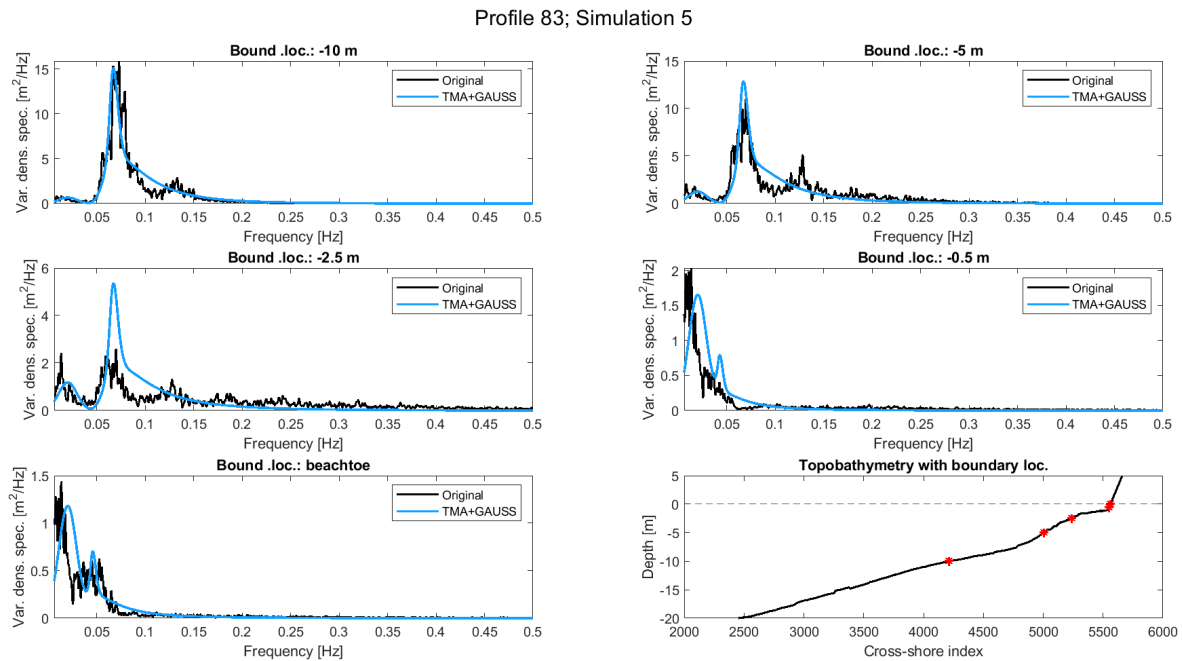
Figure 4.3: Original (black line) and fitted (blue line) spectra for the test case for Profile 83, Simulation 5 (significant wave height Hs = 3 m, peak wave period Tp = 14 s and an offshore water level $\eta = 0$ m) at each boundary location separately. Bottom right is the topobathymetry of the reef profile with the boundary locations, marked in red. For the sake of clarity, only frequencies between 0.006 Hz and 0.5 Hz are depicted.

The quality of the spectral fit with TMA+GAUSS function is evaluated with the root mean square error (RMSE) between the parameterized spectra and the original spectra. RMSE for Profile 83 of each simulation (for $\eta_0 = 0$ m) for each boundary location are depicted in Figure 4.4 (RMSE of other 5 reef profiles are included in Appendix C). The quality of the fit decreases with increasing offshore wave conditions. Moreover, the quality of the fit is the highest for the boundary locations further from the shore at depths of -10 m, -5 m and -2.5 m, where more wave energy is stored in higher frequencies which are better represented with TMA part of the function. The quality of the fit is the lowest close to the shore at a depth of -0.5 m and at the beachtoe where most of the wave energy is stored in LF part of the spectrum. There, the IG and VLF part waves are poorly represented with Gaussian part of the function because of the assumption that LF part of the spectrum has only one frequency peak at 0.02 Hz.

RMSE at each boundary location, averaged over all simulations (see Table 4.2), are not in line with the resulting errors of runup for each boundary location (see Table 4.1, BT method 3). Therefore, the accuracy of the BT method 3 is not directly affected by the quality of spectral fit[1].

---

[1]Note, that the amount of wave energy at the boundary is the same for the parameterized spectral method (BT method 3) and the direct method (BT method 1). RMSE is a result of the error introduced by the different distribution of wave energy among the frequencies.
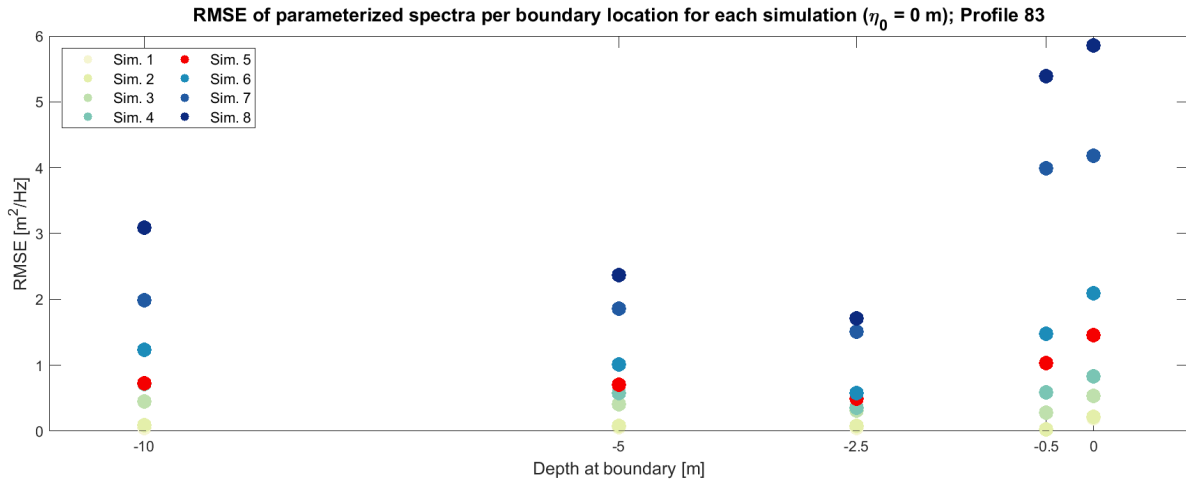
Figure 4.4: Root mean square error (RMSE) between the parameterized wave spectra and the original wave spectra per each boundary location (depth at the boundary on x-axis) and for each simulation separately (coloured dots, see Table 3.3 for the list of simulations with offshore water level $\eta_0 = 0$ m), for Profile 83. Red dots are corresponding to Simulation 5 (significant wave height Hs = 3 m, peak wave period Tp = 14 s and an offshore water level $\eta = 0$ m).

Table 4.2: Root mean square error (RMSE) between the parameterized wave spectra and the original wave spectra per each boundary location, averaged over all simulations (see Table 3.3 for the list of simulations with offshore water level $\eta_0 = 0$ m) for Profile 83.

Depth at boundary	-10 m	-5 m	-2.5 m	-0.5 m	beachtoe
Averaged RMSE [m^2/Hz]	1.05	0.89	0.64	1.60	1.92

Water level time series at the boundary

Wave spectra at the boundary locations at depths of -10 m, -2.5 m and -0.5 m are highly diverse, not only in frequency distribution, but also in the amount of energy stored in their spectra (observed in Figure 4.3). Therefore, the nonlinear wave shapes at these three boundary locations are compared for the three BT methods. A section of the time series from $t_1 = 2000$ s to $t_2 = 2400$ s when waves are assumed to be already fully developed is depicted in Figure 4.5.

To identify the nonlinear wave shapes at a certain location, the output from XB-NH+ is inspected. Waves at a depth of -10 m have long and flat troughs and high narrow crests, a phenomenon known as skewness. Closer to the shore at a depth of -2.5 m waves have even more pronounced peaky crests and flatter troughs; the waves there are again skewed. Moreover, they are pitched forward, phenomenon known as asymmetry. Due to asymmetric shape, the waves break and their energy is dissipated. Very close to the shore at a depth of -0.5 m, the large amounts of wave energy are already dissipated. The shape of waves there is still asymmetric, but they are no longer skewed.

Since BT method 1 takes output directly from XB-NH+ model to force SFINCS, all the nonlinear wave shapes are present in the water level time series. However, a large difference between the water level time series obtained with BT method 1 and BT methods 2 and 3 are observed. This is because the water level time series that are generated from the spectrum with BT methods 2 and 3 lack the wave phase information. Consequently, nonlinear wave shapes are not present. Both BT methods 2 and 3 are generated with the same random phase, which is applied for easier comparison between the methods.

The water level time series at a depth of -10 m for BT methods 2 and 3 are very similar. This is expected, as the parameterized wave spectrum at that location fits well with the original wave spectrum with RMSE of 0.73 m^2/Hz (comparison of spectra depicted in Figure 4.3). The differences between BT methods 2 and 3 are more noticeable at the shallower depths closer to the shore. The water level time series at a depth of -2.5 m generated with parameterized spectrum (BT method 3) are smoother compared to the water level time series

obtained with original spectra (BT method 2) despite the low RMSE (RMSE = 0.49 m²/Hz) between the two spectra. However, the smoother water level time series obtained with BT method 3 can still be explained by the difference between the distribution of wave energy over the HF spectral band between the parameterized and original spectra, as shown in Figure 4.3. Similar observation is noticed for the water level time series at a depth of -0.5 m where RMSE between the parameterized and the original spectra is 1.04 m²/Hz. In Figure 4.3, the parameterized spectrum at a depth of -0.5 m contains more HF wave energy concentrated in a narrow peak very close to cut-off frequency of 0.04 HZ. In contrast, the original spectrum does not contain this frequency peak and the HF wave energy is more equally spread around higher frequencies. Therefore, the water level time series generated with BT method 2 are less smooth.
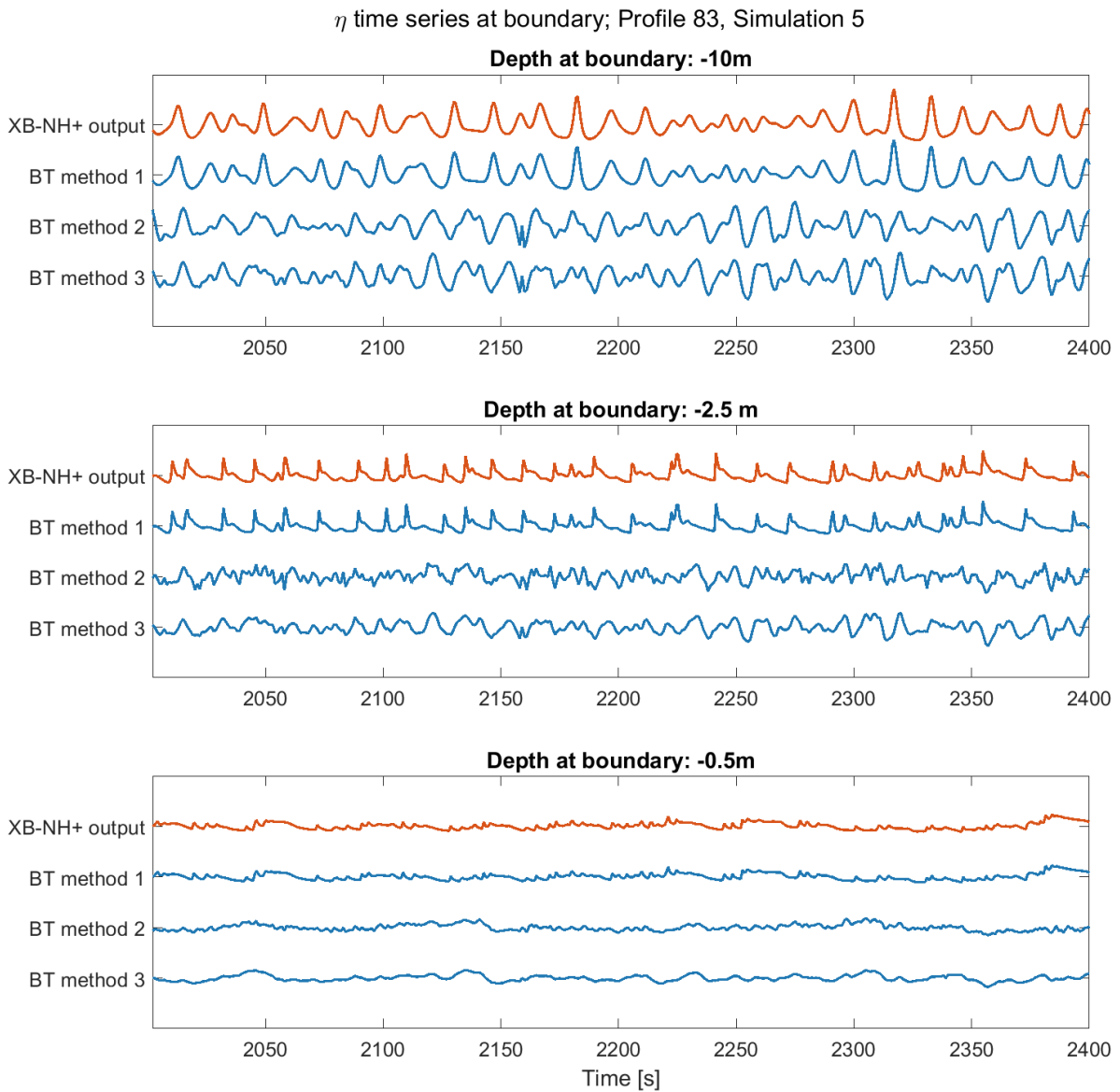
Figure 4.5: Comparison of water level time series for the test case for Profile 83, Simulation 5 (significant wave height Hs = 3 m, peak wave period Tp = 14 s and an offshore water level η = 0 m). Time series are generated with different BT methods, at the boundary locations at depths of -10 m (top), -2.5 m (middle) and -0.5 m (bottom) for the time span from t_1 = 2000 s to t_2 = 2400 s. Red line represents original water level time series at the boundary, taken from fully XB-NH+ model output. Blue lines represent water level time series generated with BT methods 1, 2 and 3. For description of BT methods, refer to Section 3.4.1.

4.2   Evolution of waves with SFINCS

The evolution of waves with SFINCS is investigated by comparing the water level time series obtained with different BT methods across the surfzone. This is researched in order to (a) understand what consequences does the use of reduced-physics model have on prediction of waves across the shore and to (b) investigate the consequences of applying the parameterization at the boundary. Only the comparison between BT methods 1 and 3 is shown, because BT methods 2 performed similarly to BT method 3. The evolution of waves with SFINCS forced with exact boundary conditions (BT method 1) is studied in Section 4.2.1. Then, the differences in evolution of waves for parameterized boundary conditions (BT method 3) are shown in Section 4.2.2. Finally, the cross-shore mean water level and variance are compared for different boundary locations in Section 4.2.3.

4.2.1   SFINCS forced with exact boundary conditions

The evolution of waves with SFINCS forced with exact boundary conditions obtained with BT method 1 is depicted in Figure 4.6. The water level time series are depicted at different locations based on the depth at that location. Additionally, at depths of -5 m, -0.5 m and at the beachtoe the time series from SFINCS (blue line in the figure) are compared to the time series from the reference model XB-NH+ (red line in the figure).

SFINCS forced far from the shore at a depth of -10 m (Figure 4.6 (a)) develops very characteristic saw tooth-shaped waves shortly after the boundary. The close-up of one section from the time series at a depth of -5 m is depicted in Figure 4.7. The asymmetry of these waves is very well predicted, but their skewness is only 22% of the skewness simulated with the reference model XB-NH+ (for the reference, the skewness of the waves predicted with XB-NH+ model is 1.34, whereas the skewness of the waves predicted with SFINCS is only 0.29 for the location at a depth of -5 m). The wave height of the waves simulated with SFINCS is therefore under-predicted. This can be explained with the simplified shallow water equations that SFINCS is based on. Since SFINCS does not include dispersion, the waves simulated with SFINCS are not dispersive. While the waves that lack dispersion are propagating towards the shore, they steepen more quickly and therefore break earlier than they should. The waves, depicted in Figure 4.7, are already partially broken, which is also evident from the cross-shore mean sea level at that location, depicted in Figure 4.11. The mean sea level, directly indicating the wave setup, is over-predicted. Therefore, the waves have indeed already partially broken while propagating towards the observed location at a water depth of -5 m. This is further explained in Section 4.2.3.

The waves predicted with SFINCS forced at a depth of -10 m have a saw tooth-like shape roughly from depths of -9 m till -2 m. Once most of their wave energy is dissipated closer to the shore, their saw tooth shape has disappeared. The difference between the waves simulated with SFINCS and with the reference model XB-NH+ model close to the shore is in the amount of HF waves. Close to the shore HF waves are generated due to wave breaking, as observed from XB-NH+ time series. SFINCS does not predict these HF waves, therefore the time series at the depth of -0.5 m and at the beachtoe are smooth (see Figure 4.8 (top) for a closer look of the time series at a beachtoe).

When SFINCS is forced closer to the shore at a depth of -2.5 m (Figure 4.6 (b)) , less energy is imposed into the system compared to the boundary locations further offshore (refer to Figure 4.3). This is because the waves are already partially broken before the boundary. The waves at the boundary are steep and asymmetric, so they break soon after the boundary without developing distinct saw tooth shapes. A closer look of the evolution of waves at a beachtoe (see Figure 4.8 (middle)) reveals that the waves are better predicted compared to the waves predicted with the simulation where SFINCS is forced at the boundary location at a depth of -10 m. The water level time series predicted with SFINCS are again smooth because no HF wave energy is generated close to the shore.

When SFINCS is forced even closer to the shore at a depth of -0.5 m (Figure 4.6 (c)), it is imposed with the HF wave energy that is lacking in the previous two examples. Intuitively, that would result in better prediction of waves at the beachtoe. However, soon after the boundary the waves become smooth again. SFINCS therefore always seems to underestimate the magnitude of the HF waves.

Differences in evolution of waves are observed for the compared boundary locations because every boundary location across the reef profile has different different wave spectra with a different LF to HF energy ratio that

SFINCS is imposed with. Nevertheless, all three tested boundary locations resulted in similar prediction of waves at the beachtoe (Figure 4.8) and over-prediction of runup between 2 cm and 9 cm, corresponding to relative errors of runup between 1.1% and 6.5%.
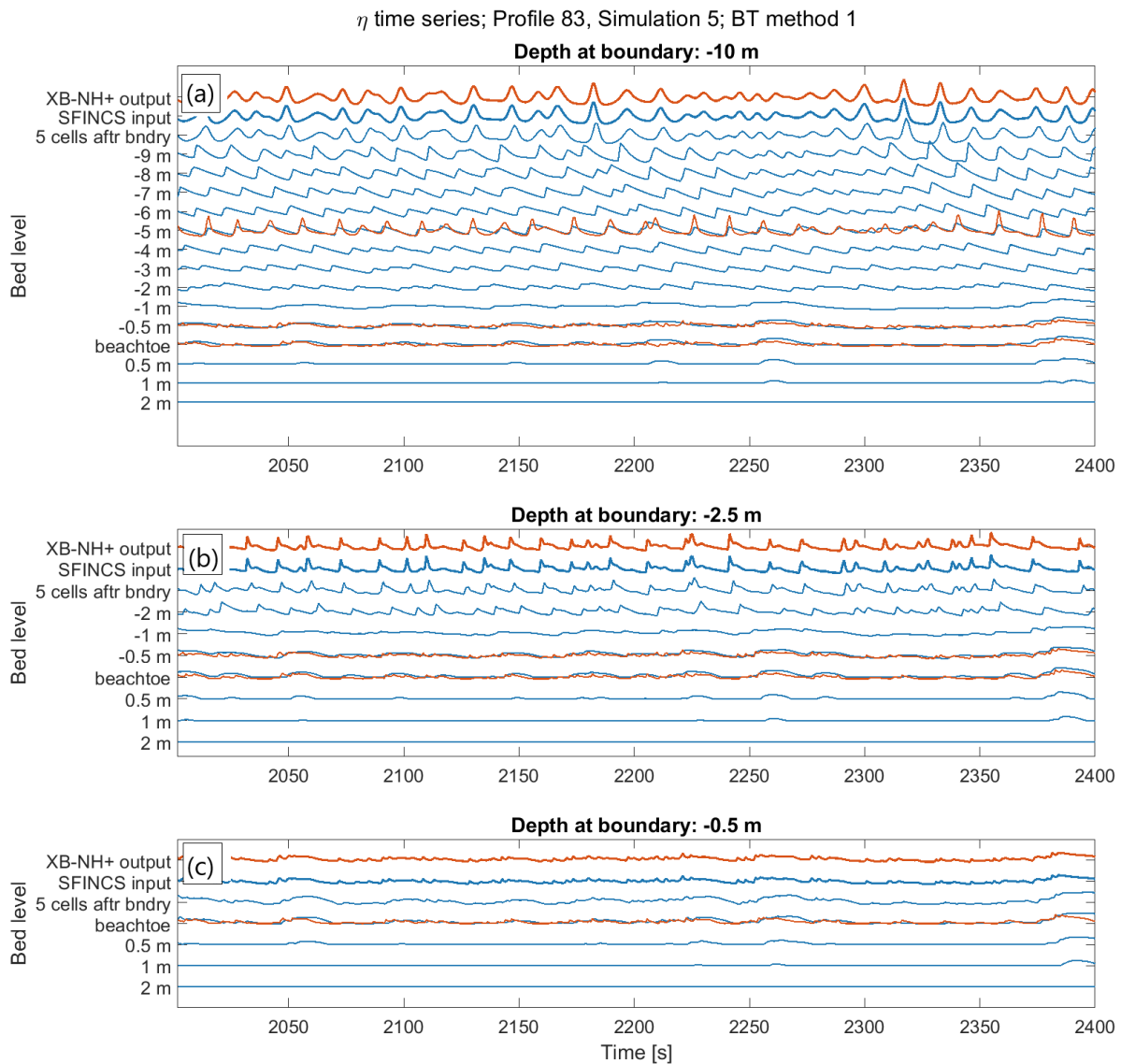
Figure 4.6: Evolution of waves across the shore with SFINCS for the test case for Profile 83, Simulation 5 (significant wave height Hs = 3 m, peak wave period Tp = 14 s and an offshore water level $\eta = 0$ m). SFINCS is forced at three different boundary locations at depths of -10 m (a), -2.5 m (b) and -0.5 m (c) with exact boundary conditions, directly obtained from XB-NH+ LUT with BT method 1 (see Section 3.4.1). Time series from SFINCS (blue line) are compared to the time series from the reference model XB-NH+ (red line). Water level time series are depicted at the selected observation locations corresponding to the water depths that are denoted on y-axis.
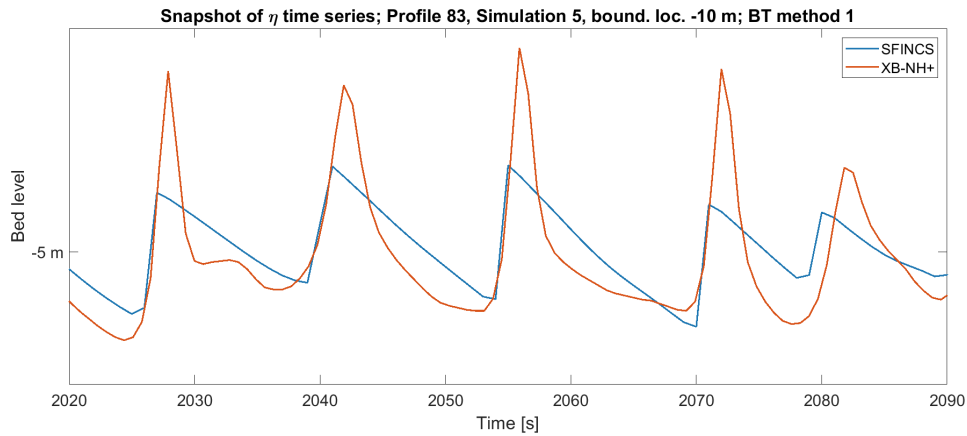
Figure 4.7: Zoomed-in graph of water level time series of SFINCS (blue line) compared with XB-NH+ (red line) at the location with the depth of -5 m when SFINCS model is forced at boundary location with depth of -10 m. For the full evolution of waves refer to Figure 4.6.
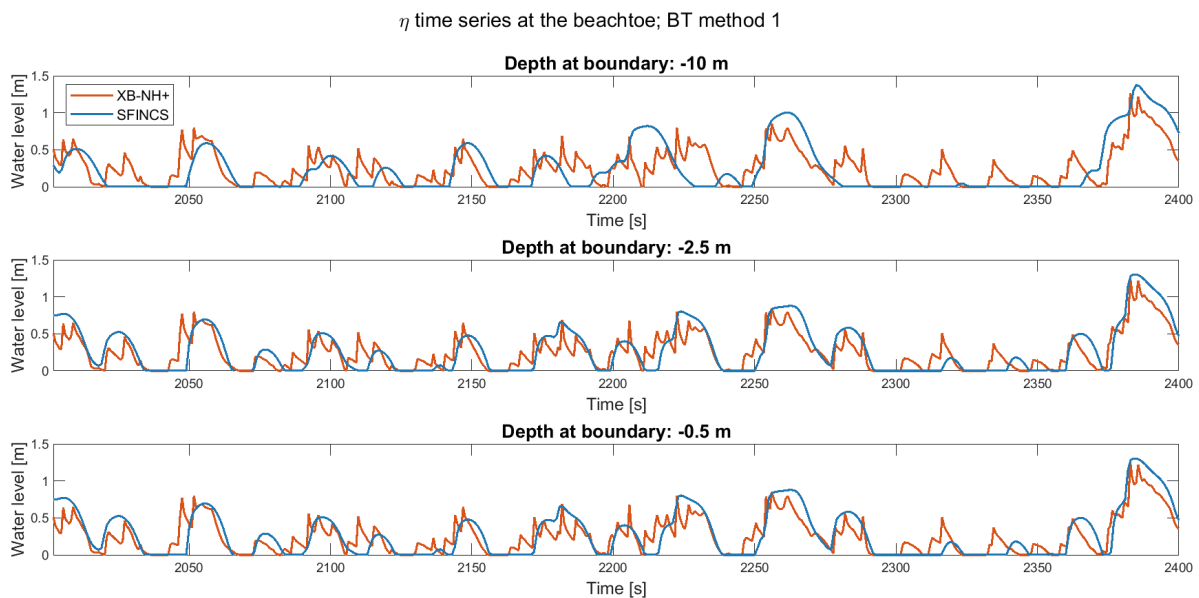
Figure 4.8: Water level time series at the beachtoe for the test case for Profile 83, Simulation 5 (significant wave height Hs = 3 m, peak wave period Tp = 14 s and an offshore water level $\eta = 0$ m). SFINCS is forced at three different boundary locations at depths of -10 m (top), -2.5 m (middle) and -0.5 m (bottom) with exact boundary conditions, directly obtained from XB-NH+ LUT with BT method 1 (see Section 3.4.1). The time series from SFINCS (blue line) are compared to the time series from XB-NH+ (red line).

4.2.2   SFINCS forced with parameterized boundary conditions

The evolution of waves with SFINCS forced with the parameterized boundary conditions obtained with BT method 3 is depicted in Figure 4.9. Parameterization is performed with the TMA+GAUSS function, as described in Section 3.4.1. The water level time series are depicted at different locations based on the depth at that location. Additionally, at depths of -5 m, -0.5 m and at the beachtoe the time series from SFINCS (blue line on the figure) are compared to time series from the reference model XB-NH+ (red line on the figure). Since the waves obtained with BT method 3 are not in phase with the waves from the reference model XB-NH+, the comparison between the two time series in that case is more difficult.

SFINCS forced far from the shore at a depth of -10 m (Figure 4.9 (a)) develops saw tooth shaped waves shortly after the boundary, similar as the case when the model was forced with the exact boundary conditions. The asymmetry of the waves at the observation location at a depth of -5 m is well predicted with SFINCS, while their skewness is under-predicted with only 43% of the skewness simulated with the reference model XB-NH+

(for the reference, the skewness of the waves predicted with XB-NH+ model is 1.34, whereas the skewness of the waves predicted with SFINCS is only 0.57 for the location at a depth of -5 m). Near the shore, SFINCS again neglects HF part of the spectrum (see the time series at the beachtoe in Figure 4.10).

Differences are detected when SFINCS is forced closer to the shore. At the boundary location at a depth of -2.5 m (Figure 4.9, (b)), SFINCS is not forced with steep and asymmetric waves, as was the case before, but with waves with a random phase. Nevertheless, SFINCS develops asymmetric waves shortly after the boundary which are mainly broken at the depth of -1 m. Near the shore SFINCS neglects HF part of the spectrum which results in smooth time series, unlike the time series from the reference model XB-NH+. At the boundary location at a depth of -0.5 m (Figure 4.9 (c)) no HF part of the spectrum is imposed into SFINCS, unlike with BT method 1. Since SFINCS does not generate HF part of the spectrum near the shore by itself, the fact that waves are smooth near the shore is not surprising. Even though these HF waves are not present, the runup is still predicted with good accuracy (relative error of runup is 1.9%).

The accuracy of runup prediction increases with decreasing depth of the offshore boundary location for forcing SFINCS. This can be explained with the fact that SFINCS is better at solving LF wave energy which is dominating close to the shore. The comparison of the water level time series simulated with SFINCS to the ones from the reference model XB-NH+ is challenging because of the different wave phase. However, similar characteristics of the waves predicted with BT method 3 are found as the characteristics of the waves predicted with BT method 1 (Section 4.2.1). Therefore, the inaccurate simulation of waves is not due to the parameterization of wave spectra and the lack of phase information at the boundary. This implies that the inaccuracy in wave prediction comes from the reduced physics in SFINCS and the numerical scheme in SFINCS which is dissipative (Leijnse et al., 2021). Nevertheless, the relative errors of runup are comparable between the two methods (BT method 1 and 3, refer back to Table 4.1). Therefore, BT method 3 has a potential in being a good method for obtaining boundary conditions for forcing SFINCS.
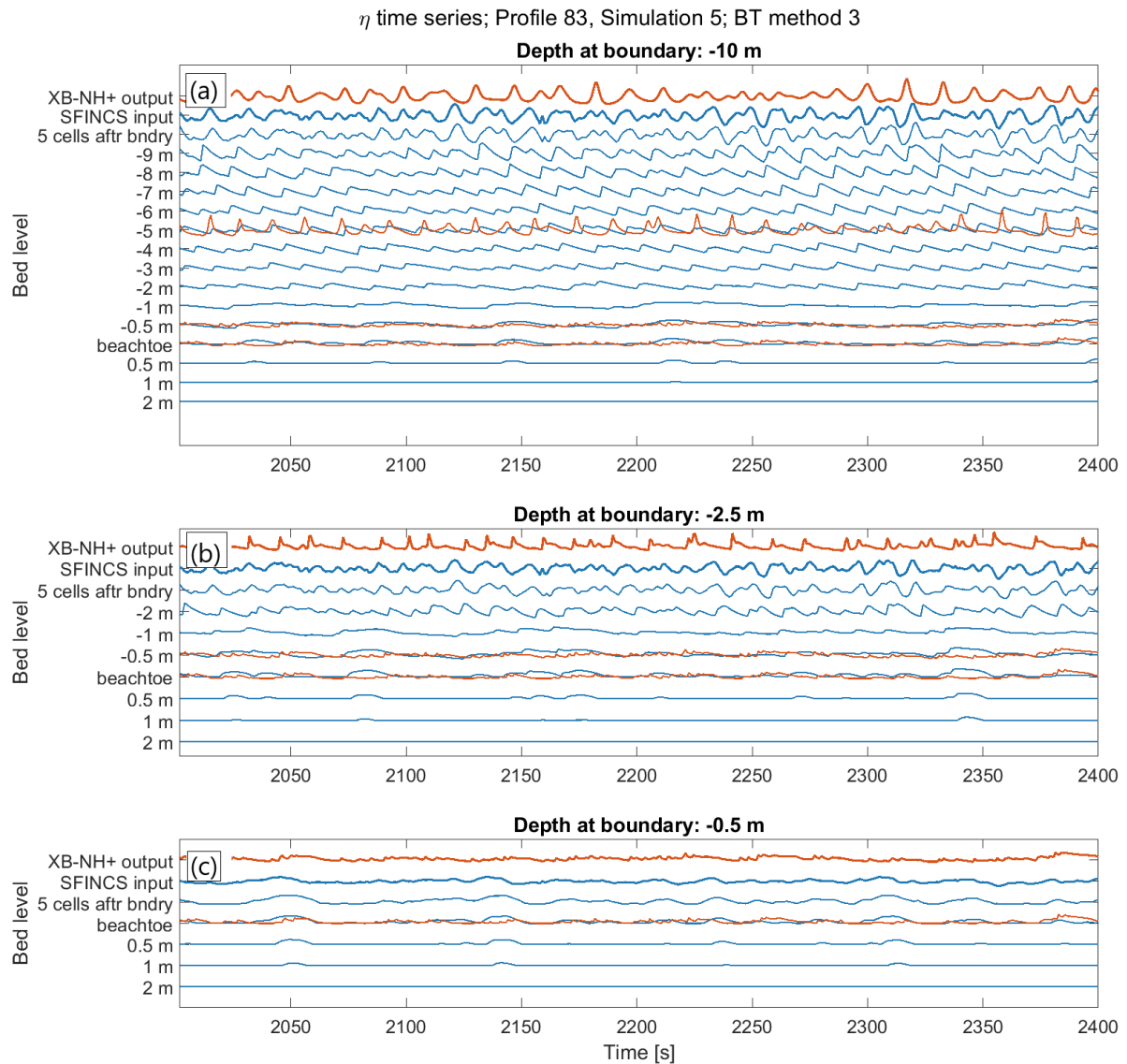
Figure 4.9: Evolution of waves across the shore with SFINCS for the test case for Profile 83, Simulation 5 (significant wave height Hs = 3 m, peak wave period Tp = 14 s and an offshore water level $\eta = 0$ m). SFINCS is forced at three different boundary locations at depths of -10 m (top), -2.5 m (middle) and -0.5 m (bottom) with parameterized boundary conditions, obtained with BT method 3 (see Section 3.4.1). Time series from SFINCS (blue line) are compared to the time series from XB-NH+ (red line).
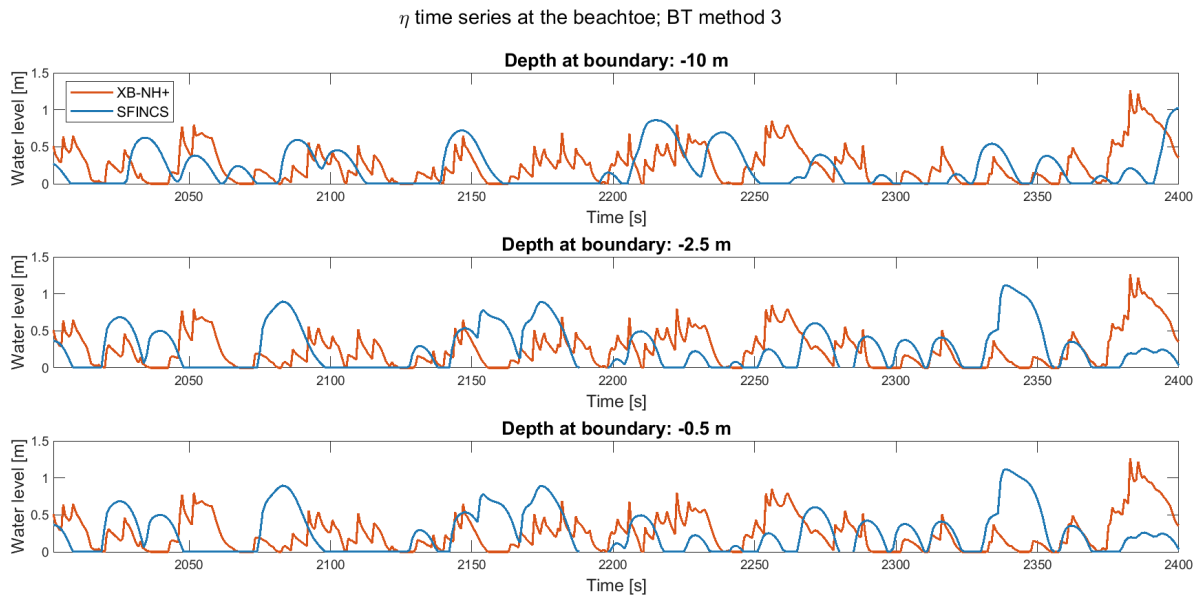
Figure 4.10: Water level time series at the beachtoe for the test case for Profile 83, Simulation 5 (significant wave height Hs = 3 m, peak wave period Tp = 14 s and an offshore water level η = 0 m). SFINCS is forced at three different boundary locations at depths of -10 m (top), -2.5 m (middle) and -0.5 m (bottom) with parameterized boundary conditions with BT method 3 (see Section 3.4.1). The time series from SFINCS (blue line) are compared to the time series from XB-NH+ (red line).

4.2.3 Wave setup and variance across the shore

Mean water level (directly indicating the wave setup) and variance (representing 1/2 of the squared wave amplitude) are calculated for the simulations with exact boundary conditions (BT method 1) and parameterized boundary conditions (BT method 3). Simulations with all tested boundary locations are compared to the reference model XB-NH+ in Figure 4.11. Results from the reference model XB-NH+ are depicted in orange colour and results from the SFINCS model, forced at different boundary locations, are of various colours. No significant differences between BT methods 1 and 3 are observed for both the mean water level and the variance. This again demonstrates that BT method 3 is comparable with BT method 1. More noticeable differences are observed between the cross-shore evolution of mean water level and variance calculated with SFINCS forced at the different boundary locations and with the reference model XB-NH+.

When SFINCS is forced far from the shore at a depth of -10 m, variance is diminished with a faster rate compared to XB-NH+ simulation. At the same time the mean water level, directly indicating the wave setup, starts to increase approximately 300 m further from the shore compared to the wave setup, computed with the reference model XB-NH+. This implies that in SFINCS breaking occurs further offshore than it is supposed to. This can be explained with (1) the lack of dispersion in SFINCS and (2) the numerical scheme implemented in SFINCS which is dissipative (Leijnse et al., 2021). The consequences of not including dispersion in the model were already observed with the analysis of the water level time series in Section 4.2.1 and Section 4.2.2.

Wave setup close to the shore (Figure 4.12 (a) for BT method 1 and Figure 4.12 (b) for BT method 3) is inaccurately predicted for all simulations with the exception of when SFINCS is forced at the beachtoe. This is not surprising, as the majority of the waves at the beachtoe are already broken and SFINCS is forced with the same wave setup for both BT methods which is directly obtained from XB-NH+. A strange sudden increase in variance is observed for the simulation with SFINCS forced at the boundary location at a depth of -0.5 m, depicted in Figure 4.12 (c and d). No explanation for this behaviour was found.

Despite the acceptable runup predictions obtained with boundary locations far from the shore, Figure 4.11 demonstrates that starting before the breakpoint with a model based on simplified shallow water equations does not predict the evolution of waves correctly. It is therefore more appropriate to set the boundary location for forcing SFINCS closer to the shore where wave propagation across the reef profile is predicted more accurately.
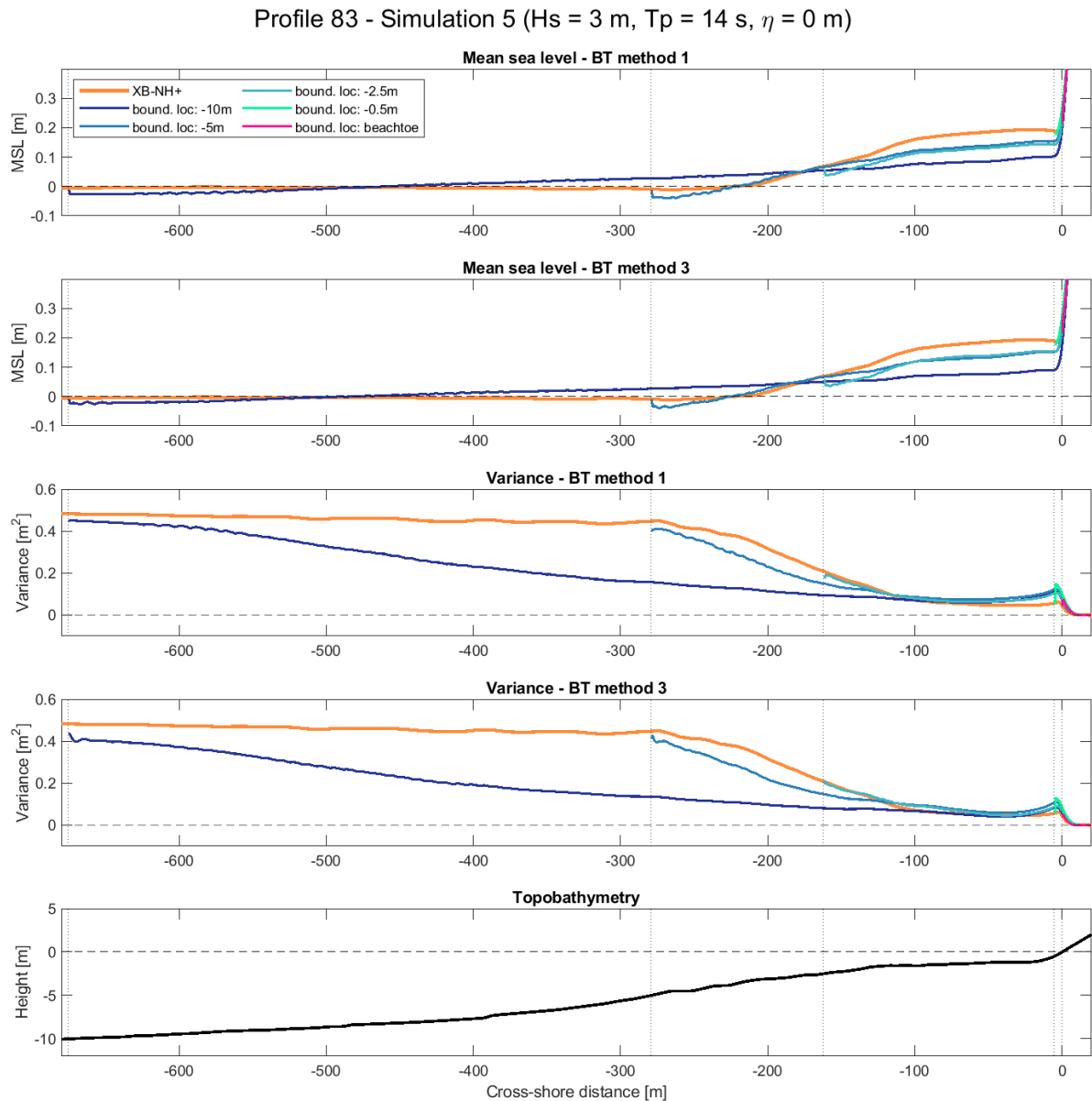
Figure 4.11: Mean sea level (MSL, first and second graph) and variance (third and fourth graph) across the shore for different boundary locations (depths of -10 m, -5 m, -2.5 m, -0.5 m and at the beachtoe, all marked as dashed vertical lines) obtained with SFINCS (various colours) and compared with the reference model XB-NH+ (orange colour). Results obtained with correct boundary conditions (BT method 1, first and third graph) are compared to results obtained with parameterized boundary conditions (BT method 3, second and fourth graph). Bottom graph depicts the topobathymetry of the reef profile (Profile 83). Test case is performed for Profile 83, Simulation 5 (significant wave height Hs = 3 m, peak wave period Tp = 14 s and an offshore water level $\eta_0 = 0$ m).
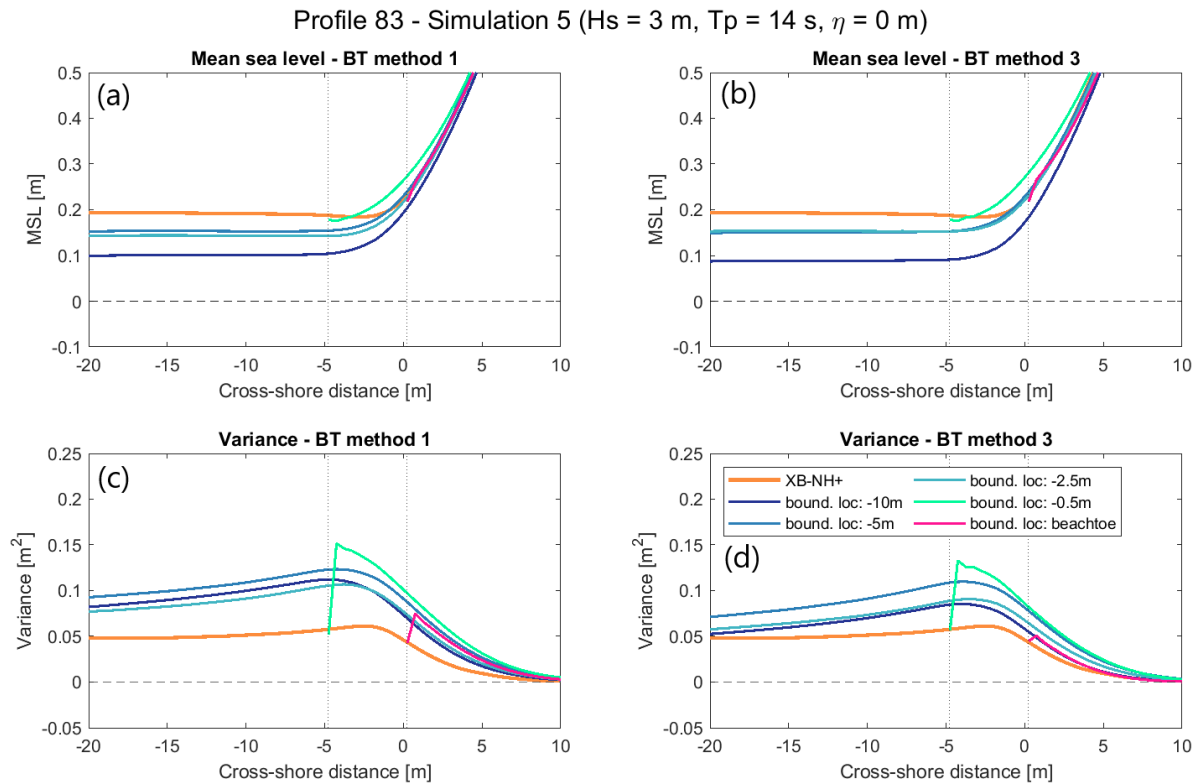
Figure 4.12: Mean sea level (MSL, Figures a and b) and variance (Figures c and d) close to the shore for different boundary locations (depths of -10 m, -5 m, -2.5 m, -0.5 m and at the beachtoe) obtained with SFINCS (various colours) and compared with the reference model XB-NH+ (orange colour). Results obtained with correct boundary conditions (BT method 1, Figures a and c) are compared to the results obtained with parameterized boundary conditions (BT method 3, Figures a and c). Test case is performed for Profile 83, Simulation 5 (significant wave height Hs = 3 m, peak wave period Tp = 14 s and an offshore water level $\eta_0 = 0$ m). The graphs are zoomed-in figures from the full cross-sectional profiles, depicted in Figure 4.11.

4.3   Analysis of boundary locations

This part of the analysis consists of identifying what is the best suitable boundary location per each profile (Section 4.3.1), identifying the possible reasons behind these findings (Section 4.3.2) and estimating the runup errors when SFINCS is forced at pre-defined boundary location (Section 4.3.3), which is defined as the most suitable boundary location for the majority of the studied cases. Different reef profiles have a different wave breaking response and LF/HF wave energy ratios at different water depths, therefore the findings of optimal water depth over a range of profiles need to be justified. The desired outcome of this section is to find the optimal boundary location that can be applicable for the majority of the reef profiles.

The simulations are performed with two different offshore water levels ($\eta_0 = 0$ m and $\eta_0 = 1$ m) in order to investigate if the preferred boundary location changes considerably depending on the mean sea level and how well is the runup estimated in that case.

A reference of runup heights from the advanced XB-NH+ model is depicted in Figure 4.13 as a reference for the interpretation of results of the following analysis. The runup increases with increasing offshore water level. Moreover, the reef profiles 12, 24 and 38 generally result in higher runup compared to the reef profiles 83, 271 and 526. The reef profiles 83, 271 and 526 have generally a mild slope and wide reef flat, therefore dissipation of wave energy due to wave breaking is more pronounced on these profiles (followed from the hypotheses stated in Table 3.2). The difference in wave runup is largely observed for lower offshore water level ($\eta_0 = 0$ m) and for stormy conditions (simulation numbers 5-8).
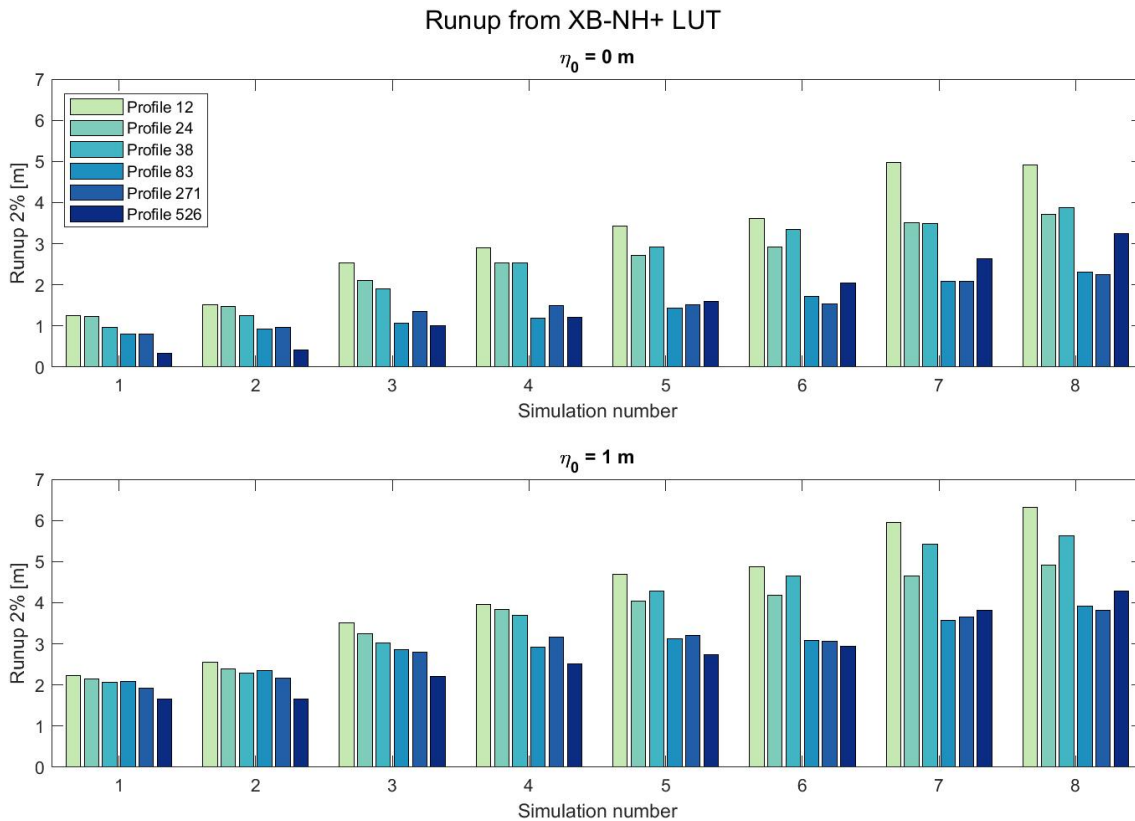
Figure 4.13: Runup heights from the advanced XB-NH+ model per reef profile (colours) per simulation (numbers 1 to 8 where 1-4 are for swell scenario and 5-8 are for storm scenario) for two offshore water levels ($\eta_0 = 0$ m on the top and $\eta_0 = 0$ m on the bottom).

4.3.1 The best suitable boundary location

The best suitable boundary location is defined as the boundary location that leads to the least error of runup simulated with SFINCS. The runup is compared to the runup simulated with the reference model XB-NH+. The best suitable boundary locations vary considerably for each reef profile, BT method and an offshore water level. The following question needs to be answered: *How does the optimal boundary location vary with the offshore wave conditions and bathymetric profile?*

Offshore water level η_0 = 0 m

The best suitable boundary locations for each applied BT method (three columns) per reef profile (rows) per simulation (denoted as numbers 1-8 in rows) for offshore water level of 0 m are depicted in Figure 4.14 (a). The results are depicted as heatmaps; each boundary location that results in the least amount of error is marked with different colour in order to easily detect the possible characteristics of the results. The relative and absolute errors of runup, associated with the best suitable boundary locations, are depicted in Figure 4.14 (b) and (c), respectively. These results are also depicted as the heatmap tables where the more intense colours represent the higher errors.

Characteristic features are observed for simulations when SFINCS is forced with parameterized boundary conditions (BT method 3, the third column in Figure 4.14 (a)). The reef profiles that result in higher runup due to steep fore reef slope and/or narrow reef flat (Profiles 24 and 38) perform better when SFINCS is forced at the boundary location at a depth of -2.5 m. The reef profiles that result in lower runup due to high amounts of wave energy dissipated on wide reef flat and/or mild fore reef slope (Profiles 83 and 271) perform better when SFINCS is forced at the boundary location closer to the shore at a depth of -0.5 m. Similar behaviour can be observed for simulations when SFINCS is forced with random phased time series generated with original spectrum (BT method 2, the second column in Figure 4.14 (a)), but not for simulations when SFINCS is forced with correct boundary conditions (BT method 1, the first column in Figure 4.14 (a)).

Another observation lies in the bathymetric features of the active domain in SFINCS for the considered reef profiles. SFINCS has its active domain which starts from the forcing offshore boundary location and ends on the top of the (semi-infinite) shore. All reef profiles are decreasing in depth shore-ward from the best suitable boundary location. Therefore, the SFINCS domain does not include reef flat, nor the lagoon. In other words, best results are obtained when SFINCS is forced shore-ward from the reef flat.

The runup is underestimated for most cases, regardless of the applied BT method, shown in Figure 4.14 (c) (all three columns). Some of the highest relative errors of runup (Figure 4.14 (b)) are observed for the swell scenario (Simulations 1-4), when the offshore wave conditions are less intense. The steepest reef profile, Profile 12, is an example of that behaviour with the relative error of runup of 40% for the most gentle offshore conditions and BT method 3. The simplified reef profile, Profile 526, resulted in the lowest errors of runup. No indication of the best suitable boundary location is observed for this profile. This result could be because of simplicity of the reef profile and therefore more clear location of wave breaking.

The average relative errors of runup can be found in Figure 4.15 per reef profile (columns 1-6) and for all profiles together (column 7) for three tested BT methods. The reef profiles that lead to higher runup (between 20% and 140% higher than the rest of the profiles, refer to Figure 4.13) due to their bathymetric characteristics (Profiles 12, 24 and 38) result in larger relative and absolute errors of runup compared to the reef profiles resulting in lower runup (Profiles 83, 271 and 526). This behaviour is observed for all applied BT methods. The relative errors of runup, averaged over all profiles (Figure 4.15, the last column), are almost the same for BT methods 1 and 3. This means that parameterization of wave spectra and the lack of phase information at the boundary does not introduce any significant error.
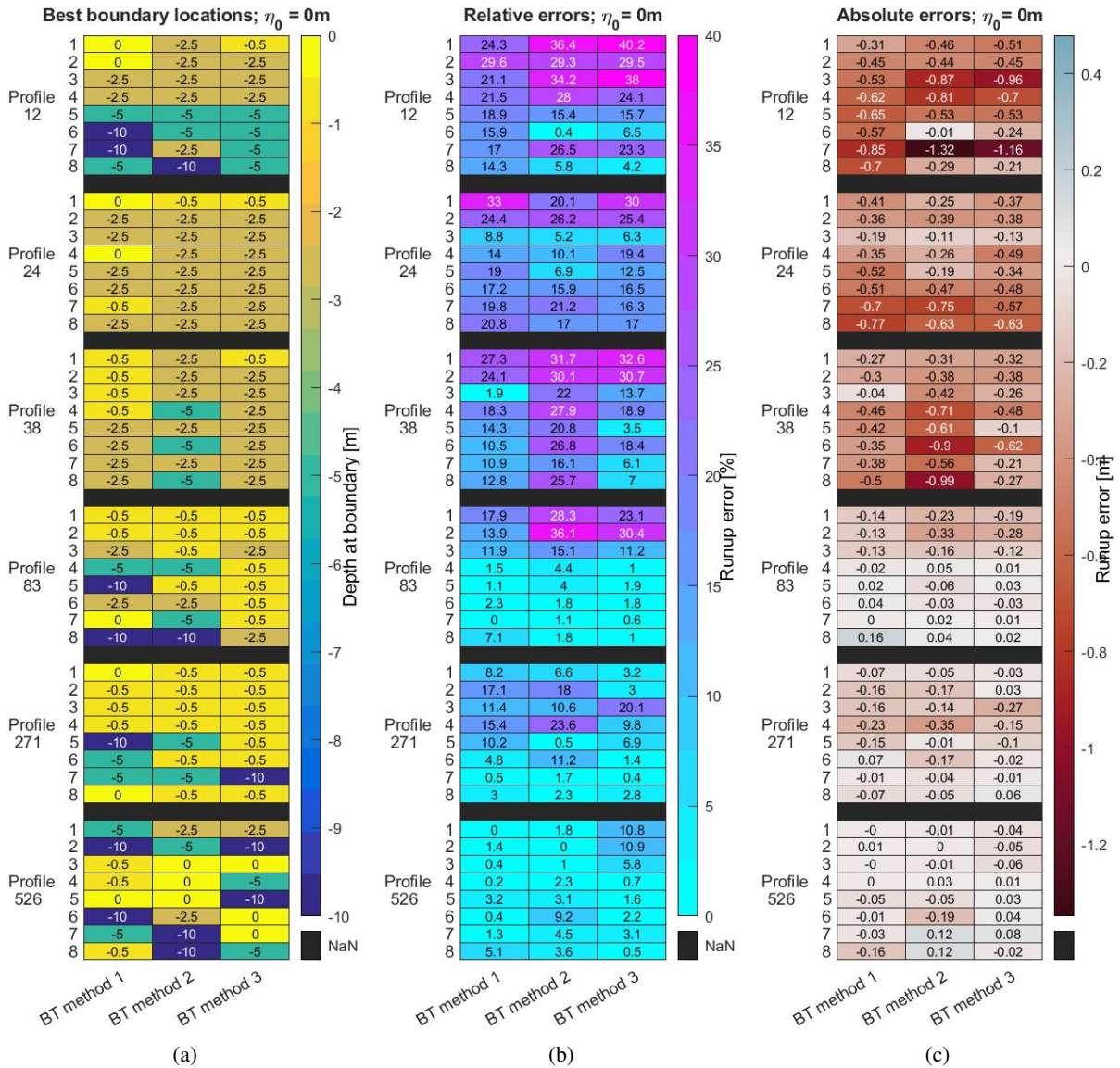
Figure 4.14: (a) The best suitable boundary locations are the locations that lead to the lowest relative errors of runup. The results are shown per reef profile (rows) per simulation (numbers 1 to 8, rows), for offshore water level $\eta_0 = 0$ m as heatmap tables where the colours represent the depth at the boundary. (b) The associated relative errors and (c) the absolute errors of runup are depicted with heatmap tables where colours represent the values of the errors of runup (b and c; more intense colours are associated with larger errors).
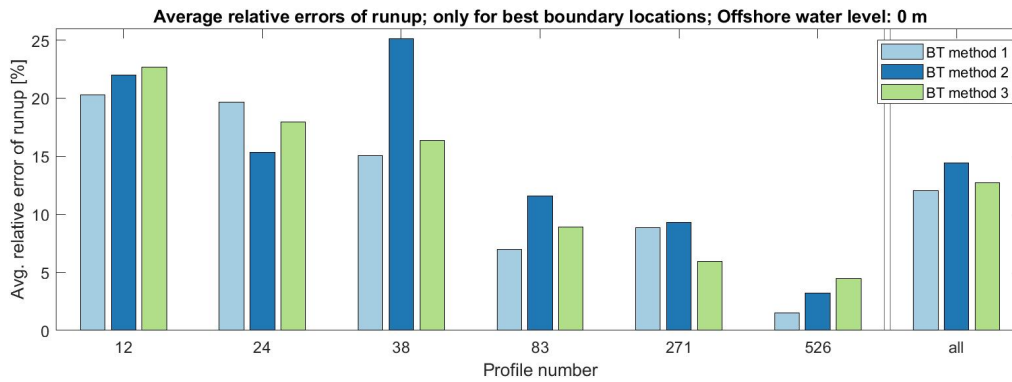
Figure 4.15: Average relative errors of runup for best boundary locations, depicted in Figure 4.14 for offshore water level $\eta_0 = 0$ m. The values are averaged over the 8 tested simulations with different offshore conditions for each reef profile separately (bars 1-6) and for all reef profiles together (bar 7) for each BT method separately.

Offshore water level $\eta_0 = 1$ m

The best suitable boundary locations for each applied BT method (three columns) per reef profile (rows) per simulation (denoted as numbers 1-8 in rows) for offshore water level of 1 m are depicted in Figure 4.16 (a). The results are depicted as heatmaps; each boundary location that results in the least amount of error is marked with different colour in order to easily detect the possible characteristics of the results. The relative and absolute errors of runup, associated with the best suitable boundary locations, are depicted in Figure 4.16 (b) and (c), respectively. These results are also depicted as the heatmap tables where the more intense colours represent the higher errors.

Similarities are observed between simulations with offshore water levels $\eta_0 = 0$ m and 1 m with parameterized boundary conditions (BT method 3). Reef profiles that result in higher runup (Profiles 12, 24 and 38) perform better when forced at the boundary further from the shore compared to other tested profiles. This is consistent with the previous finding with the offshore water level of 0 m. The most common optimal boundary locations when BT method 3 is applied are at water depths of -2.5 m, -0.5 m and at the beachtoe (Figure 4.16 (a), the third column, BT method 3). Therefore, the best suitable boundary location of all tested profiles is now shifted closer to the shore. The reference level for the definition of boundary locations is still at a 0 m water level, however now the mean water level excluding the wave setup is at 1 m height. This means that the best suitable boundary location is at the actual still water level between -3.5 m and -1 m, which is similar to the previous findings[2].

The shifted optimal boundary location can also be explained by the configuration of SFINCS domain. SFINCS prefers to have a certain number of wet cells between the boundary and the shoreline. Boundary location at the beachtoe was not a good option when offshore water level was 0 m, because SFINCS does not have enough wet cells in the domain to correctly simulate waves till shore. However, enough wet cells are present between the pre-defined beachtoe and the mean water level of at least 1 m height. Therefore, in this case the optimal boundary location was often found to be at the (pre-defined) beachtoe.

Larger mean sea level results in better runup estimates with the highest relative error of runup of 23% (Figure 4.16 (b), third column, Profile 12) and the average error of runup between 6% and 7% (Figure 4.17, the last column, errors averaged over all reef profiles). Errors of runup are low regardless of the type of boundary conditions. Therefore, BT method 3 is again confirmed to be the good method for generating the boundary conditions for forcing SFINCS.

Additionally, the second and the third best boundary locations were analyzed. The results showed that the good accuracy of runup prediction is achieved in that case as well. The largest error of runup of up to 60% is observed with simulations when SFINCS is forced with parameterized boundary conditions (BT method 3).

---

[2]Note that the boundary location at the beachtoe is the shallowest tested location. Therefore, it was not possible to find out if the better boundary location in case of offshore water level of 1 m could be at even shallower water depths.
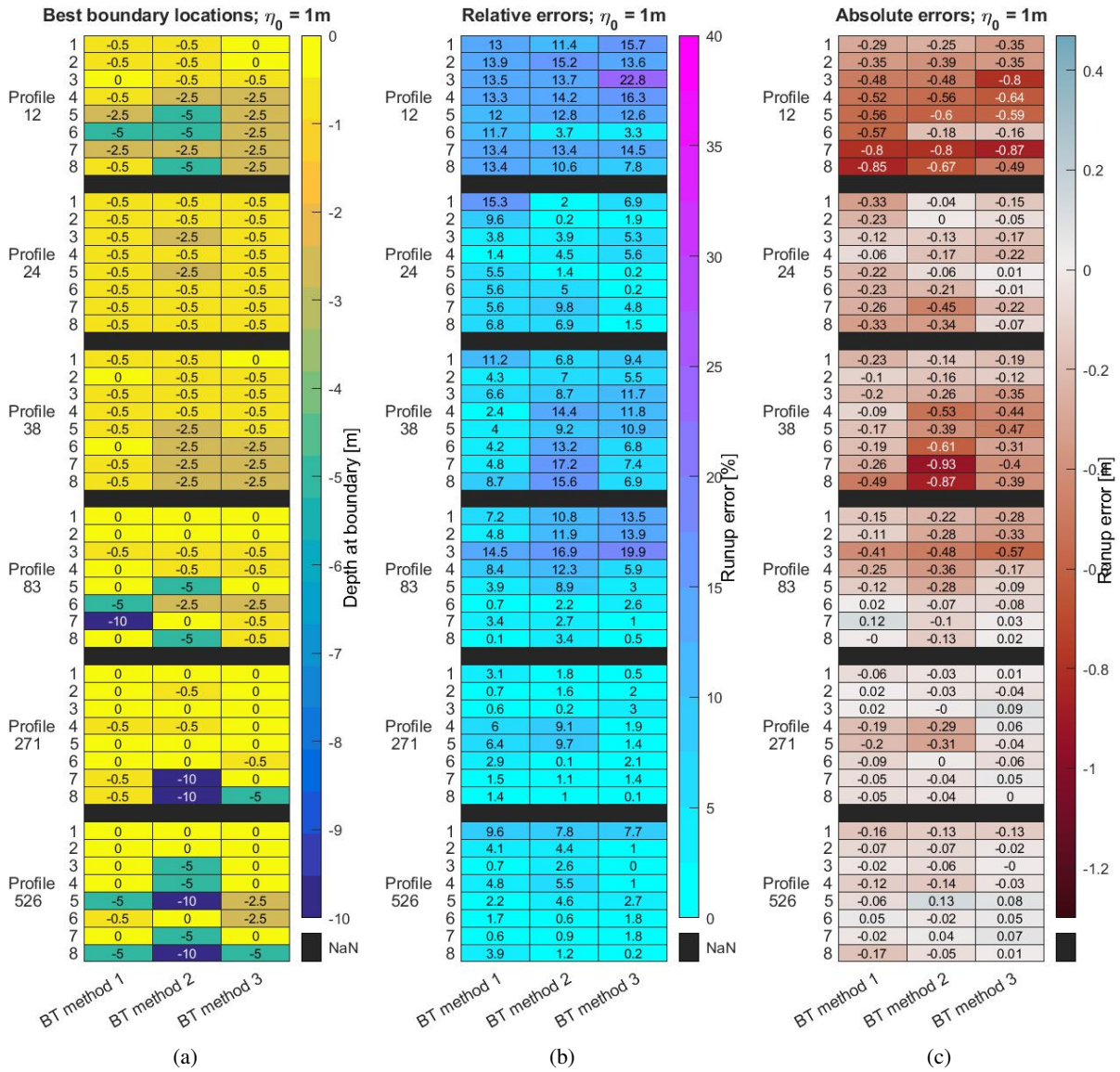
Figure 4.16: (a) The best suitable boundary locations are the locations that lead to the lowest relative errors of runup. The results are shown per reef profile (rows) per simulation (numbers 1 to 8, rows), for offshore water level $\eta_0 = 1$ m as heatmap tables where the colours represent the depth at the boundary. (b) The associated relative errors and (c) the absolute errors of runup are depicted with heatmap tables where colours represent the values of the errors of runup (b and c; more intense colours are associated with larger errors).
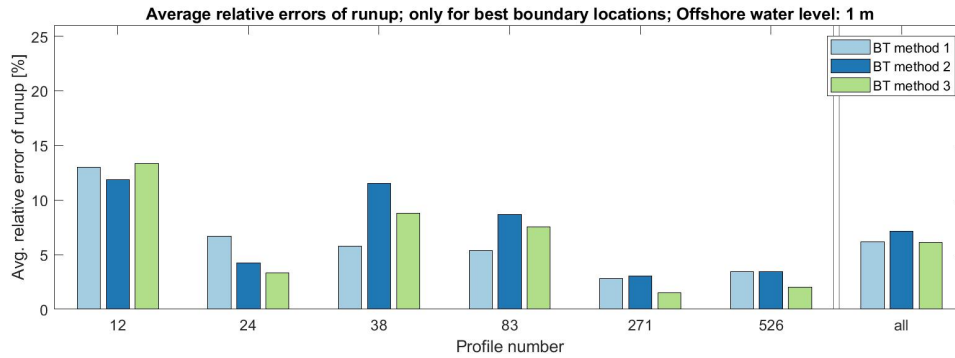
Figure 4.17: Average relative errors of runup for best boundary locations, depicted in Figure 4.16 for offshore water level $\eta_0 = 1$ m. The values are averaged over the 8 tested simulations with different offshore conditions for each reef profile separately (bars 1-6) and for all reef profiles together (bar 7) for each BT method separately.

The optimal boundary location

The following can be concluded from the analysis above:

  – The best results are obtained when SFINCS is forced shore-ward from the reef flat.

  – The best suitable boundary location is at the actual still water level between -3.5 m and -0.5 m.

  – The reef profiles that dissipate large amounts of wave energy on the wide and shallow reef flat and/or mild fore-reef slope (dissipative reef profiles) perform better when forced at the boundary closer to the shore compared to the reef profiles that have steep fore-reef and/or narrow and deeper reef flat (or no reef flat). These reef profiles also result in lower errors of runup.

  – Parameterizing wave spectrum and the lack of phase information at the boundary does not introduce any significant error.

  – There is an indication that the errors of runup decrease with increasing offshore water level.

4.3.2 Analysis of wave parameters at boundary

Previous analysis revealed that the reef profiles that result in higher runup due to their bathymetric characteristics (Profiles 24 and 38) have a clear preference for boundary location at a greater depths compared to the reef profiles that result in lower runup (Profiles 83 and 271), when forced with parameterized boundary conditions (BT method 3). This section attempts to answer the following question: *What do these profile-couples have in common?*

Possible reasons behind the similar behaviour of profile-couples are their bathymetric features and the value of their runup, as already indicated in Section 4.3.1. However, a deeper analysis on the wave parameters at the boundaries is performed in order to reason the behaviour with the parameters describing physical characteristics which can potentially be generalized to other reef profiles.

Following is a list of wave parameters, calculated at the boundaries, that did not reveal any direct correlation between their values and the relative errors of runup:
  – dispersion (kd);
  – Ursell number;
  – asymmetry;
  – skewness;
  – the amount of IG wave energy; and
  – the amount of HF wave energy.

The nonlinearities in the sea-swell wave fields, defined as the ratio between significant wave height of HF waves (sea-swell) and the depth (i.e. H_{ss}/d), gave an indication on the position of the boundary within the nearshore zone. Results are depicted in Figure 4.18 for offshore water level of 0 m and in Figure D.1 for offshore water level of 1 m. All reef profiles except from the simplified reef profile (Profile 526) result in lower error of runup when SFINCS is forced with an optimal amount of sea-swell nonlinearities at the boundary. Every reef

profile has a different optimal value, though.
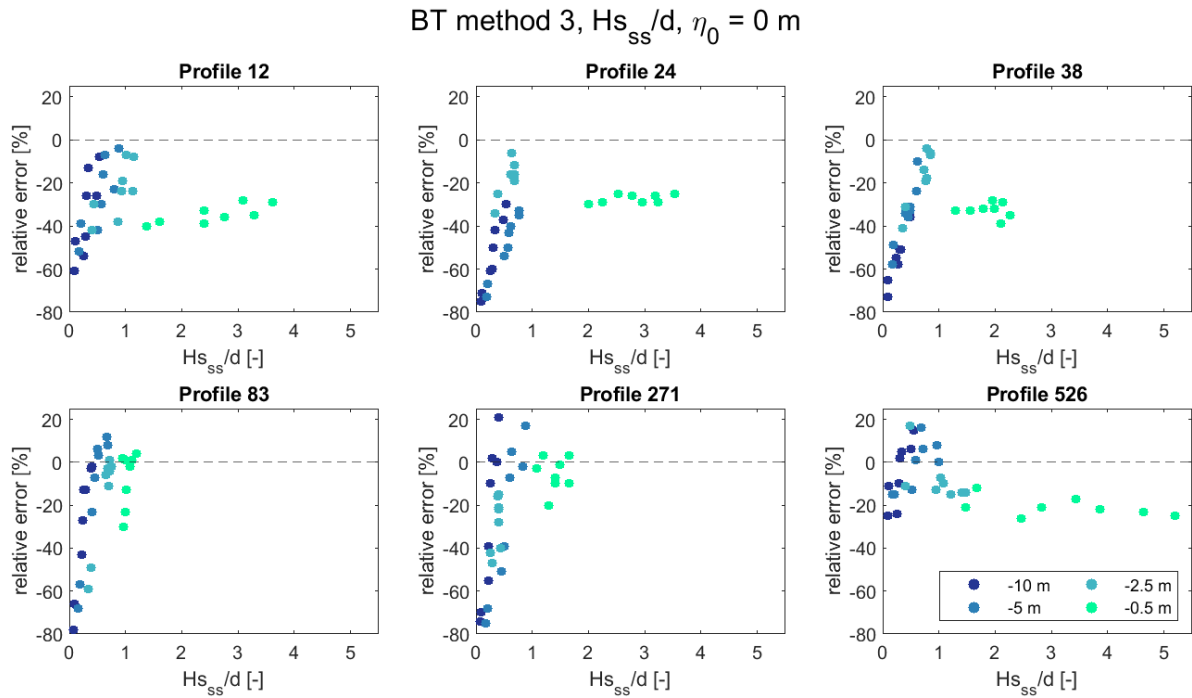
Figure 4.18: The ratio between the significant wave height of HF waves (sea-swell) and the depth (H_{ss}/d) at the boundary locations in relation with the associated relative errors of runup. Results are depicted for each reef profile separately for all simulations (8 different cases, based on different offshore wave conditions). Offshore water level is $\eta_0 = 0$ m and parameterized boundary conditions are applied (BT method 3, see Section 3.4.1). Various colours depict 4 different boundary locations that SFINCS is forced at. Boundary location at the beachtoe is not depicted because the ratio H_{ss}/d cannot be calculated (depth = 0 m).

Sea-swell nonlinearities increase with decreasing depth. Moreover, relative error of runup decreases with increasing amount of sea-swell nonlinearities. Figure 4.18 clearly indicates this when comparing H_{ss}/d of the same boundary location (depicted with the same colour) to the relative error of runup. However, this observation is inconsistent for points representing boundary location at a depth of -0.5 m (similar phenomenon is present also for the offshore water level of 1 m, shown in Figure D.1). There, a difference between the profile-couples is shown. Despite the different amounts of sea-swell nonlinearities at the boundary, the relative errors of runup for Profiles 12, 24 and 38 (Figure 4.18, top row) are nearly constant. A possible reason for different behaviour at the boundary location at a depth of -0.5 m for Profiles 12, 24 and 38 (Figure 4.18, top row) is that this boundary location is too close to the shore. SFINCS, when forced too close to the shore, might not have enough wet cells in its domain. Therefore, when large rundown occurs and consequently the water leaves the SFINCS domain, SFINCS does not deal properly with this phenomena. The errors of runup for these cases are nearly constant between 20 and 40%. This could also explain why the boundary location at the beachtoe is often not the best suitable boundary location for forcing SFINCS. The errors when SFINCS is forced at the beachtoe are not the highest, but they are not the lowest either (referring back to Section 4.3.1).

The ratio between the significant wave height of LF waves (IG and VLF together) and the depth (i.e. H_{LF}/d) gave similar results because the amount of LF wave energy is dependent on the amount of HF wave energy. The dependence is not linear (see Figure D.2 and Figure D.3), and consequently the correlation between the LF waves nonlinearities (H_{LF}/d) and the errors of runup are not completely apparent.

4.3.3   Errors associated with pre-defined boundary locations

Following is the analysis performed on errors of runup associated with the pre-defined boundary locations. The question that is being answered here is: *How large are the runup errors if the model is forced at the same*

boundary location regardless of the reef profile or the offshore wave conditions applied?

Two boundary locations are considered, defined at depths of -2.5 m and -0.5 m. These boundary locations are chosen because they appeared most often in the previous analysis in Section 4.3.1. Only BT methods 1 and 3 are analysed, associated with correct and parameterized boundary conditions, respectively. Results are depicted in Figure B.1 and Figure B.2 for offshore water levels of $\eta_0 = 0$ m and $\eta_0 = 1$ m, respectively.

Forcing the model at a depth of -0.5 m results in better runup estimates for the majority of cases for both offshore water levels. This is supported with Figure 4.19, showing average relative errors of runup for both boundary locations and both offshore water levels and all BT methods. There is also an indication that the errors of runup are decreasing with increasing mean sea level. Some of the highest relative errors of runup can be found for the simulations with parameterized boundary conditions (BT method 3) and the offshore water level of 0 m, with the errors up to 60% (Figure B.1 (a), second column, Profile 83, swell scenario). Note, that the errors are usually lower and on average between 19% and 22 % depending on the boundary location. Second, reef profiles that promote larger runup (Profiles 12, 24 and 38) and are forced at a boundary depth of -0.5 m resulted in nearly constant relative errors of runup between 24% and 40%. This behaviour is already observed in Figure 4.18 and cannot be explained with sea-swell nonlinearities at the boundary. Some indication for this behaviour are suggested in Section 4.3.2.

Relative errors of runup, averaged over all simulations and all reef profiles together (Figure 4.19, the last error bars of all four graphs), showed that forcing SFINCS with parameterized boundary conditions (BT method 3) leads to comparable errors of runup as forcing SFINCS with the exact boundary conditions. This is true even when SFINCS is forced at the pre-defined boundary location at depths of either -2.5 m or -0.5 m. This finding supports the previous results in Section 4.2.2, Section 4.2.3 and Section 4.3.1. In these sections, the analyses showed that with parameterized wave spectrum and with the lack of phase information at the boundary, no significant error is introduced. The main source of error is the reduced physics in SFINCS. As it was shown in Section 4.2.2, SFINCS highly underestimates HF waves while it is better at solving evolution of LF waves across the shore including the simulation of asymmetric shape of waves. Since the HF waves are neglected with SFINCS, this leads to under-estimation of runup. In general, a majority of HF waves are already dissipated close to the shore, while LF waves are dominating the wave spectrum. Forcing SFINCS at the optimal boundary location close to the shore leads to less error because the accurate amount of LF waves is put in the system. The observed errors are mainly the under-prediction of HF waves.

The finding suggest that the parameterized boundary conditions are appropriate for forcing SFINCS at both considered boundary locations at depths of -2.5 m and -0.5 m with the average error of runup between 10 and 20% and the maximum error of runup of up to 60%.
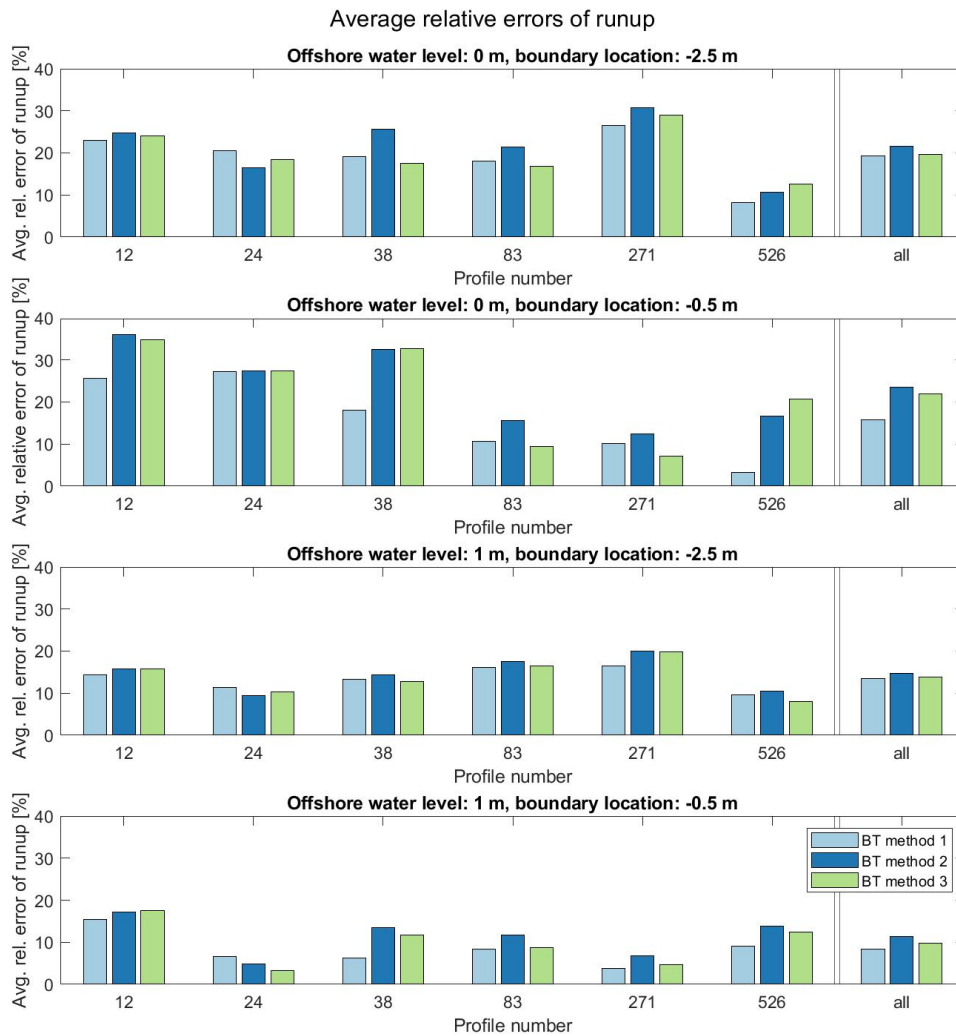
Figure 4.19: Average relative errors of runup for pre-defined boundary locations at depths of -2.5 m (first and third bar plot) and -0.5 m (second and fourth bar plot), for offshore water levels $\eta_0 = 0$ m (first and second bar plot) and $\eta_0 = 1$ m (third and fourth bar plot). The values are averaged over the 8 tested simulations with different offshore conditions for each reef profile separately (bars 1-6) and for all reef profiles together (bar 7) for each BT method separately. Full sets of results are depicted in Figure B.1 and Figure B.2.

4.4 Computational time

Computational efficiency of the new method can be assessed by comparing the computational time of the developed method with the computational time of the conventional method. Computational time can be determined by the amount of time needed for the model to perform the desired simulation. Since the developed method only applies modeling from the chosen boundary location to the shore, the computational time of the method is expected to be significantly lower than by using the model along the entire reef profile. Moreover, by using reduced-physics model SFINCS, the computational demands are furthermore lowered.

Currently it is only possible to model wave-driven flooding on coral reef-lined coasts by using computationally demanding models such as XB-NH+ along the entire reef profile. To assess the computational efficiency of the developed method, the computational time of SFINCS along the active cells is compared to the computational time of physics-based model XB-NH+ along the entire reef profile.

1D model XB-NH+ simulates coastal flooding in 350 s on average for the studied reef profiles (simulated with the real-time forcing of 4000 s). SFINCS, on the other hand, needs significantly less time. Computational time highly depends on the number of active cells. The number of active cells also differs per reef profile. Average computational times depending on the boundary location (and thus on the number of active cells) are listed in Table 4.3. The computational time averages 9.6 s for the real-time forcing of 3600 s. Moreover, the computational time of SFINCS that is forced at the optimal boundary location at the optimal depth of either -2.5 m or -0.5 m is 6.8 s. This is a **relative speed-up factor of about 50 compared to the XB-NH+ model simulating hydrodynamic processes along the entire reef profile**.

Table 4.3: Average computational times and average number of active cells of SFINCS based on the boundary location. The average is computed over the reef profiles. Computational time and a number of active cells averaged over all profiles are included in the bottom row. The model was run with the real-time forcing of 3600 s.

Depth at boundary	Number of active cells	Computational time [s]
-10 m	1724	16.3
-5 m	1316	12.5
-2.5 m	839	7.9
-0.5 m	688	5.6
beachtoe	597	5.8
Average	**1032**	**9.6**

4.5   Conclusion

A sensitivity analysis was performed (a) to understand the influence of parameterized boundary conditions for forcing SFINCS and (b) to find the most optimal boundary location for forcing SFINCS with the parameterized boundary conditions. Additionally, the amount of error introduced with the proposed method was estimated. These results are used directly for further analysis on the interpolation methods in Chapter 5.

The evolution of waves with SFINCS was compared to the results from the reference model XB-NH+. SFINCS forced with exact boundary conditions develops asymmetric waves shortly after the boundary, while the skewness of the waves is highly under-predicted. Furthermore, SFINCS dissipates HF wave energy, which results in smooth water level time series close to the shore. The wave setup and the variance across the shore are falsely predicted as well, because SFINCS develops saw-tooth shaped waves which grow rapidly and break further from the shore compared to the reference model XB-NH+. These results were obtained for the exact boundary conditions, derived directly from the reference model XB-NH+. The observed behaviour is therefore a consequence of reduced physics in SFINCS.

Parameterized boundary conditions are generated with a random phase, i.e. they lack the wave phase information. Therefore, nonlinear wave shapes are not present at any considered boundary location (analysed for the locations at depths of -10 m, -2.5 m and -0.5 m). Moreover, the frequency distribution of wave energy in the parameterized spectrum differs from the original spectrum, while the amount of wave energy at both spectra is the same. Despite the differences between the parameterized and exact boundary conditions, the evolution of waves with SFINCS for the two cases is comparable. In general, parameterizing wave spectrum and the lack of phase information at the boundary does not introduce any significant error.

Forcing SFINCS with parameterized boundary conditions requires the optimal forcing location. The best results are obtained when SFINCS is forced shore-ward from the reef flat. Furthermore, this corresponds with the best suitable boundary location at the actual still water level between -3.5 m and -0.5 m. The reef profiles that dissipate large amounts of wave energy on the wide and shallow reef flat and/or mild fore-reef slope (dissipative reef profiles) perform better when forced at the boundary closer to the shore compared to the reef profiles that have steep fore-reef and/or narrow and deeper reef flat (or no reef flat). The nonlinearities it the sea-swell wave field at the boundary are responsible for this behaviour. These reef profiles also result in lower errors of runup. There is an indication that the errors of runup also decrease with increasing offshore water level.

Boundary locations at depths of -2.5 m and -0.5 m most often appeared as the best suitable boundary locations for the considered offshore wave and water level conditions and the reef profiles. On average, they resulted in relative errors of runup between 10% and 20% with the highest errors of up to 60% for the tested cases. The computational time of SFINCS forced at the optimal boundary location averages 6.8 s for the real-time forcing of 1 h, which results in a relative speed-up factor of about 50 compared to the XB-NH+ model simulating hydrodynamic processes along the entire reef profile.

Based on the results, obtained with sensitivity analysis, the further analysis on interpolation methods is performed with parameterized boundary conditions obtained with TMA+GAUSS function and the boundary locations at depths of -2.5 m and -0.5 m.

5

Interpolation of boundary conditions

An interpolation of boundary conditions is needed in order to force SFINCS with boundary conditions that match the desired offshore wave and water level conditions. Interpolation is performed over the closest offshore wave and water level conditions from XB-NH+ LUT, i.e. the most similar conditions to the target offshore conditions. For instance the LUT includes wave heights of $H_s = 1$ & 3 m and offshore water levels of $\eta_0 = 0$ & 1 m, while at a certain time-frame the boundary conditions for $H_s = 1.8$ m and $\eta_0 = 0 = 0.25$ m are wanted.

An analysis is performed to find the interpolation method that results in (a) the most accurate estimate of the boundary conditions and (b) the most accurate estimate of runup. The simulations are applied to two offshore wave and water level scenarios, gentle swell and stormy conditions, and to two boundary locations at depths of -2.5 m and -0.5 m. All cases are performed with BT method 3 (parameterized boundary conditions), as this method was shown to work with good accuracy (e.g., Section 4.3.3). The method includes the parameterization of the spectrum with three parameters using the TMA+GAUSS function and the generation of random time series as input for SFINCS. The three spectral parameters and the wave setup are interpolated to obtain the most accurate estimate of the boundary conditions. 9 different interpolation methods are tested. Their algorithms are described in Section 3.5.

A schematic representation of the analysis of interpolation methods is depicted in Figure 5.1. This figure shows the set-up of the analysis, which includes testing the interpolation methods and evaluating the importance of each interpolated parameter. Moreover, the set-up of two control cases is depicted as well. Control case consisting of full XB-NH+ simulations serves for comparing the resulted runup with the correct runup. The control case consisting of model train with XB-NH+ and SFINCS serves for comparing (a) interpolated parameters at the boundary with the correct ones and (b) the influence of errors of interpolated parameters to the resulting runup. The letter is performed by *semi-interpolating* the parameters at the boundary, i.e. by interpolating each parameter individually, while the other parameters have the exact values. A scheme also refers to the sections in which the results of each performed analysis are presented. The interpretation of the results is discussed in Section 5.5.
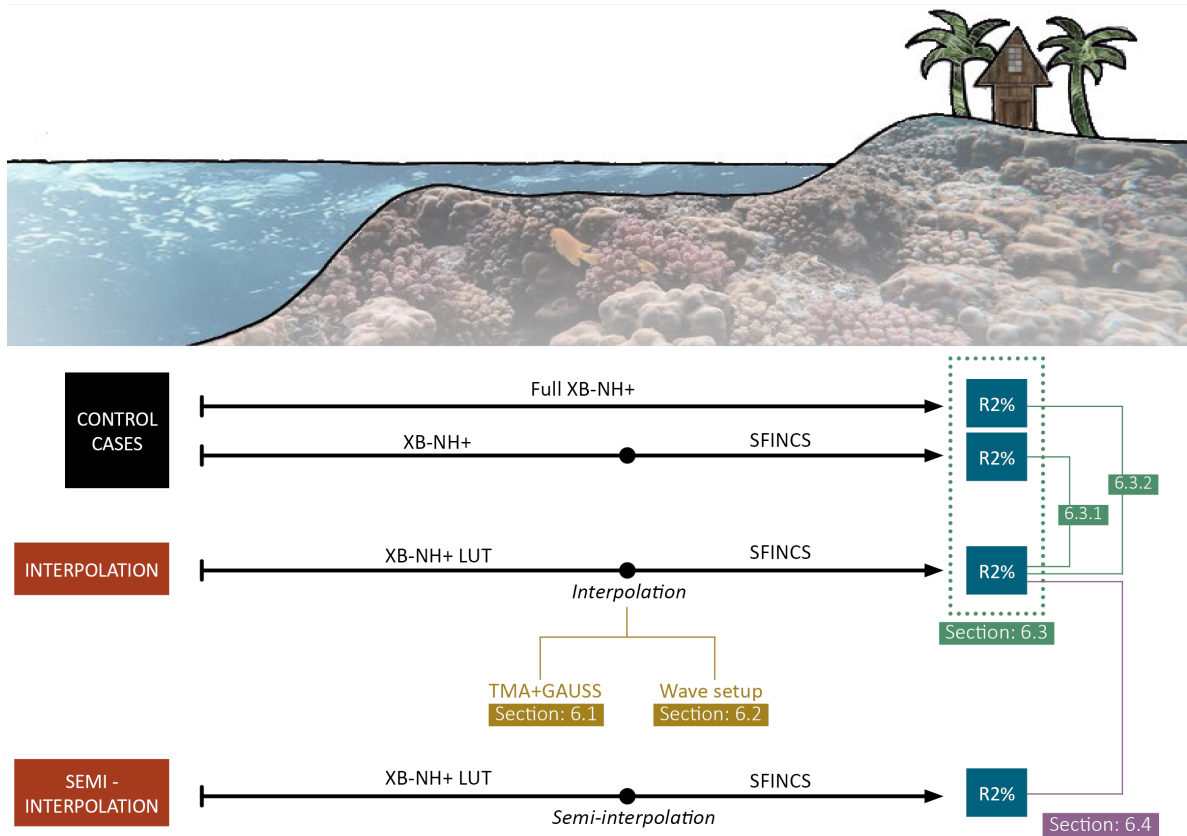
Figure 5.1: Schematic representation of the elements that form the analysis of interpolation methods. All the elements are represented as the simplified cross-section of 1D reef bathymetric profile from the offshore (left) till the shore (right) and the model/look-up-table that are used. Each element refers to the section where the analysis is described. Two control cases are used to calculate the associate errors of (a) estimated spectral and wave setup parameters and (b) resulted runup (R2%). *Semi-interpolation* of the parameters at the boundary refers to interpolating each parameter individually, while the other parameters have the exact values.

5.1 Interpolated spectral parameters

The parameterized wave spectrum is described with three parameters: frequency peak of HF part of the spectrum, HF wave energy and LF wave energy. These three parameters together form the TMA+GAUSS shape of the spectrum. At the boundary each TMA+GAUSS spectral parameter is interpolated over the values associated with the closest offshore wave and water level conditions. 9 different interpolation methods are tested, as described in Section 3.5 and listed in Table 3.4. The first indication of the quality of performance of the applied interpolation methods is the ability to estimate the TMA+GAUSS parameters with good accuracy. The interpolated TMA+GAUSS parameters are compared to the correct values, calculated with the reference model XB-NH+.

Mean and standard error of the sample mean[1] of the relative errors of predicted TMA+GAUSS spectral parameters are calculated for each applied interpolation method. Results are depicted in Figure 5.2 where different colours represents the interpolation methods. Relative errors of predicted TMA+GAUSS spectral parameters for each profile and each scenario separately can be found in Appendix E.
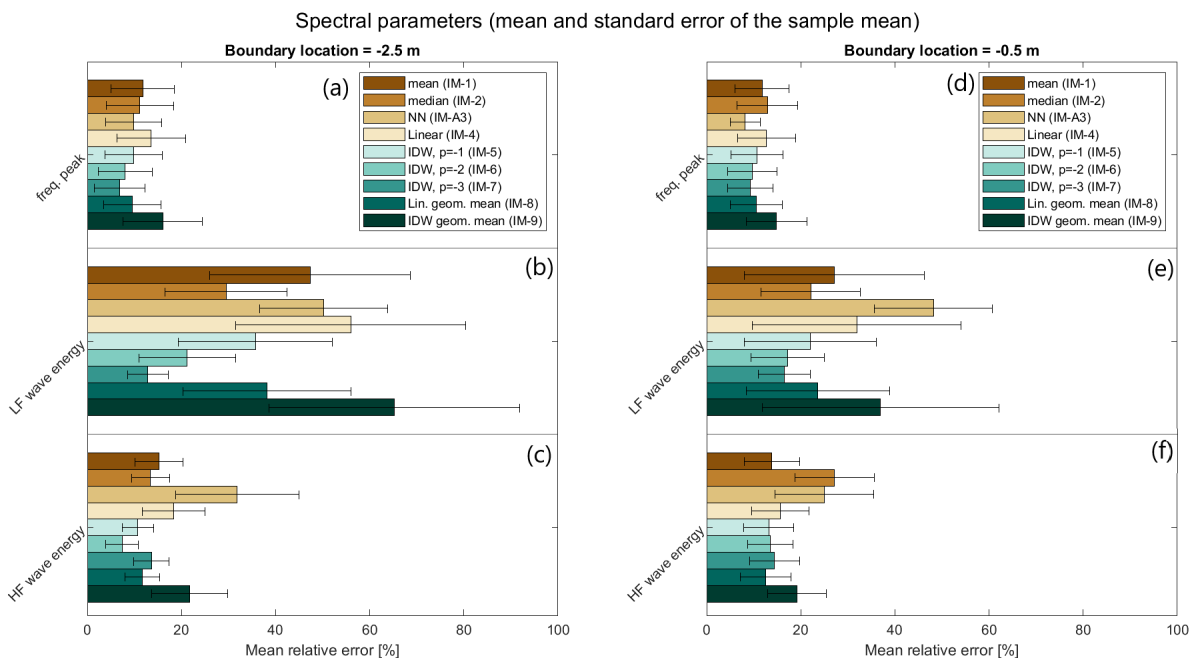
Figure 5.2: Mean and standard error of the sample mean of relative errors of predicted TMA+GAUSS spectral parameters that form the parameterized wave spectrum, consisting of frequency peak of HF part of the spectrum (a and d), LF wave energy (b and e) and HF wave energy (c and f) (see Section 3.4.1 for the description of the parameterization). Interpolated parameters are compared to the correct values of parameters. 9 different interpolation methods are compared (listed in Table 3.4, NN = Nearest Neighbour, IDW = Inverse Distance Weighting), each marked with different colour. Methods are applied to two boundary locations at the depths of -2.5 m (a, b and c) and -0.5 m (d, e and f). Standard error of the sample mean is calculated as 1.96-times the standard deviation and it represents the 95% confidence interval of the calculated mean.

Frequency peak is estimated with similar accuracy for all tested interpolation methods for both boundary locations (Figure 5.2 a and d). The mean error of prediction is between 10 and 20 %. The errors are highly dependent on the offshore wave conditions (i.e. scenarios) with mainly overestimation of frequency peak for swell and underestimation for storm, as observed in Figure E.1. Often the relative error of the frequency peak shows greater dependency on the reef profile and the offshore wave conditions, and not on the applied interpolation method.

---

[1]Standard error of the sample mean estimates how far the sample mean is likely to be from the population mean (Altman and Bland, 2005).

The relative error is generally much higher for LF wave energy (Figure 5.2 b and e) than for the frequency peak . The best accuracy can be achieved with IDW method with p=-3 for both boundary locations. Further from the shore, the interpolation methods are mostly overestimating the LF wave energy, whereas closer to the shore they are mostly underestimating it, as observed in Figure E.3.

HF wave energy (Figure 5.2 c and f) is generally better predicted than LF wave energy, but not as good as the frequency peak. Closer to the shore for most cases the amount of HF wave energy is underestimated, as observed in Figure E.2. No correlation is observed between the reef profiles and the amount of error as well as between the offshore wave conditions (scenarios) and the amount of error. The highest accuracy can be achieved with the IDW interpolation method with the power of p=-2.

Overall, the IDW method with p=-2 or p=-3 (IM-6 and IM-7 in Figure 5.2, respectively) was shown to be the optimal method for interpolating spectral parameters at the boundaries with depths of -2.5m and -0.5m. With this method applied, the expected relative error of prediction based on the sample mean for each spectral parameter can be up to 30%, but is often lower.

5.2   Interpolated wave setup

In order to accurately predict the water level at the boundary, wave setup must be interpolated. Wave setup at the considered boundary locations varies from negligible values in order of 1 mm to 1 cm (reef profiles with mild slopes and gentle swell conditions) to up to 40 cm (idealized reef profile with wide and shallow reef flat, Profile 526, for storm scenario close to the shore). Assessing the performance of the methods cannot be appropriately presented with relative errors, since the relative errors are consequently rather high for the cases where true setup is nearly zero (can be up to order of 1000%). Therefore, the errors in this section are calculated as the differences in predicted and true wave setup as $\Delta\eta = \eta_{\text{interpolated}} - \eta_{\text{true}}$ in [m]. Results per profile and scenario are depicted in Figure 5.3.
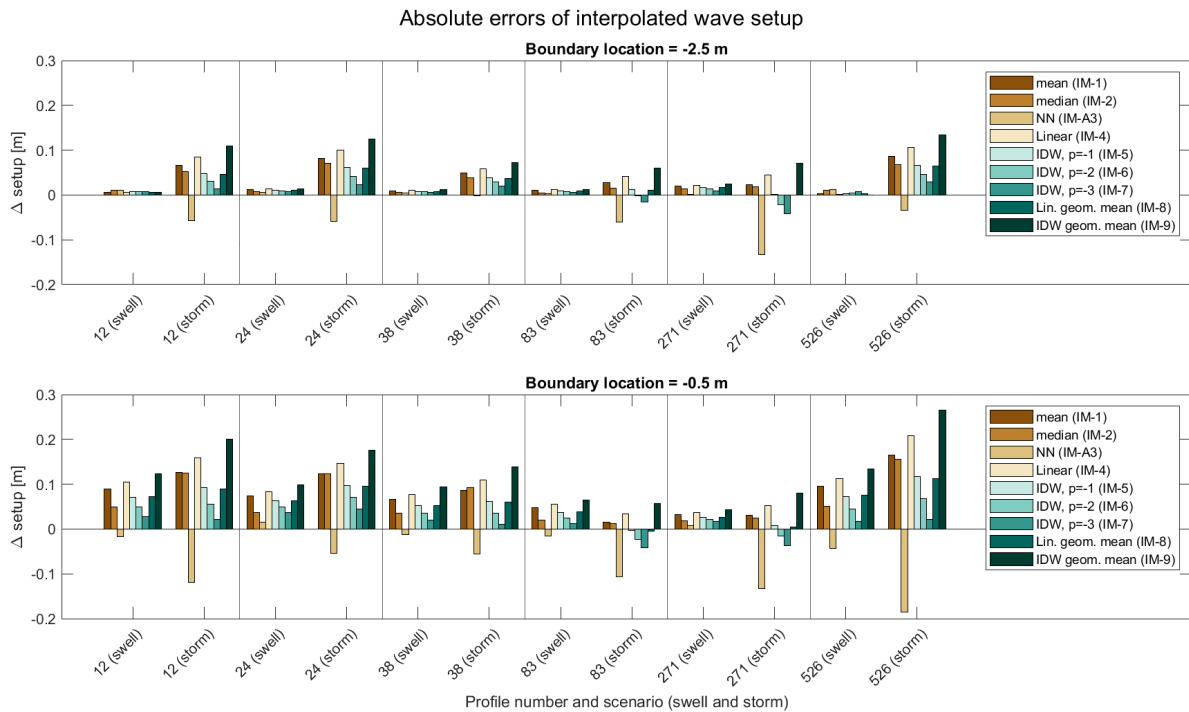
Figure 5.3: Errors of predicted wave setup computed as $\Delta\eta = \eta_{\text{interpolated}} - \eta_{\text{true}}$ per profile, for the two forcing scenarios (swell and storm). Interpolated wave setup values are compared to correct wave setup values. 9 different interpolation methods are compared (listed in Table 3.4, NN = Nearest Neighbour, IDW = Inverse Distance Weighting), each marked with different colour. Methods are applied to two boundary locations at depths of -2.5 m (top) and -0.5 m (bottom).

The wave setup is predominantly overestimated with all interpolation methods except for NN interpolation method. It is not expected that the NN interpolation method ideally predicts the wave setup, as the wave setup is highly dependent on the offshore wave conditions. Moreover, for the boundary location at a depth of -0.5 m a clear trend can be observed between the applied interpolation method and the value of Δ setup. This indicates that close to the shore the accuracy of the interpolation method to estimate the wave setup is independent of the bathymetric features of cross-shore profiles and of the offshore wave conditions.

Mean and standard error of the sample mean of Δ wave setup are depicted in Figure 5.4. Errors of estimated wave setup are higher for the boundary location at a depth of -0.5 m. This is expected, as the wave setup closer to the shore is generally higher. For both boundary locations the IDW interpolation method with the power of p=-3 performs with the highest accuracy. The expected mean error is between 1 cm and 3 cm.
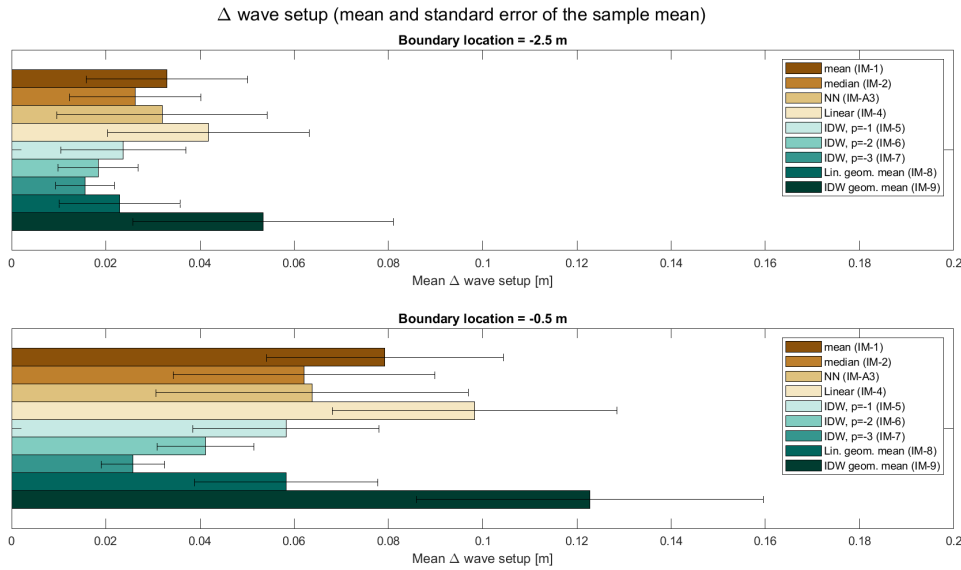
Figure 5.4: Mean and standard error of the sample mean of the errors of predicted wave setup computed as $\Delta\eta = \eta_{\text{interpolated}} - \eta_{\text{true}}$ per profile, for the two forcing scenarios (swell and storm). Interpolated wave setup values are compared to correct wave setup values. 9 different interpolation methods are compared (listed in Table 3.4, NN = Nearest Neighbour, IDW = Inverse Distance Weighting), each marked with different colour. Methods are applied to two boundary locations at depths of -2.5 m (top) and -0.5 m (bottom). Standard error of the sample mean is calculated as 1.96-times the standard deviation and it represents the 95% confidence interval of the calculated mean.

5.3 Errors in predicted runup

The main objective of analysing the performance of various interpolation methods is to find the method that introduces the least additional error of runup. Therefore, Section 5.3.1 deals with analysing the additional error of runup compared to the exact (parameterized) boundary conditions. Nevertheless, the outcome that is important for evaluating the overall developed method is the relative error of runup compared to the exact runup, simulated with full XB-NH+ model. This is analysed in Section 5.3.2.

5.3.1 Comparison with simulations with exact parametrized boundary conditions

In this section the runup simulated with each applied interpolation method is compared with runup simulated with the same model train where SFINCS is forced with the correct values of TMA+GAUSS parameters and wave setup at the boundary. The additional error due to the introduced interpolation at the boundary is calculated as the relative error of runup. The aim is to find a method that will result in the most similar runup estimates as if SFINCS was forced with the exact values of parameters at the boundary.

Runup errors per reef profile for both scenarios and both boundary locations are depicted in Figure 5.5. When the NN interpolation method is applied, the significant underestimation of runup of up to 20% can be observed for all profiles and all simulations. In Section 5.1 and Section 5.2 it was observed that with NN interpolation method HF wave energy, LF wave energy and wave setup were all underestimated for most cases[2]. Therefore, the underestimation of runup is expected.

Figure 5.5: Relative errors of runup per profile, for the two forcing scenarios (swell and storm). Predicted runup is compared with runup simulated with correct boundary conditions. 9 different interpolation methods are compared (listed in Table 3.4, NN = Nearest Neighbour, IDW = Inverse Distance Weighting), each marked with different colour. Methods are applied to two boundary locations at depths of -2.5 m (top) and -0.5 m (bottom).

Correlation between the offshore wave conditions (swell and storm scenarios) and the performance of interpolation methods is observed for the boundary location at a depth of -0.5 m, for the reef profiles with more pronounced reef flat, excluding the idealized profile. For swell scenario, the runup is underestimated, while for stormy conditions the runup is accurately predicted or overestimated. The opposite is observed for interpolation of frequency peak, as described in Section 5.1 and depicted in Figure E.1. A possible correlation can be detected: when the frequency peak is underestimated, the runup is overestimated, and vice versa. This, however, requires further analysis with more reef profiles and more offshore wave scenarios, as other factors can play a role as well.

An apparent overestimation of runup is observed for the idealized reef profile (Profile 526) with up to 20% relative error of runup. At first sight, this is counter-intuitive as in sensitivity analysis, Chapter 4, the runup over the idealized profile was calculated with the highest accuracy. However, these results indicate that SFINCS is sensitive to its input at the boundary. Overestimation of wave setup, as seen in Figure 5.3, and overestimation of LF wave energy, as seen in Figure E.3, are observed for the idealized reef profile. This can partially be the reason for the overestimation of runup. Detailed investigation on the influence of each interpolated parameter to the final runup is furthermore described in Section 5.4.

Mean relative errors of runup and the associated standard errors of the sample means are depicted in Figure 5.6. IDW method with p=-2 performed with the highest accuracy, resulting in 2-7% mean error of runup. A link between the performance of the method at the boundary and the resulted runup prediction is observed. Although the most accurate method for the interpolation of parameters at the boundary was IDW method with the power of

---

[2]Note that the underestimation most probably occurred because the nearest neighbouring (NN) simulation for both studied scenarios had less intense offshore wave conditions than the target offshore conditions. It can also happen that the resulting NN simulation has more intense offshore conditions and thus the over-estimation of the parameters can occur.

p=-3, it was followed by the IDW method with p=-2.

NN interpolation method resulted in the largest mean relative error of runup for both boundary locations with mean error of up to 10% higher compared to other interpolation methods. Looking back at results of interpolated parameters at the boundary, this outcome can only be directly linked to the poor interpolation of LF and HF wave energy values with NN interpolation method, depicted in Figure 5.2.
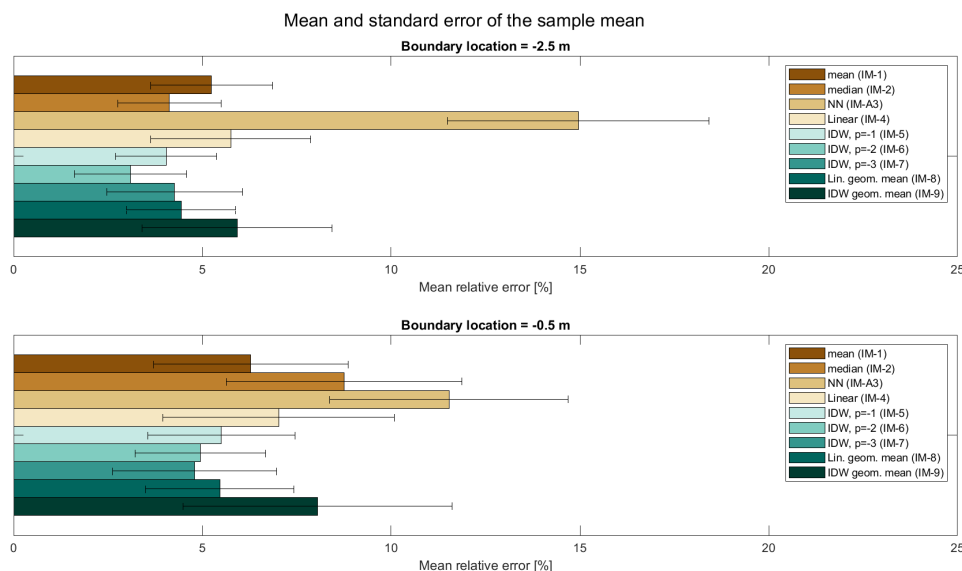
Figure 5.6: Mean and standard error of the sample mean of the relative errors of runup. Predicted runup is compared with runup simulated with correct boundary conditions. 9 different interpolation methods are compared (listed in Table 3.4, NN = Nearest Neighbour, IDW = Inverse Distance Weighting), each marked with different colour. Methods are applied to two boundary locations at depths of -2.5 m (top) and -0.5 m (bottom). Standard error of the sample mean is calculated as 1.96-times the standard deviation and it represents the 95% confidence interval of the calculated mean.

5.3.2   Comparison with full XBeach-NH+ simulations

SFINCS simulations forced with 1) exact wave and water level conditions from an XB-NH+ run and 2) interpolated wave and water level conditions from the XB-NH+ LUT are compared to full XB-NH+ simulations. Note that all simulations with SFINCS are performed with a parameterized spectrum (BT method 3), therefore they all lack phase information at the boundary. The resulting relative errors in runup prediction are depicted in Figure 5.7. The yellow colour represents the relative runup error simulated with SFINCS forced with the exact wave and water level conditions. All other colours are linked to the applied interpolation methods.

Runup is underestimated for most cases. This corresponds to the results from the sensitivity analysis (Chapter 4). NN interpolation once again attracts attention with its consistent underestimation of runup for nearly all cases.

Contrary to sensitivity analysis, runup is significantly inaccurately predicted for the idealised reef profile (Profile 526) with relative error of up to 25% when interpolation is applied, but also very high with no interpolation (15% underestimation for the swell scenario close to the shore). Idealised reef profile is more sensitive to interpolation compared to other reef profiles. This can be explained by the poor interpolation of wave setup. The idealized reef profile resulted in 40 cm of wave setup for stormy conditions at the boundary depth of -0.5 m. Figure 5.4 shows that 5 out of 9 interpolation methods (over)estimated wave setup by at least 15 cm for that case. The exact same interpolation methods also (over)estimated the runup, seen in Figure 5.7.
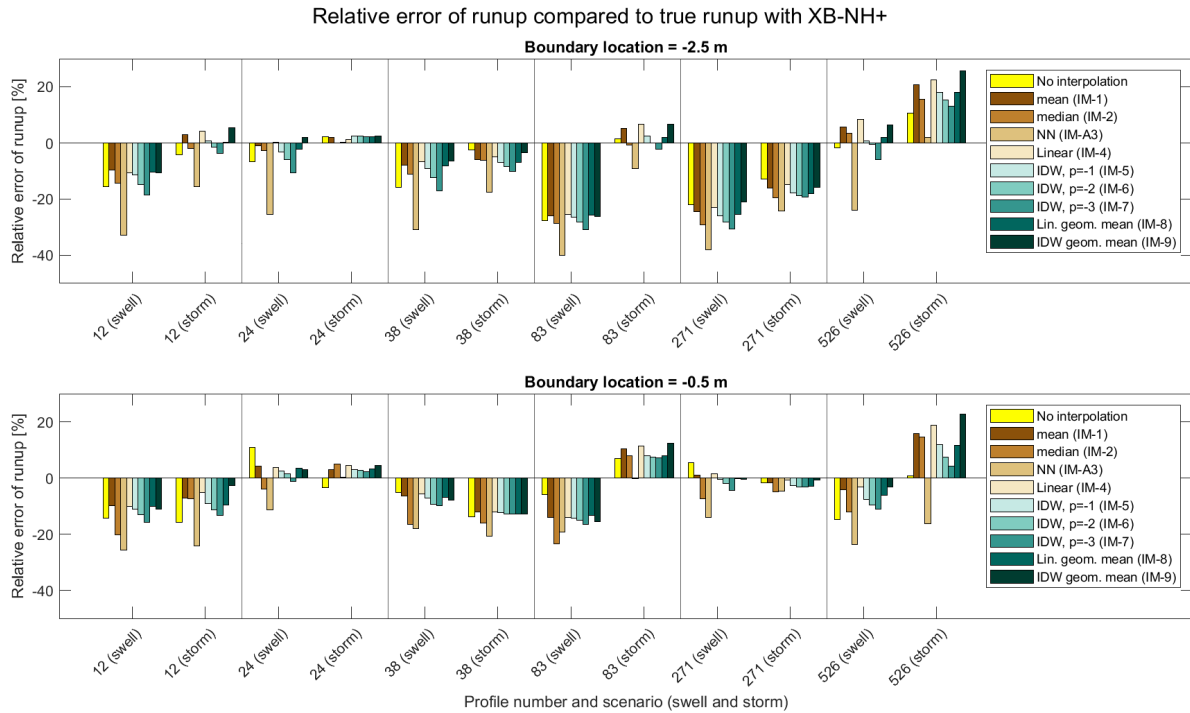
Figure 5.7: Mean and standard error of the sample mean of the relative errors of runup. Predicted runup is compared with runup computed with full XBeach-NH+ simulations. 9 different interpolation methods are compared (listed in Table 3.4, NN = Nearest Neighbour, IDW = Inverse Distance Weighting), each marked with different colour. The yellow colour represents the relative runup error for the SFINCS simulation forced with the correct TMA+GAUSS spectral parameters and the correct wave setup. Methods are applied to two boundary locations at depths of -2.5 m (top) and -0.5 m (bottom).

Mean relative errors of runup and the associated standard errors of the sample means are depicted in Figure 5.8. NN interpolation method performed with the lowest accuracy for both boundary locations, whereas all other methods are comparable with the simulations applying the exact (parameterized) boundary conditions. The comparable performance of interpolation methods can be explained by the amount of energy forced at the boundary. Section 5.3.1 showed that for some cases (e.g. steep reef profile, Profile 12, with the boundary at a depth of -0.5 m) runup was over-predicted compared to runup simulated with SFINCS forced with correct boundary conditions. At the same time the amount of LF wave energy (Figure E.3) and the wave setup (Figure 5.3) were over-predicted as well. On the other hand, HF wave energy (Figure E.2) was under-predicted. It is possible that forcing SFINCS with higher amount of LF wave energy, lower amount of HF wave energy and a higher wave setup compensated for the errors made due to lack of phase information at the boundary and neglected processes within the SFINCS model.

Relative errors of runup are decreasing with decreasing depth at the boundary from 10% for the -2.5 m boundary depth, to around 7.5% for the -0.5 m boundary depth. Similar characteristics were already observed in the sensitivity analysis (Chapter 4). These results indicate that as long as the appropriate interpolation method is applied, it is no longer the main source of error. The main sources of error are in the reduced physics in SFINCS, as already explained in the sensitivity analysis (Chapter 4).
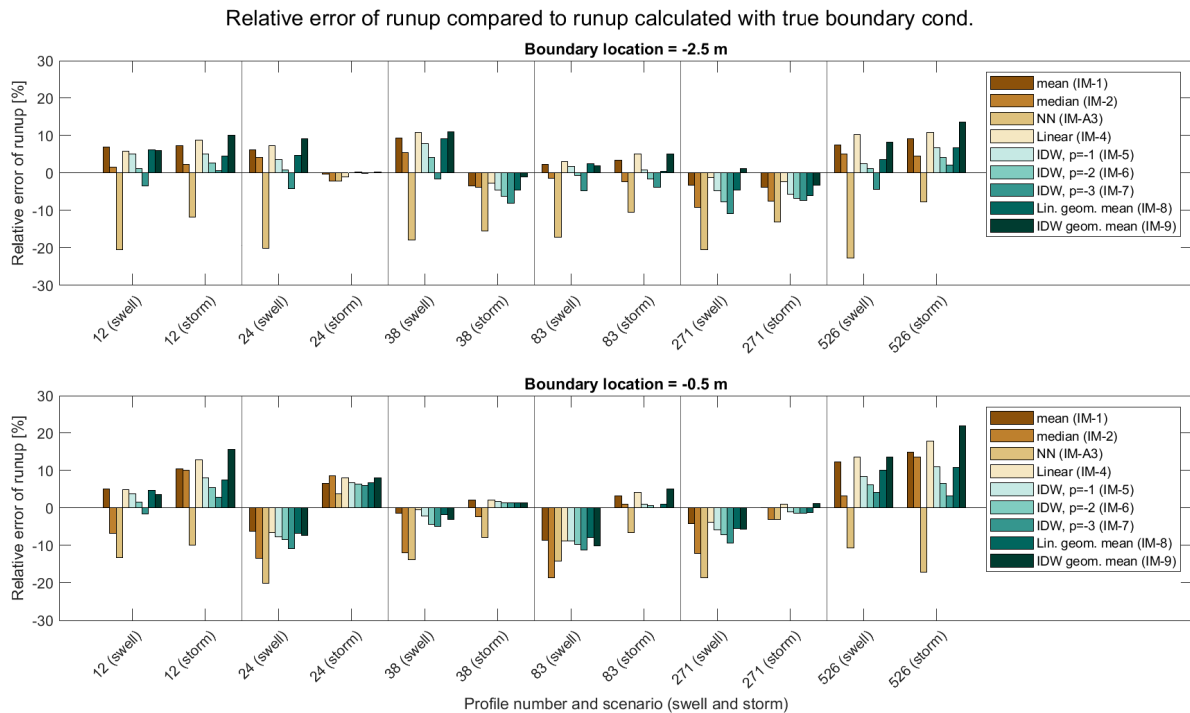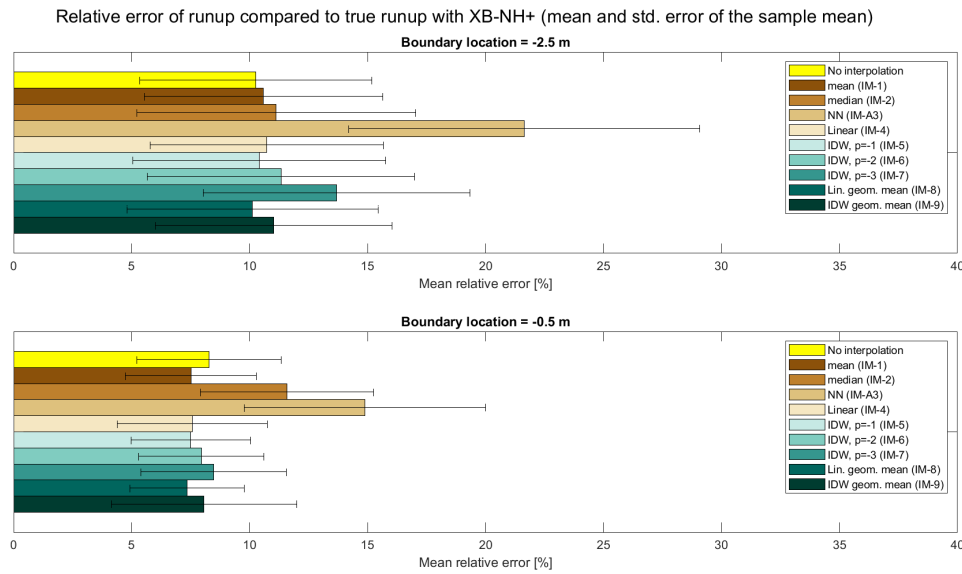
Figure 5.8: Relative errors of runup per profile, for the two forcing scenarios (swell and storm). Predicted runup is compared with runup computed with full XBeach-NH+ simulations. 9 different interpolation methods are compared (listed in Table 3.4, NN = Nearest Neighbour, IDW = Inverse Distance Weighting), each marked with different colour. The black colour represents the relative error of runup for the SFINCS simulation forced with the correct TMA+GAUSS spectral parameters and the correct wave setup. Methods are applied to two boundary locations at depths of -2.5 m (top) and -0.5 m (bottom). Standard error of the sample mean is calculated as 1.96-times the standard deviation and it represents the 95% confidence interval of the calculated mean.

5.4 Sensitivity of interpolated parameters

Multiple additional simulations were performed in order to investigate how sensitive is the final runup to each interpolated TMA+GAUSS spectral parameter and the wave setup separately. This was performed by *semi-interpolating* the parameters at the boundary, i.e. by interpolating each parameter individually, while the other parameters have the exact values. The simulations and their characteristics are listed in Table 5.1. By separating the influence of each parameter it is possible to identify which interpolation method is the best for estimating each parameter. Depending on the outcome of the analysis, customised interpolation can be applied for each parameter to increase the accuracy of the runup prediction.

Runup resulted from each test simulation is compared with runup simulated with the same model setting where SFINCS is forced with the correct values of all TMA+GAUSS parameters and wave setup at the boundary. Therefore, the additional runup error resulting from the interpolation of each parameter can be detected independently. Mean relative errors of predicted runup and the associated standard errors of the sample means of test simulations are depicted in Figure 5.9.

The interpolated value of wave setup at the boundary depth of -2.5 m has a very small influence on the final runup estimation (mean error of runup up to 3%), regardless of the interpolation method. This can be observed for the test simulations IMB (spectrum) as well as for the IMC (wave setup). The wave setup at that boundary location is generally low for the applied scenarios, compared to wave setup closer to the shore. For the swell scenario, all profiles have a wave setdown of up to 2 cm at that location, or lower. As shown in Figure 5.4 (Section 5.2), the performance of all interpolation methods was more accurate for the boundary location at a depth of -2.5 m as well. On the other hand, wave setup is less accurately predicted for the boundary location closer to the shore, where larger errors of relative runup are observed as well (Figure 5.9, right). Higher values of wave setup are observed there too. Following these observations, the interpolation of wave setup is more important for boundary locations where the values of wave setup are larger, as already concluded in Section 5.2. Moreover, just like in Section 5.2, the runup is best predicted with IDW interpolation method with the power of p=-3.

Table 5.1: List of test simulations in order to investigate the influence of each interpolated parameter to the final runup estimation. IMA (all-original) case is the case with all the parameters interpolated and detailed results are shown in the previous sections. All other cases have some parameters interpolated and some exact, as calculated with the XBeach-NH+ model with the target offshore wave and water level conditions.

| Name	Frequency peak	HF wave energy	LF wave energy	wave setup
IMA all-original	interpolated	interpolated	interpolated	interpolated
IMB spectrum	interpolated	interpolated	interpolated	exact
IMC wave setup	exact	exact	exact	interpolated
IMD freq. peak	interpolated	exact	exact	exact
IME HF energy	exact	interpolated	exact	exact
IMF LF energy	exact	exact	interpolated	exact
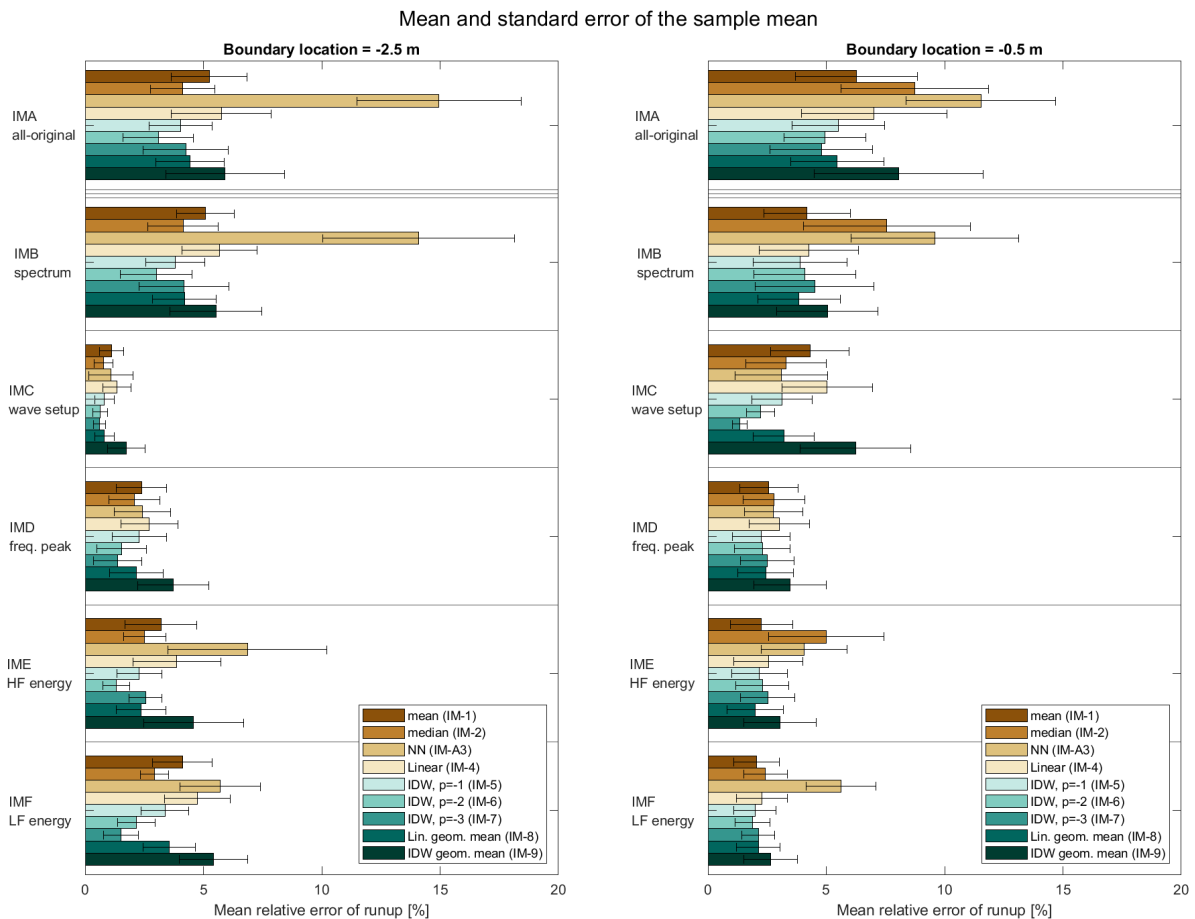
Figure 5.9: Mean and standard error of the sample mean of the relative errors of runup. Predicted runup is compared with runup simulated with correct boundary conditions. 6 different test simulations are compared (rows). Their name indicates the parameters at the boundary that are interpolated. All other parameters are exact. Within each test simulation, 9 different interpolation methods are compared (listed in Table 3.4, NN = Nearest Neighbour, IDW = Inverse Distance Weighting), each marked with different colour. Methods are applied to two boundary locations at depths of -2.5 m (left) and -0.5 m (right). Standard error of the sample mean is calculated as 1.96-times the standard deviation and it represents the 95% confidence interval of the calculated mean.

Interpolation of all TMA+GAUSS spectral parameters has an important role in the final runup estimation. The mean of the relative errors of runup when only one of the parameters is interpolated (test cases IMD-freq. peak, IME-HF energy and IMF-LF energy) varies between 2 and 7% depending on the applied interpolation method. Each TMA+GAUSS spectral parameter has an equal importance in the accuracy of the final runup prediction. Moreover, IDW interpolation method with the power of either p=-2 or p=-3 performs with good accuracy and often outperforms other methods (e.g. at the boundary at a depth of -2.5 m for the test cases IME-HF energy and IMF-LF energy).

5.5 Discussion

In this section the interpretation of results is discussed. By combining the results from the analysis of the interpolation methods (Chapter 5) with the results from the sensitivity analysis (Chapter 4), the most optimal method can be determined. The optimal method consists of the most accurate interpolation of boundary conditions and the best suitable boundary location for forcing SFINCS. This method is model-specific, i.e. it is appropriate when the wave-driven modeling is performed with the LUT that is used in this analysis and with the reduced-physics model SFINCS or another model with similar characteristics. If another model and/or another LUT is used, the sensitivity analysis is required in order to achieve the desired accuracy.

The most accurate interpolation method

The primary purpose of the analysis of interpolation methods is to find a method that can approximate the TMA+GAUSS spectral parameters and the wave setup with the acceptable accuracy at the boundary in order to accurately simulate runup (and thus accurately predict the coastal flooding). The interpolated parameters at the boundary are used to generate the new water level time series that serve as the boundary conditions for forcing SFINCS. The IDW interpolation with the Euclidean distance and the power of p=-3 resulted in the most accurate estimation of spectral parameters and wave setup, as seen in Section 5.1 and 5.2. By applying this interpolation method, the boundary conditions can be as close to the desired conditions as possible, aiming towards the conditions obtained with the reference model XB-NH+. Consequently, the spectral parameters can be predicted with less than 20% error on average and the wave setup can be predicted with less than 4 cm difference on average from the wave setup, calculated with the reference model XB-NH+. Logically, the accuracy of runup prediction would be increased with increased accuracy of parameters at the boundary. But, is it this straightforward?

A link is indeed observed between the good prediction of parameters at the boundary and the lower relative errors of runup when comparing the runup simulated with the interpolated parameters to the runup simulated with the correct parameters at the boundary (comparing Figures 5.2 and 5.4 to Figure 5.6). Relative errors of runup are in fact the lowest for the IDW interpolation method with Euclidean distance and a power of p=-2 or p=-3; same method that predicts the parameters at the boundary with the best accuracy. However, that does not necessarily lead to the most accurate runup estimates when compared to the runup simulated with the reference model XB-NH+. In fact, only the NN interpolation method showed a direct link between the accuracy of the interpolated parameters at the boundary and the accuracy of the resulted runup. Note that this is the method that performed poorly for most cases. All other methods are comparable to each other when only the final runup is considered, referred to Figure 5.8.

In sensitivity analysis (Chapter 4) it was already demonstrated that by using the XB-NH+ LUT till the boundary, parameterizing the given spectrum at the boundary and generating random time series that are used as input for SFINCS, the relative errors in runup prediction are on average between 10 and 20% and can be up to 60% depending on the boundary location, offshore wave conditions and the reef profile characteristics. The good runup predictions are therefore not only dependent on the correct amount of energy put into the system, but also on the other processes neglected by the reduced-physics model. Therefore, putting the right amount of energy into the system does not necessarily lead to better final results. This can be illustrated with the performance of the method *mean*, the simplest interpolation method. As seen in Figure 5.8 for boundary location at a depth of -0.5 m, this method resulted in lower errors of runup prediction compared to the simulations where the correct amount of energy was put into the system (i.e. simulations without interpolation). The *mean* interpolation method particularly stood out with its over-prediction of wave setup (Figure 5.4), whereas LF wave energy was not ideally predicted either (Figure 5.2). This difference in interpolated and exact amount of energy, and the

increased wave setup probably compensated for the errors (instead of increasing them) that are introduced with the use of reduced-physics model SFINCS. The method therefore resulted in a good runup prediction despite the errors introduced at the boundary.

In general, no evident link is observed between the amount of over- or under-predicted TMA+GAUSS spectral parameters (Figure 5.2) at the boundary and the reduced overall error of runup (compared to full XB-NH+ simulations, Figure 5.8). However, the over-prediction of the wave setup could potentially cause the decreased errors of runup prediction. *How?* In sensitivity analysis (Chapter 4) it was shown that runup is mostly under-predicted. By introducing the higher wave setup at the boundary close to the shore, the mean water level is increased and consequently the runup is increased as well.

Results introduced in Section 5.1 and Section 5.2 suggest that the IDW interpolation with Euclidean distances and a power of p=-3, followed by the power of p=-2, leads to the most accurate prediction of the spectral parameters and the wave setup at the boundary. However, the results in Section 5.3.2 suggest that the IDW interpolation with Euclidean distances and a power of p=-1 or p=-2 lead to slightly better prediction of runup compared to the same method with the power of p=-3[3]. Here, the accuracy is calculated based on how well is the runup estimated compared to the runup simulated with the full XB-NH+ model. Since the runup is a common measure of flooding, it is important that it is estimated with the highest possible accuracy. With this in mind, **the most optimal method to interpolate the boundary conditions from the XB-NH+ LUT for forcing SFINCS is the IDW interpolation with Euclidean distances and a power of p=-2.**

The errors of the resulted runup could potentially be different when the method is applied to another reduced-physics model with different assumptions from those in SFINCS. This is because, as already mentioned before, the accuracy of runup is in large part dependent on the processes neglected by the reduced-physics model. In order to propose a more generalised method, the focus should be in estimating the boundary conditions as accurately as possible while keeping the errors of runup prediction acceptably low. In that case, a more appropriate method is the IDW interpolation method with Euclidean distances with the power of p=-3.

How important is the interpolation of wave setup?

Wave setup generally increases with decreasing distance from the shore. In front and around the break-point it is even negative, the phenomenon named setdown. The location of a break-point and the amount of setdown are dependent on the offshore wave and water level conditions. Therefore, there will always be different values of setup (setdown), obtained from XB-NH+ LUT, that need to be interpolated. However, the absolute values of setdown are usually lower than the values of setup close to the shore. Consequently, the setup can be more accurately predicted further from the shore, as was the case in Figure 5.4. In fact, most of the correct values of setup at the boundary location at a depth of -2.5 m for the considered scenarios were negative (i.e. setdown was observed). By either increasing offshore water level or decreasing offshore wave conditions, the error of wave setup is expected to decrease as well. Note, however, that the absolute errors of wave setup (i.e. Δ wave setup) are considered. It is *logical* that the absolute errors are lower when the interpolation is performed over lower values of setup from the XB-NH+ LUT. Nevertheless, the preferred location for interpolation of wave setup is still further from the shore.

The accuracy of predicted wave setup is highly important for the accurate prediction of runup because it determines the initial mean water level of the SFINCS domain and the constant mean water level at the boundary. Even if the errors of predicted wave setup are not significantly large (in order of cm), it can still have considerable consequences on the wave transformation and dissipation of wave energy towards the shore. After all, these processes are dependent on the water level. It is therefore important to handle the interpolation of wave setup with great care, especially when setting a boundary close to the shore.

Re-evaluating the optimal boundary location

The largest influence of the boundary location is observed in interpolation of wave setup. The preferred location for interpolation of wave setup is further from the shore, based on the analysis of the interpolation methods.

---

[3]Of course, other interpolation methods performed with good accuracy as well, but since the IDW interpolation is accurate at predicting the boundary conditions, this method is desired. The question is, which power is the most appropriate.

Different conclusions can be drawn from the sensitivity analysis. The test case (Section 4.2) revealed that the wave setup was not simulated well across the shore with SFINCS when SFINCS was forced at the boundary location at greater depths, including a depth of -2.5 m. Variance across the shore is better captured with SFINCS forced closer to the shore as well. Moreover, the resulting runup is better estimated when SFINCS is forced at a depth of -0.5 m (Figure 5.8). By taking all these factors into the consideration, **in the current XB-NH+ LUT – SFINCS couple the most optimal boundary location is at a water depth of -0.5 m.**

It should be emphasized that these observation can only apply to physics-reduced models that are based on the same or similar equations as SFINCS. The optimal boundary location is therefore model-specific. By making the method more general and model-neutral, the accurate interpolation of parameters at the boundary should be a primary source of the decision. In that case, the wave setup and the TMA+GAUSS spectral parameters are better predicted further from the shore at a water depth of -2.5 m.

5.6   Conclusion

Analysis of the interpolation methods gave insight on the importance of correctly estimated boundary conditions for forcing SFINCS. Three aspects of interpolation were studied. First, the accuracy of interpolated spectral parameters and wave setup was calculated. Next, the performance of SFINCS with interpolated boundary conditions was assessed with relative errors of runup. This was performed by assessing (a) the additional error of runup introduced by the interpolation and (b) the final error of runup as a result of the overall methodology, which consists of parameterization, interpolation and the use of physics-reduced model SFINCS. Finally, an attempt is made to estimate how important is the accurate interpolation of each parameter at the boundary.

A link between the performance of the interpolation method at the boundary and the resulted runup prediction is observed. The most optimal method to simulate the runup by interpolating the boundary conditions (the TMA+GAUSS spectral parameters and the wave setup) is the IDW interpolation method with Euclidean distances and a power of p=-2. The wave setup is better predicted when the boundary location is at greater depths (in the tested case at a depth of -2.5 m). In the current XB-NH+ LUT – SFINCS couple the most optimal boundary location is at a water depth of -0.5 m.

Validation of results with the reference model XB-NH+ revealed that by applying interpolation at the boundary, the accuracy of the method is comparable with the accuracy of applying the exact boundary conditions. Together with the findings from the sensitivity analysis (Chapter 4) it is confirmed that the reduced physics in SFINCS is the primary source of error. The average error of runup when interpolated parameterized boundary conditions are applied at the boundary location at a water depth of -0.5 m is around 10%.

6

Discussion: a critical view on the developed methodology

The methodology developed in this thesis opens new opportunities for simulating and forecasting flooding on coral reef-lined coasts around the globe. The course of the research was primarily focused on the accuracy and computational efficiency of the method within the boundaries of the method itself. At the same time, the method was tested for different reef bathymetries and offshore wave and water level scenarios. The application on a more global scale was thus assessed. A critical view of the applied approach to tackle these challenges is discussed in Section 6.1.

Besides the limitation of the developed method itself (e.g. the accuracy of the reduced-physics model SFINCS), other constraints of the method need to be addressed as well. In Section 6.2, these constrains are described together with their possibilities of improvement.

6.1   Approach to the problem

The main goal of this research is to develop a methodology to model wave-driven flooding on coral reef-lined coasts in a fast and efficient way. One of the prospects of this methodology is to implement it into a flood risk assessment tool that can be applicable on a global scale. With this in mind, the following question was driving the course of the research: *Can the method be valid for different coral reef morphologic types and hydrodynamic regimes?*

The attempt to create a method which can be generalized to an arbitrary reef morphology and arbitrary offshore wave and water level conditions was realised in two steps: (1) by using the XB-NH+ LUT that consists of a large number of representative reef profiles and a large number of offshore wave and water level conditions and (2) by testing the sensitivity of the method on conceptual cases with various characteristics.

A design of conceptual cases was limited to six reef profiles and two offshore wave scenarios. Results show that a variety of hydrodynamic regimes were captured with conceptual cases. The interpretation of results based on different reef profiles and different offshore conditions is included in Section 6.1.1 and Section 6.1.2, respectively. Another goal of this research is to develop a method that is computationally efficient. A balance between the cost and accuracy was achieved primarily by applying simple computationally efficient methods while assessing the accuracy. This aspect is further discussed in Section 6.1.3.

6.1.1   Chosen reef profiles

A complexity of coral reef bathymetric profiles is recognized based on the work by Scott et al. (2020) and Roelvink (2019). Consequently, hydrodynamic processes along the reef differ considerably between the reef profiles. The challenge to develop a generalized method that can be applicable to a larger number of coral reefs around the globe was tackled with conceptual cases. Five reef profiles were chosen from Scott et al. (2020)'s database consisting of real measured bathymetries from Puerto Rico, United States Virgin Islands, Florida and Hawaii. The five profiles can be divided in two subsets based on their bathymetric features and consequently on the magnitude of their runup (depicted in Figure 6.1 (a)). The two subsets are (1) Profiles 12, 24 and 38 that have deep and narrow reef flat and/or steep fore-reef (Figure 6.1, row (b)) and (2) Profiles 83 and 271 that have wide and shallow reef flat and/or mild fore-reef slope (Figure 6.1, row (c)). The subset from row (b) in Figure 6.1 results in larger magnitude of runup compared to the subset from row (c) for the same offshore wave conditions.

The two subsets of the five studied reef profiles differ in their bathymetric features and their hydrodynamic response to the offshore wave conditions. Sensitivity analysis (Chapter 4) revealed that despite these differences, the two subsets are similar in four aspects. (1) All reef profiles that include reef flat (therefore excluding Profile 12) perform better when forced at the boundary location landward from the reef flat. (2) This is connected to the amount of sea-swell nonlinearities at the offshore boundary of SFINCS (defined with the ratio H_{ss}/d). Typical values of H_{ss}/d are present landward from the reef flat. The values of H_{ss}/d differ between the studied reef profiles when the same offshore conditions are applied. However, they often increase with decreasing distance from the shore. The errors of runup also generally decreases with increasing values of H_{ss}/d at the offshore boundary of SFINCS (and thus with decreasing distance from the shore). (3) SFINCS generally underestimates the amount of runup regardless of the reef profile. (4) The errors of runup decrease with increasing offshore water level regardless of the reef profile. All these similarities suggest that the different reef profiles react similarly to the developed methodology. Thus, **the method has a potential to be applied to an arbitrary reef profile**. However, in order to be confident with this conclusion, the method needs to be further tested on a larger number of reef profiles from Scott et al. (2020)'s database.

Sensitivity analysis (Chapter 4) also revealed some differences among the two subsets of the reef profiles. Reef profiles from the first subset (Profiles 12, 24 and 38 in row (b) in Figure 6.1) perform better when forced at the boundary location that is further from the shore compared to the reef profiles form the second subset (Profiles 83 and 271 in row (c) in Figure 6.1). This information is not convenient, because in reality comparison between the profiles is often unavailable. Therefore, a more general rule is to determine the boundary location at a depth of -0.5 m (based on the offshore water level of 0 m). This conclusion is supported with the sensitivity analysis (Chapter 4) and the analysis of interpolation methods (Chapter 5).
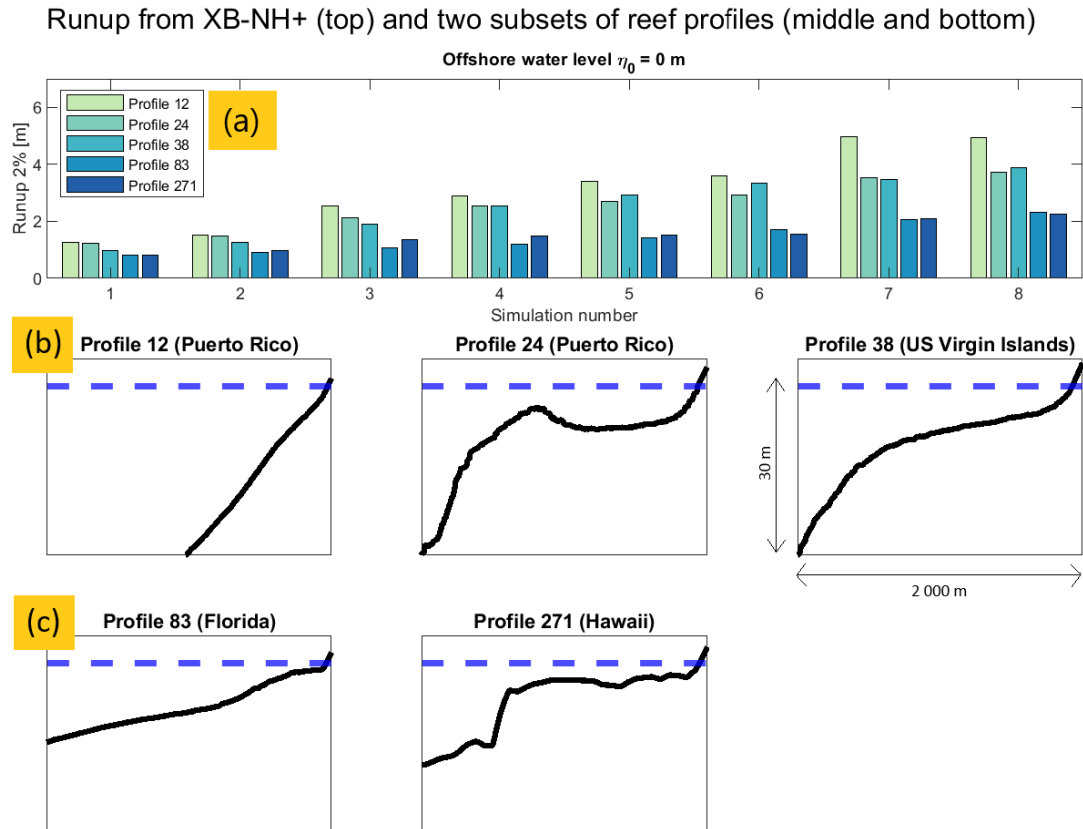
Figure 6.1: (a) Runup calculated with the reference model XB-NH+ for each of the 8 offshore wave conditions and offshore water level of $\eta_0 = 0$ m (simulations on x-axis where 1-4 corresponds to swell and 5-8 corresponds to stormy conditions; the full list of simulations can be found in Table 3.3). (Row b) Profiles 12, 24 and 38 that have deep and narrow reef flat and/or steep fore-reef slope. (Row c) Profiles 83 and 271 that have wide and shallow reef flat and/or mild fore-reef slope. The five profiles are taken from Scott et al. (2020)'s database consisting of real measured bathymetries from Puerto Rico, United States Virgin Islands, Florida and Hawaii. All profiles on the figures show 2 km width (x-axis) and 30 m depth (y-axis), as demonstrated on Profile 38.

Besides the five realistic reef profiles, one simplified reef profile (Profile 526) from Pearson et al. (2017)'s research was tested as well. Two valuable outcomes resulted from the analysis of this profile. First, sensitivity analysis (Chapter 4) showed that SFINCS performed with the highest accuracy when implemented on the simplified reef profile. Second, analysis of interpolation methods (Chapter 5) revealed that when interpolation is applied, the simplified profile no longer resulted in the least error (compared to other reef profiles). While the simplified reef profile was not particularly sensitive to the parameterization of wave spectra at the boundary, it was more sensitive to the interpolation at the boundary. In order to draw general conclusions, the simplified reef profile should be compared to the observed reef profile with similar characteristics (e.g., reef flat width and depth, fore-reef slope). However, the aim of this study is not to simplify the method even further. Since the XB-NH+ LUT consists of the observed reef profiles, the benefits of this feature are acknowledged. In reality, the newly observed reef bathymetry will likely match (one or more) measured reef bathymetries from Scott et al. (2020)'s database. Simplified reef profiles are not essential for further development of the method.

A general conclusion, drawn from a set of reef profiles and shown sensitivity analysis (Chapter 4, particualry in Section 4.3.1) is that **dissipative coastlines lead to more accurate prediction of wave-driven flooding** when SFINCS is forced close to the shore and the mean sea water level is low (0 m in the studied case). In this study, dissipative coastlines are defined as the coastlines that dissipate large amounts of wave energy on their wide and shallow reef and/or gentle fore-reef slope (profiles from the second subset in row (c) in Figure 6.1). Closer to the shore a lot of wave energy is already dissipated (especially when the mean sea water level is low as well). Therefore, the boundary location at a depth of -0.5 m is after the wave breaking. The wave breaking is a complex process. SFINCS does not account for dispersion and under-estimates skewness (seen in Section 4.2). Consequently, it does not accurately simulate wave breaking (supported with the cross-section of the variance in Figure 4.11). If all these processes are captured with the advanced model XB-NH+ in the LUT across the shore,

SFINCS is left with the boundary conditions that consist of a (large) value of wave setup and small amounts of the remaining wave energy near the coast. The predictions of runup are consequently more accurate as if SFINCS was forced with more energetic boundary conditions. This outcome is encouraging because the most typical reefs are in fact highly dissipative. Atoll islands are a good example, where facing the problem of flooding is the government's highest priority. An example is a simulation of coastal flooding for the combination of a low tide and highly energetic swell waves on reefs with wide and shallow reef flats.

6.1.2   Chosen offshore conditions

Wave-driven flooding on coral reef-lined coasts can occur due to waves with various combinations of significant wave height and peak wave period propagating from the offshore towards the shore (Ford et al., 2018). The characteristics of waves generated offshore are responsible for hydrodynamics regimes that develop on the reef profile. Two typical offshore wave conditions were chosen for conceptual cases: gentle swell and stormy conditions. The differences in results for these two scenarios revealed that the developed method is sensitive to offshore conditions.

In sensitivity analysis (Chapter 4), each offshore scenario resulted in 8 different combinations of offshore wave and water level conditions; in total 16 different combinations. This approach was chosen because it was convenient to apply sensitivity analysis on the offshore wave conditions which are going to be interpolated in the analysis of interpolation methods. Consequently, sensitivity analysis did not give any insight into a large number of various offshore scenarios. However, sensitivity analysis revealed that often the accuracy of the method is higher for stormy conditions as opposed to swell conditions. There is also an indication that the accuracy of the method increases with increasing offshore water level. Figure 4.19 (Section 4.3.3) showed that the accuracy of the method increased from the average error of runup of 20% for the offshore water level of 0 m to 10% for the offshore water level of 1 m. This outcome is encouraging because more intense offshore conditions lead to a higher risk of coastal flooding, so it is most critical that our method is accurate under these conditions. To back up the preliminary conclusions based on sensitivity analysis, future research should consider applying the method to a larger set of offshore scenarios.

6.1.3   Computational efficiency of the method

A computationally efficient method is primarily achieved by combining the physics-reduced model SFINCS with a look-up-table consisting of pre-run simulations with the advanced model XB-NH+ (i.e. XB-NH+ LUT). The first two steps towards the computational efficiency were achieved through the sensitivity analysis (Chapter 4): (1) parameterized boundary conditions gave almost as accurate results as the correct boundary conditions; and (2) the boundary location close to the shore is both computationally efficient and an accurate option. Because the outcome of the sensitivity analysis was positive, no other computationally more demanding methods were tested (e.g. machine learning techniques).

Interpolation at the boundary was primarily performed using methods with very low computational demand. Throughout the analysis of interpolation methods (Chapter 5), a majority of the methods resulted in an accurate prediction of spectral parameters and wave setup at the boundary and accurate prediction of resulting wave runup. When runup simulated with interpolated values at the boundary was compared to the runup simulated with the exact values at the boundary (Section 5.3.2) the accuracy was comparable (averaged relative error of runup around 10% for both cases, shown in Figure 5.8). As a result, the IDW interpolation method was shown to be accurate. Therefore, there was no need to test other more computationally demanding methods (e.g., kriging).

Overall results showed that **by applying parameterization and interpolation at the boundary, the accuracy of the method is comparable with the accuracy of applying exact boundary conditions**. The use of the physics-reduced model SFINCS is therefore the main source of errors.

6.2 Constrains of the method

The developed methodology is both computationally efficient and accurate with the main source of error arising from the use of the physics-reduced model SFINCS. These errors are acceptable as long as the user is aware of them. The method could be further improved by improving the parameterization at the boundary, e.g., by analysing the best cut-off frequency between LF and HF parts of the spectrum, or by improving the interpolation at the boundary by further exploring the most optimal interpolation method. However, the results showed that the developed method is adequate for the intended applications.

Other, less obvious limitations of the method need to be addressed in order to understand the boundaries of applicability of the method and the possibilities of improvement. These include the limitations of capturing of hydrodynamic regimes (Section 6.2.1), 2-dimensional applicability of the method (Section 6.2.2), and limitations of applied computational models (Section 6.2.3).

6.2.1 Capturing the hydrodynamic regimes

While the conceptual cases captured different hydrodynamic regimes, not all possibilities were covered. As already mentioned in Section 6.1, by testing the method on a larger set of reef profiles and offshore wave conditions from XB-NH+ LUT, more generalized results can be obtained. However, this can broaden the understanding of the method and not necessarily the applicability of it. The method is limited to a certain amount of hydrodynamic regimes that it can capture (e.g., the highest offshore significant wave height from the XB-NH+ LUT). The following question will be answered here: *What are the acknowledged boundaries of the applicability of the method and how could the method be improved?*

First, the reef profiles from the field will (almost[1]) always differ from the ones from Scott et al. (2020)'s database which are included in the XB-NH+ LUT. By matching the reef profile from the field with the one from the database, the error is introduced. In the matching process, the percentage of similarity between the field and the database profile is estimated. However, the matched profile could be so different that the hydrodynamic regimes are falsely predicted. Follow-up work should therefore include the application of this methodology to a real case study and the errors introduced due to matching the reef profiles should be identified. If needed, the XB-NH+ LUT could be extended by increasing the number of reef profiles.

Second, the current version of the XB-NH+ LUT has a limited number of offshore wave conditions. Limits are mainly in the maximum values of significant wave height, peak wave period and offshore water level. Often, large flooding events occur due to intense offshore wave conditions. Two solutions are possible: either the XB-NH+ LUT extends its database or the method to extrapolate the boundary conditions is developed. It is advised that both options are considered in the follow-up research.

Third, the TMA+GAUSS function is limited. In the HF part of the spectrum, the TMA shape of the spectrum can only capture one frequency peak, while other peaks are ignored. In the LF part, the Gaussian shape of the spectrum assumes that the frequency peak is in the middle at the frequency of 0.02 Hz. With this step, the VLF part of the spectrum is completely ignored, while its energy is transferred to the IG part of the spectrum. At greater water depths this does not pose a large problem, however, close to the shore where VLF motions are present (see Figure 4.3), the method can cause inaccuracies. Moreover, generalizing the peak of the IG waves at 0.02 Hz is inaccurate as well. As shown in Gawehn et al. (2016), IG waves and VLF motions are important phenomena on coral reefs and in some occasions can result in resonant motions that can cause flooding. A more detailed analysis on the influence of the Gaussian part of the parameterized spectrum in cases when the resonance can occur is needed.

Another scenario when the resonant motion could be under-predicted is during the interpolation of the boundary conditions. For instance, the target hydrodynamic regime should include the occurrence of resonance on the reef flat. The neighbouring simulations from XB-NH+ LUT do not promote resonant motion. Consequently, no resonant motion is simulated and the runup predictions are highly underestimated. This can be dangerous, therefore a detailed analysis on the possibilities of capturing resonant motion on coral reefs is needed. One possible solution is to empirically estimate whether the chosen reef profile from the field has a potential of

---

[1]Of course if the same reef profile is measured as the one from Scott et al. (2020)'s database, the match can be 100%.

promoting the resonant motions (e.g., does the dominant frequency on the reef match the theoretical resonant frequency based on water depth and reef width?). If yes, the profile is labeled with this feature and the modeller is aware of it.

Lastly, the spatially variant reef roughness is not taken into the account. Since reef roughness is highly variable across the different reef platforms (e.g., Roelvink (2019)), this aspect cannot be efficiently included in the method. Moreover, the bottom friction in XB-NH+ LUT is pre-determined. The same bottom friction is applied to all simulations in the LUT over the entire reef profiles. The influence of bottom friction can further be studied.

6.2.2   Application in 2D

The method is currently developed only for 1-dimensional (1D) cross-shore profiles. The forcing in 1D modeling is shore-normal and the effects such as lateral flow and directional spreading are not taken into the account (Guza and Feddersen (2012), Quataert et al. (2015)). Therefore, **1D modeling represents a conservative estimate for wave runup.**

Flood hazard mapping for coastal flood risk assessment is performed in 2 dimensions over a certain area of interest. Since the developed method in this thesis is limited to 1D, one challenge is to apply it to 2D modeling such that it can be successfully applied for coastal flood risk assessment purposes. SFINCS can be applied to 2D, but the boundary conditions from 1D simulations from XB-NH+ LUT need to be addressed. A definition of the offshore boundary location for forcing SFINCS at a depth of -0.5 m (based on the offshore water level of 0 m) is practical. If the boundary location is pre-defined at the same water depth for all reef profiles, it is easier to apply the methodology in 2D. First, the 0.5 m depth contour is identified for the chosen coastline based on the zero offshore water level. The 2D grid domain is built for SFINCS shore-ward from the 0.5 m depth contour. Then, the 1D bathymetric cross-sections from the offshore boundary (deep water) towards the 0.5 m depth contour are identified and matched with the bathymetric reef profiles from the XB-NH+ LUT. The matched reef profiles provide the boundary conditions for forcing SFINCS which simulates flooding of the land. However, in order to put this in practice, a more detailed analysis needs to be performed. Some of the remaining research questions are, for instance: *How many boundary points are sufficient for forcing SFINCS? How can this method account for directional spreading?*

Follow-up work should first start with analysing the practical application of XB-NH+ LUT for forcing SFINCS. This includes the number of cross-shore profiles from the LUT, computational grid resolution of SFINCS in 2D, variable reef profiles along the coast, variable offshore conditions along the coast and interpolation of boundary conditions from 1D XB-NH+ LUT simulations to 2D model grid in SFINCS. At the same time, accuracy and computational demand of methodology in 2D need to be addressed.

Often, wave forcing from the offshore comes from a certain direction which is not necessarily shore-normal. Moreover, on curvilinear coastlines wave forcing is not the same for the entire coastline. Therefore, in order to take these effects into the account, the directional spreading needs to be analysed. This can be done by either parameterizing directional spreading into the methodology or acknowledging the amount of error that is potentially produced due to lack of directional spreading. Some ideas can be drawn from the study performed by Veldt (2019). Furthermore, alongshore variability of the wave runup needs to be further understood (Winter et al., 2020). The lack of knowledge could be first tackled with field and laboratory observations, and then applied to computational modeling techniques.

6.2.3   Improving the models

Limitations of SFINCS in terms of accuracy are acknowledged both in the knowledge of the lack of the physics processes (described in Section 2.3.2) and with analysis in sensitivity analysis (Chapter 4). Two of the most important limitations are (a) the use of simplified shallow water equations (and thus the lack of non-hydrostatic term) and (b) the use of first order explicit scheme which is dissipative. Acknowledged consequences are the smoothing of HF waves, the lack of dispersion and as a result the underestimation of wave runup. SFINCS can further be developed to improve the accuracy.

Another less obvious limitation is the use of XB-NH+ model to validate the methodology. In this thesis XB-NH+ model serves as *reality*. However, the applicability of the model to coral reef environments in still not assured yet. The model was only validated with irregular waves on a fringing reef using laboratory data (de Ridder et al. (2021), see Section 2.3.1). This validation gave good results, however, the model still needs to be validated with field data. The next step in improving the modeling is therefore to perform extensive fieldwork for validation of the model, e.g., by measuring wave heights along the reef flat and around the reef crest. Ideally, the fieldwork is performed in such a way to capture high varieties of hydrodynamic conditions. However, in reality the highly energetic wave conditions are difficult to measure.

Lastly, morphodynamic processes are not included in the modeling. Coral reefs generally consist of rigid structures, but less known processes lie in the transport of sand across the reef towards the coastline. Masselink et al. (2020) found that SLR can cause the coral reef islands to accrete vertically. However, sediment production and reef-to-shore transport is still not a well known process (Winter et al., 2020). These processes are important especially close to the shore where SFINCS is potentially applied. While SFINCS does not model sediment transport, it is worth noting that for flood risk assessment applications these processes need to be acknowledged. Moreover, energetic wave conditions can modify the nearshore profile by eroding the beach. These issues first needs to be tackled by extending the knowledge of the processes, and then by finding the ways to implement these processes in the model.

7

Conclusions and recommendations

Throughout the research project, a preliminary method to accurately and efficiently model wave-driven flooding on coral-reef lined coasts was developed. Key findings of the research are outlined in Section 7.1 by answering the research questions, introduced in Chapter 1. Advances of the conducted research are acknowledged in Section 7.2.

The method has a potential for application to flood risk assessment or as a support for Early Warning Systems (EWS). However, in order to be implemented in these systems, the method needs to be developed further. Recommendations for follow-up work are outlined in Section 7.3. Finally, in Section 7.4 some of the prospects of the method are described. Besides coupling the method with flood risk assessment tools and a support for EWS, the method can also be applied to other coastal environments, or the LUT can be coupled with other inundation models.

7.1   Key findings

In this thesis a new method for modeling wave-driven flooding on coral reef-lined coasts is proposed. The method combines a look-up-table (LUT) consisting of the process-based phase-resolving numerical wave model XBeach Non-Hydrostatic+ simulations (XB-NH+ LUT) with a reduced-physics model SFINCS to simulate 1-dimensional (1D) coastal inundation in an accurate and computationally efficient way. Key findings of the performed research are outlined by answering the research questions that were introduced in Chapter 1.

> (1.) How can the output of process-based phase-resolving numerical wave model be used as an input wave boundary condition close to the shore for forcing a reduced-physics numerical model?

The results showed that forcing SFINCS with parameterized boundary conditions results in comparable accuracy with the accuracy of applying exact boundary conditions. Parameterized boundary conditions are obtained by generating new random water level time series from parameterized wave spectrum at the offshore boundary of SFINCS. The output from XB-NH+ LUT can therefore be used as an input for forcing SFINCS with the following steps:

- obtain water level time series from XB-NH+ LUT at a chosen location along the reef profile;
- perform Fast Fourier transform on time series to obtain the associated wave spectrum;
- parameterize the spectrum with TMA+GAUSS function, as proposed by Athif (2020), using three spectral parameters (the amount of LF wave energy, the amount of HF wave energy and the frequency peak of the HF part of the spectrum);
- generate random water level time series from the obtained parameterized spectrum.

As a general outcome it was concluded that forcing SFINCS shore-ward from the reef flat results in the highest accuracy. In the current XB-NH+ LUT – SFINCS couple this corresponds to the most optimal boundary location at a depth between -2.5 m and -0.5 m (based on the offshore water level of 0 m). Additionally, the performance of the method is better when the waves are more nonlinear at the offshore boundary of SFINCS (determined with the ratio between significant wave height of HF waves (sea-swell) and the water depth).

> (2.) What interpolation method is the most appropriate to calculate the desired time series from the given offshore conditions with the use of discretized runs from XB-NH+ LUT?

The most accurate method to interpolate spectral parameters and wave setup at the boundary is the Inverse Distance Weighting interpolation with Euclidean distances and a power of -2. This method results in the most accurate prediction of wave runup compared to the runup simulated with SFINCS forced with the exact boundary conditions, obtained directly from the XB-NH+ model. In the current methodology with interpolation, the most optimal boundary location is shore-ward from the reef flat at a water depth of -0.5 m (based on the offshore water level of 0 m).

Validation of results with the physics-based model XB-NH+ revealed that by forcing SFINCS with interpolated boundary conditions, the accuracy of the method is comparable with the accuracy of applying exact boundary conditions.

> (3.) Can the methodology be generalized to all types of reef geometries and hydrodynamic regimes?

The results of the sensitivity analysis (Chapter 4) revealed that the developed methodology has a potential to be applied to an arbitrary reef profile. Dissipative coastlines lead to more accurate prediction of wave-driven flooding when SFINCS is forced close to the shore and the mean sea water level is low (0 m in the studied case). In this study, dissipative coastlines are defined as the coastlines that dissipate large amounts of wave energy on their wide and shallow reef and/or gentle fore-reef slope. Note that these results are based on a limited number of reef profiles (6) and offshore wave scenarios (2). The more detaned understanding of the method can be achieved by applying the method to a larger variety of hydrodynamic regimes and more reef bathymetries.

Often, the accuracy of the method is higher for stormy conditions as opposed to swell conditions. There is also an indication that the accuracy of the method increases with increasing offshore water level. The method is

currently limited to the maximum values of significant wave height, peak wave period and offshore water level, that are pre-determined in XB-NH+ LUT. However, XB-NH+ LUT database can be extended in order to capture a larger range of hydrodynamic regimes.

> **(4.) What are the performance and computational efficiency of the developed methodology?**

The accuracy of the developed method is high with mean error of runup between 10% and 20% based on the offshore water level. The maximum error of runup is up to 60%. Runup is under-predicted in most cases. The research demonstrated that the reduced physics in SFINCS is the main source of errors. Since SFINCS is based on simplified shallow water equations, it neglects non-hydrostatic pressure term and it does not account for dispersion. This results in inaccurate prediction of wave breaking across the shore.

A computationally efficient method is primarily achieved by combining physics-reduced model SFINCS with a look-up-table consisting of pre-run simulations with advanced model XB-NH+ (i.e. XB-NH+LUT). Furthermore, computational efficiency is achieved by parameterizing boundary conditions with a simple TMA+GAUSS function that consists of three parameters only. The interpolation is performed with Inverse Distance Weighting interpolation which has practically no computation demand. The computational time of SFINCS forced at the optimal boundary location is averaged 6.8 s for the real-time forcing of 1 h. SFINCS performs with a relative speed-up factor of about 50 compared to the XB-NH+ model simulating hydrodynamic processes along the entire reef profile.

7.2 Advances

Research performed by Athif (2020) proposed the application of the TMA+GAUSS function for parameterizing wave spectrum at the boundary. Untill now, the function was only applied to one specific reef profile. However, with this thesis it was shown that parameterized boundary conditions can be applied to an arbitrary reef profile. Moreover, untill now no such interpolation of boundary conditions was performed. The research demonstrated an accurate method to interpolate boundary conditions with low computational demand.

While attempts were already made before to simulate wave runup in computationally efficient and accurate way (BEWARE by Pearson et al. (2017) and HyCreWW by Rueda et al. (2019)), no efficient method was yet developed to compute flooding in a dynamic way that has a potential to be applied on a global scale. With the outcome of this thesis, we are one step closer to achieving this goal.

Lastly, it was shown that SFINCS, forced with parameterized boundary conditions, performs better when the waves are more nonlinear at the offshore boundary (determined with the ratio between significant wave height of HF waves (sea-swell) and the water depth). While the amount of sea-swell nonlinearities differs per reef profile, it is worth knowing that the performance of SFINCS depends on this parameter.

7.3 Recommendations

Many recommendations for further development of the method are already mentioned in Section 6.2. Follow-up work should first focus on the application to real-life reef profiles and later on the translation from 1D modelling to 2D. The following flow chart (Figure 7.1) summarizes some ideas on how these issues can be tackled with two aspects: further development of methodology and expanding the validity of the methodology.

DEVELOPING METHODOLOGY	EXPANDING VALIDITY

OBSERVED REEF PROFILES

- assessing the errors introduced by
  matching the new observed reef profiles
  with Scott et al. (2020)'s database
- option: interpolation over several reef
  profiles from the database

2D MODELING

- conceptual cases with different scenarios
  (curved coastline, variable offshore forcing,
  variable reef profiles along the coast, ...)
- assessing the optimal grid resolution in
  SFINCS
- interpolation of boundary conditions in 2D
- including directional spreading

IMPLEMENTATION

flood risk assessment:
coupling with Delft-FIAT

HYDRODYNAMIC REGIMES

- expanding XB-NH+ LUT
- sensitivity to resonant motions on reef flats
- spatially varying reef roughness
- morphologic changes

VALIDITY OF XB-NH+ MODEL

conducting field observations and testing
the model with collected data

IMPROVING SFINCS

- parameterization of non-hydrostatic
  pressure term
- numerical scheme

**EXTEND THE CURRENT KNOWLEDGE ON
REEF HYDRODYNAMICS**

- wave breaking on fore-reef
- sediment production and dynamics
- development of coastline
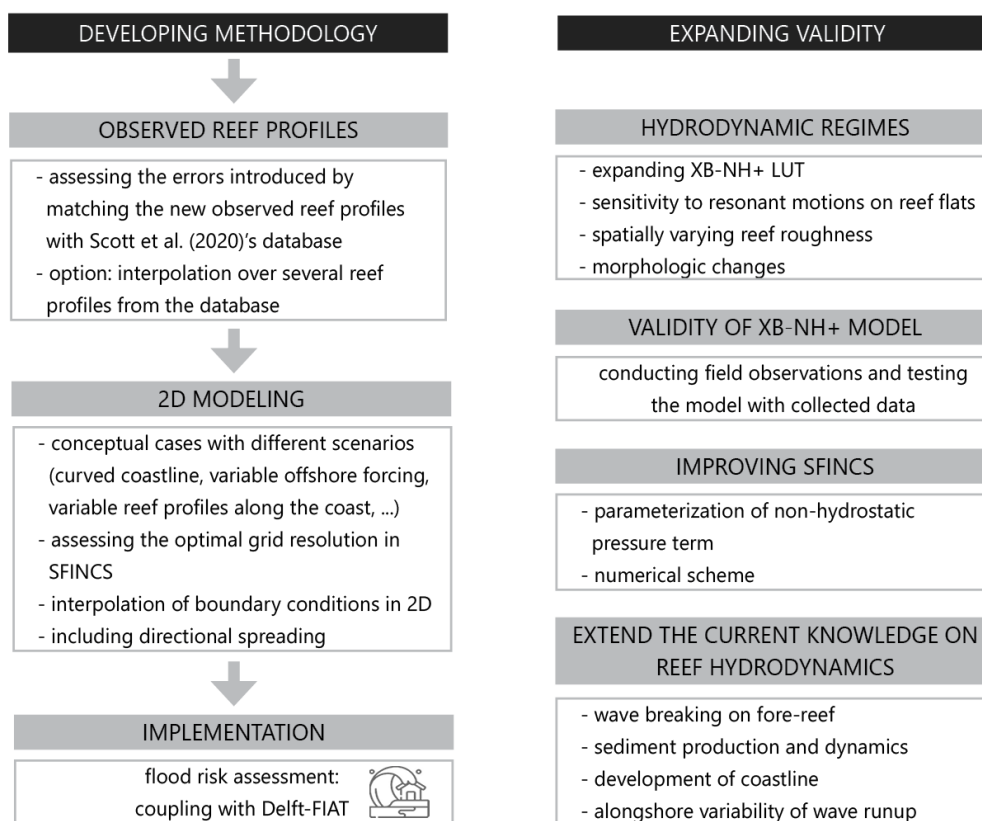- alongshore variability of wave runup

Figure 7.1: A flow chart of recommendations for the follow-up work. The follow-up work needs to be tackled in two ways: follow-up development of methodology and extending the validity of the methodology.

Further development of the methodology

– In order to better understand the accuracy of the method, the method should first be applied to the observed reef profiles that are not included in Scott et al. (2020)'s database. Errors introduced by matching the new reef profiles with the database should be addressed.

– 2D modeling with the proposed method can be investigated by first designing conceptual cases with different scenarios and later by applying it to the real case study. Research objectives can include investigation of the influence of curved coastlines, variable offshore wave forcing and variable reef profiles along the coast on the accuracy of the method. Moreover, the optimal grid size in SFINCS and the effects of (the lack of) directional spreading on the accuracy should be addressed together with interpolation of boundary conditions in 2D modeling.

– After the method is successfully developed for 2D modeling, it can be implemented into flood risk assessment tool, such as Delft-FIAT. The accuracy and computational efficiency of the model train need to be addressed before the method can be finalized and put into practice.

Expanding the validity of the methodology

– The validity of the method can be expanded by extending the amount of hydrodynamic regimes that the method can capture. This can include expansion or extrapolation of XB-NH+ LUT and testing of the method on the validity of predicting resonant motions.

– The method is currently validated with physics-based model XB-NH+. The validity of the XB-NH+ model should be investigated by conducting field observations on coral reef coastlines and testing the model with the collected data.

– The model SFINCS can furthermore be developed to capture HF waves in shallow water while keeping the computational time low.

– The current knowledge of the coral reef hydrodynamics can be expanded by studying the wave breaking on fore-reef, alongshore variability of wave runup, reef development and sediment production, sediment

transport from the reef towards the shore and its response to SLR. Filling these knowledge gaps is important for better and more accurate flood risk assessment and EWS.

7.4   Possible applications

Flooding events on coral reef-lined coasts are expected to occur more frequently and with more severe consequences in the future (Winter et al., 2020). It is expected that severity of coastal hazards will occur mainly due to sea level rise (SLR), changes in weather patterns and degradation of coral reefs. Development of decision support tools for disaster managers and coastal planners is highly prioritized in areas where high risks of flooding are predicted. Tools that need to be developed can be applicable for short term forecast in Early Warning Systems (EWS) and for long term coastal adaptation strategies (scenario modelling tool or flood risk assessment tool).

The main advantages of the developed method in this thesis are that it is computationally efficient, applicable to a high variety of nearshore bathymetries and it has a potential to be applicable in 2D modeling for mapping of coastal hazards. Possible applications of the developed method therefore include implementation in flood risk assessment tools, a support to EWS and application to other coastlines which do not necessarily include coral reefs. In this section, some ideas for the application of the method are presented. The following question will be answered: *What are the prospects of the method?*

Flood risk assessment tool

Frequent flooding of coastal communities can threaten people's lives, damage infrastructure and increase the risk of salt water contamination of the fresh water lenses (Winter et al., 2020). Without mitigation strategies, the land in high risk areas could soon be uninhabitable (Storlazzi et al., 2015). Communities living in these areas can either relocate or implement coastal adaptation strategies. Hopefully, latter is possible for most communities. Coastal adaptation strategies require time for thorough planning and adaptation to build resilience. Therefore, a need for an efficient and accurate flood risk assessment tool is prioritized.

The developed methodology in this thesis can be coupled with a flood risk assessment tool such as Delft-FIAT (Slager et al., 2016). For input in Delft-FIAT, a 2D water depth map and impact functions are needed. The 2D water depth map can be obtained with SFINCS when the developed method is further extended to 2D applications. The final outcome of the coupled models is the damage map which can serve for flood risk assessment purposes.

The main objective of the scenario modeling tool is to assess what the predicted damage can be based on the future climate change scenarios. Thus, the developed tool is mainly applied to intense wave and water level conditions. It is therefore especially important to accurately model various hydrodynamic regimes under intense circumstances. Validation of such cases should be a priority before the method is fully implemented for real-life purposes.

A support to the Early Warning Systems

Early Warning Systems (EWS) produce short-term forecasts, typically up to 7 days in advance (Winter et al., 2020). With these forecasts, local authorities are able to prepare for the event and plan evacuation measures. Until now, most EWS are implemented on sandy coastlines. Implementation on coral reef-lined coasts is difficult due to complex bathymetries and the unique evolution of waves across the shore (for details refer to Chapter 2). BEWARE (Pearson et al., 2017) and HyCreWW (Rueda et al., 2019) are some of the first developed tools that implement EWS on coral reef environments. However, both tools are performed on simplified reef profiles and they both have an output in terms of wave runup. A second version of BEWARE, currently under development, aims to increase the accuracy of prediction of coastal flooding for EWS. However, its output is still only in terms of probability distribution of wave runup prediction.

Predicted runup values are a good first estimate for early warning of a certain area. However, in order to develop EWS even further, water levels and runup values from tools such as BEWARE and HyCreWW need to be translated into a meaningful measure of flooding, which is always site-specific (Winter et al., 2020). In other words, a flooding map is needed to more accurately predict the areas where flooding is expected to be the most

substantial and where evacuation needs to be prioritized. In the future, improved remote sensing techniques will provide more accurate nearshore and topographic data. There is therefore the potential to create more detailed EWS. A way to do this is to implement the methodology that was developed throughout this thesis into the EWS together with detailed topographic data as a supporting tool to EWS.

In order for the methodology to be used together with EWS, the methodology needs to be further developed in 2D, similarly to the applications of flood risk assessment. Additionally, EWS need to take into account other factors contributing to coastal flooding, such as fluvial, pluvial, tidal and wind-driven processes. All these processes need to be addressed in order to develop an accurate method.

Other opportunities

The highlighted computational model in this thesis is reduced-physics model SFINCS. However, other models can be used instead of SFINCS as well. For example, the LUT could provide the boundary conditions for forcing a process-based numerical wave model, such as XBeach (e.g., XBeach with surf-beat mode or non-hydrostatic mode; Roelvink et al. (2009)). While XBeach is computationally demanding model, forcing it close to the shore still decreases computational demand considerably (compared to modeling across the entire reef profile). With this application, the accuracy can be increased while computational demands are sufficiently low. Nevertheless, this application cannot be performed without thorough sensitivity analysis such as the one from this thesis (Chapter 4). Note that the optimal boundary location that was found in this thesis is only optimal when implemented to SFINCS.

This thesis is primarily focusing on coral reef-lined coasts. Another potential of the developed methodology is by applying it to other coastal environments, such as gravel beaches, rocky shores and sandy coastlines. As shown in sensitivity analysis (Chapter 4), methodology can be applied on a number of different bathymetries. The steepest profile (Profile 12 in Table 3.2) is not a typical reef profile, but can also represent a typical profile on sandy coastline. The results of the sensitivity analysis revealed that the steepest reef profile resulted in some of the highest errors of runup, however this should not restrain the potential of its application. In order to develop the method for different coastlines, similar steps as in this thesis can be taken and a new LUT can be built.

Bibliography

Altman, D. G. and Bland, J. M. (2005). Standard deviations and standard errors. *Bmj*, 331(7521):903.

Arakawa, A. and Lamb, V. R. (1977). Computational design of the basic dynamical processes of the ucla general circulation model. *General circulation models of the atmosphere*, 17(Supplement C):173–265.

Athif, A. A. (2020). Computationally efficient modelling of wave driven flooding in Atoll Islands: Investigation on the use of a reduced-physics model solver SFINCS. Master's thesis, IHE, the Netherlands.

Baldock, T. E., Golshani, A., Callaghan, D. P., Saunders, M. I., and Mumby, P. J. (2014). Impact of sea-level rise and coral mortality on the wave dynamics and wave forces on barrier reefs. *Marine Pollution Bulletin*, 83(1):155–164.

Barber, N. F. and Ursell, F. (1948). The generation and propagation of ocean waves and swell. i. wave periods and velocities. *Philosophical Transactions of the Royal Society of London. Series A, Mathematical and Physical Sciences*, 240(824):527–560.

Bates, P. D., Horritt, M. S., and Fewtrell, T. J. (2010). A simple inertial formulation of the shallow water equations for efficient two-dimensional flood inundation modelling. *Journal of Hydrology*, 387(1):33–45.

Battjes, J., Bakkenes, H., Janssen, T., and van Dongeren, A. R. (2004). Shoaling of subharmonic gravity waves. *Journal of Geophysical Research: Oceans*, 109(C2).

Beam, R. M. and Warming, R. F. (1976). An implicit finite-difference algorithm for hyperbolic systems in conservation-law form. *Journal of computational physics*, 22(1):87–110.

Beck, M. W., Losada, I. J., Menéndez, P., Reguero, B. G., Díaz-Simal, P., and Fernández, F. (2018). The global flood protection savings provided by coral reefs. *Nature Communications*, 9.

Becker, J. M., Merrifield, M. A., and Ford, M. (2014). Water level effects on breaking wave setup for Pacific Island fringing reefs. *Journal of Geophysical Research: Oceans*, 119:914–935.

Blanchon, P. (2011). *Geomorphic Zonation*, pages 469–486. Springer Netherlands, Dordrecht.

Bosserelle, C., Reddy, S., and Lal, D. (2015). Wacop wave climate reports. marshall islands, majuro. Technical report. Available at http://gsd.spc.int/wacop/.

Bouws, E., Günther, H., Rosenthal, W., and Vincent, C. (1985). Similarity of the wind wave spectrum in finite depth water: 1. spectral form. *Journal of Geophysical Research: Oceans*, 90(C1):975–986.

Cheriton, O. M., Storlazzi, C. D., and Rosenberger, K. J. (2016). Observations of wave transformation over a fringing coral reef and the importance of low-frequency waves and offshore water levels to runup, overwash, and coastal flooding. *Journal of Geophysical Research: Oceans*, 121(5):3121–3140.

Cui, H., Pietrzak, J., and Stelling, G. (2014). Optimal dispersion with minimized poisson equations for non-hydrostatic free surface flows. *Ocean Modelling*, 81:1–12.

Day, W. H. and Edelsbrunner, H. (1984). Efficient algorithms for agglomerative hierarchical clustering methods. *Journal of classification*, 1(1):7–24.

de Ridder, M. P., Smit, P. B., van Dongeren, A. R., McCall, R. T., Nederhoff, K., and Reniers, A. J. (2021). Efficient two-layer non-hydrostatic wave model with accurate dispersive behaviour. *Coastal Engineering*, 164:103808.

Dekkers, J. (2018). Undular bore development over coral reefs: An experimental study.

Elgar, S. and Guza, R. (1985). Observations of bispectra of shoaling surface gravity waves. *Journal of Fluid Mechanics*, 161(1):425–448.

Ferrario, F., Beck, M. W., Storlazzi, C. D., Micheli, F., Shepard, C. C., and Airoldi, L. (2014). The effectiveness of coral reefs for coastal hazard risk reduction and adaptation. *Nature communications*, 5(1):1–9.

Ford, M., Merrifield, M. A., and Becker, J. M. (2018). Inundation of a low-lying urban atoll island: Majuro , Marshall Islands. *Natural Hazards*, 91(3):1273–1297.

Gallagher, B. (1972). Some qualitative aspects of nonlinear wave radiation in a surf zone. *Geophysical Fluid Dynamics*, 3(4):347–354.

Gawehn, M., van Dongeren, A., van Rooijen, A., Storlazzi, C. D., Cheriton, O. M., and Reniers, A. (2016). Identification and classification of very low frequency waves on a coral reef flat. *Journal of Geophysical Research: Oceans*, 121(10):7560–7574.

Gentry, R. C. (1968). *Hurricanes: one of the major features of air-sea interaction in the Caribbean Sea*. National Hurricane Research Laboratory, Environmental Science Services . . . .

Gourlay, M. (1996). Wave set-up on coral reefs. 2. set-up on reefs with various profiles. *Coastal Engineering*, 28(1-4):17–55.

Grue, J., Pelinovsky, E., Fructus, D., Talipova, T., and Kharif, C. (2008). Formation of undular bores and solitary waves in the strait of malacca caused by the 26 december 2004 indian ocean tsunami. *Journal of Geophysical Research: Oceans*, 113(C5).

Guza, R. and Feddersen, F. (2012). Effect of wave frequency and directional spread on shoreline runup. *Geophysical Research Letters*, 39(11).

Guza, R. and Thornton, E. B. (1982). Swash oscillations on a natural beach. *Journal of Geophysical Research: Oceans*, 87(C1):483–491.

Hasselmann, K. F., Barnett, T. P., Bouws, E., Carlson, H., Cartwright, D. E., Eake, K., Euring, J., Gicnapp, A., Hasselmann, D., Kruseman, P., et al. (1973). Measurements of wind-wave growth and swell decay during the joint north sea wave project (jonswap). *Ergaenzungsheft zur Deutschen Hydrographischen Zeitschrift, Reihe A*.

Heemsoth, A. (2014a). Reef types, coral reef ecology curriculum. Technical report, Education Department of the Khaled bin Sultan Living Oceans Foundation.

Heemsoth, A. (2014b). Reef zonation, coral reef ecology curriculum. Technical report, Education Department of the Khaled bin Sultan Living Oceans Foundation.

Hench, J. L., Leichter, J. J., and Monismith, S. G. (2008). Episodic circulation and exchange in a wave-driven coral reef and lagoon system. *Limnology and Oceanography*, 53(6):2681–2694.

Holman, R. (1986). Extreme value statistics for wave run-up on a natural beach. *Coastal Engineering*, 9(6):527–544.

Holthuijsen, L. H. (2010). *Waves in oceanic and coastal waters*. Cambridge university press.

Hopley, D. (1982). *The Geomorphology of the Great Barrier Reef*. Wiley New York.

Hunt, I. (1959). Design of seawalls and breakwaters. *Jour. Waterways and Harbors Div., Proc. Am. Soc. Civil Eng.*, 3:123–152.

Jevrejeva, S., Grinsted, A., and Moore, J. (2009). Anthropogenic forcing dominates sea level rise since 1850. *Geophysical Research Letters*, 36(20).

Kitaigordskii, S., Krasitskii, V., and Zaslavskii, M. (1975). On phillips' theory of equilibrium range in the spectra of wind-generated gravity waves. *Journal of Physical Oceanography*, 5(3):410–420.

Kopp, R. E., Horton, R. M., Little, C. M., Mitrovica, J. X., Oppenheimer, M., Rasmussen, D., Strauss, B. H., and Tebaldi, C. (2014). Probabilistic 21st and 22nd century sea-level projections at a global network of tide-gauge sites. *Earth's future*, 2(8):383–406.

Leijnse, T., van Ormondt, M., Nederhoff, K., and van Dongeren, A. (2021). Modeling compound flooding in coastal systems using a computationally efficient reduced-physics solver: Including fluvial, pluvial, tidal, wind-and wave-driven processes. *Coastal Engineering*, 163:103796.

Longuet-Higgins, M. and Stewart, R. (1964). Radiation stresses in water waves; a physical discussion with applications. *Deep-Sea Research*, 11:529–562.

Lugo-Fernandez, A., Roberts, H., Wiseman Jr, W., and Carter, B. (1998). Water level and currents of tidal and infragravity periods at tague reef, st. croix (usvi). *Coral Reefs*, 17(4):343–349.

Lugo-Fernández, A. and Roberts, H. H. (2011). *Reef Front Wave Energy*, pages 876–881. Springer Netherlands, Dordrecht.

Masselink, G. (1995). Group bound long waves as a source of infragravity energy in the surf zone. *Continental Shelf Research*, 15(13):1525–1547.

Masselink, G., Beetham, E., and Kench, P. (2020). Coral reef islands can accrete vertically in response to sea level rise. *Science Advances*, 6(24):eaay3656.

Medellín, G., Brinkkemper, J., Torres-Freyermuth, A., Appendini, C. M., Mendoza, E. T., and Salles, P. (2016). Run-up parameterization and beach vulnerability assessment on a barrier island: a downscaling approach. *Natural Hazards and Earth System Sciences*, 16(1):167.

Monismith, S. G., Rogers, J. S., Koweek, D., and Dunbar, R. B. (2015). Frictional wave dissipation on a remarkably rough reef. *Geophysical Research Letters*, 42(10):4063–4071.

Munk, W. H., Miller, G., Snodgrass, F., and Barber, N. F. (1963). Directional recording of swell from distant storms. *Philosophical Transactions of the Royal Society of London. Series A, Mathematical and Physical Sciences*, 255(1062):505–584.

Munk, W. H. and Sargent, M. C. (1948). Adjustment of Bikini Atoll to ocean waves. *Transactions of the American Geophysical Union*, 29(6):855–860.

Nakaza, E., Tsukayama, S., and Hino, M. (1990). Bore-like Surf Beat on Reef Coasts. *Coastal Engineering*.

Nwogu, O. and Demirbilek, Z. (2010). Infragravity wave motions and runup over shallow fringing reefs. *Journal of waterway, port, coastal, and ocean engineering*, 136(6):295–305.

Pearson, S. and Tissier, M. (2018). The curious undular bore.

Pearson, S. G., Storlazzi, C. D., van Dongeren, A. R., Tissier, M. F. S., and Reniers, A. J. H. M. (2017). A Bayesian-Based System to Assess Wave-Driven Flooding Hazards on Coral Reef-Lined Coasts. *Journal of Geophysical Research: Oceans*, 122:10099–10117.

Péquignet, A.-C. N., Becker, J. M., and Merrifield, M. A. (2014). Energy transfer between wind waves and low-frequency oscillations on a fringing reef, i pan, g uam. *Journal of Geophysical Research: Oceans*, 119(10):6709–6724.

Péquignet, A. C. N., Becker, J. M., Merrifield, M. A., and Aucan, J. (2009). Forcing of resonant modes on a fringing reef during tropical storm man-yi. *Geophysical Research Letters*, 36(3).

Pomeroy, A., Lowe, R., Symonds, G., Dongeren, A. V., and Moore, C. (2012). The dynamics of infragravity wave transformation over a fringing reef. *Journal of Geophysical Research*, 117:1–17.

Quataert, E., Storlazzi, C., Dongeren, A. V., and Mccall, R. (2020). The importance of explicitly modelling sea-swell waves for runup on reef-lined coasts. *Coastal Engineering*.

Quataert, E., Storlazzi, C., Rooijen, A., Cheriton, O., and Dongeren, A. (2015). The influence of coral reefs and climate change on wave-driven flooding of tropical coastlines. *Geophysical research letters*, 42:6407–6415.

Richmond, R. H. (1993). Coral reefs: present problems and future concerns resulting from anthropogenic disturbance. *American Zoologist*, 33(6):524–536.

Roberts, H. H. and Suhayda, J. N. (1983). Wave-current interactions on a shallow reef (nicaragua, central america). *Coral Reefs*, 1(4):209–214.

Roeber, V. and Bricker, J. D. (2015). Destructive tsunami-like wave generated by surf beat over a coral reef during Typhoon Haiyan. *Nature Communications*, 6(7854).

Roelvink, D., McCall, R., Mehvar, S., Nederhoff, K., and Dastgheib, A. (2018). Improving predictions of swash dynamics in xbeach: The role of groupiness and incident-band runup. *Coastal Engineering*, 134:103–123.

Roelvink, D., Reniers, A., Dongeren, A. V., Thiel, J. V., Vries, D., Mccall, R., and Lescinski, J. (2009). Modelling storm impacts on beaches, dunes and barrier islands. *Coastal Engineering*, 56(11-12):1133–1152.

Roelvink, F. (2019). Coral Restoration for Coastal Hazard Risk Reduction: The effect of coral restoration on wave transformation over various reef morphologies and the resulting runup. Master's thesis, Delft University of Technology, the Netherlands.

Rueda, A., Cagigal, L., Pearson, S., Antolínez, J. A., Storlazzi, C., van Dongeren, A., Camus, P., and Mendez, F. J. (2019). Hycreww: a hybrid coral reef wave and water level metamodel. *Computers & Geosciences*, 127:85–90.

Scott, F., Antolinez, J. A. A., Mccall, R., Storlazzi, C., Reniers, A., and Pearson, S. (2020). Hydro-Morphological Characterization of Coral Reefs for Wave Runup Prediction. *Frontiers in Marine Science*, 7(May):1–20.

Seelig, W. N. (1983). Laboratory study of reef-lagoon system hydraulics. *Journal of waterway, port, coastal, and ocean engineering*, 109(4):380–391.

Slager, K., Burzel, E., Bos, K., de Bruijn, D., Wagenaar, H., Winsemius, L., Bouwer, M., and van der Doef (2016). *User Manual Delft-FIAT version 1*. website: publicwiki.deltares.nl/display/DFIAT/Delft-FIAT+Home.

Slangen, A., Carson, M., Katsman, C., Van de Wal, R., Köhl, A., Vermeersen, L., and Stammer, D. (2014). Projecting twenty-first century regional sea-level changes. *Climatic Change*, 124(1):317–332.

Smit, P., Janssen, T., Holthuijsen, L., and Smith, J. (2014). Non-hydrostatic modeling of surf zone wave dynamics. *Coastal Engineering*, 83:36–48.

Stockdon, H. F., Holman, R. A., Howd, P. A., and Sallenger Jr, A. H. (2006). Empirical parameterization of setup, swash, and runup. *Coastal engineering*, 53(7):573–588.

Storlazzi, C. D., Elias, E. P., and Berkowitz, P. (2015). Many atolls may be uninhabitable within decades due to climate change. *Scientific reports*, 5:14546.

Storlazzi, C. D., Reguero, B. G., Cole, A. D., Lowe, E., Shope, J. B., Gibbs, A. E., Nickel, B. A., McCall, R. T., van Dongeren, A. R., and Beck, M. W. (2019). Rigorously valuing the role of us coral reefs in coastal hazard risk reduction. Technical report, US Geological Survey.

Symonds, G., Huntley, D. A., and Bowen, A. J. (1982). Two-dimensional surf beat: Long wave generation by a time-varying breakpoint. *Journal of Geophysical Research: Oceans*, 87(C1):492–498.

Tajima, Y., Shimozono, T., Gunasekara, K. H., and Cruz, E. C. (2016). Study on locally varying inundation characteristics induced by super typhoon haiyan. part 2: Deformation of storm waves on the beach with fringing reef along the east coast of eastern samar. *Coastal Engineering Journal*, 58(1):1640003–1.

Talley, L. D. (2011). *Descriptive physical oceanography: an introduction*. Academic press.

Tissier, M., Dekkers, J., Reniers, A., Pearson, S., and van Dongeren, A. (2018). Undular bore development over a laboratory fringing reef. *Coastal Engineering Proceedings*, (36):53–53.

van Engelen, T. E. (2016). Towards a rapid assessment flood forecasting system for the Southern California coast. Master's thesis, Delft University of Technology, the Netherlands.

Veldt, T. (2019). The effect of wave directional spread on coastal hazards at coastlines fronted by a coral reef. Master's thesis, Delft University of Technology, the Netherlands.

Vetter, O., Becker, J. M., Merrifield, M. A., Pequignet, A.-C., Aucan, J., Boc, S. J., and Pollock, C. E. (2010). Wave setup over a pacific island fringing reef. *Journal of Geophysical Research: Oceans*, 115(C12).

Vousdoukas, M. I., Voukouvalas, E., Mentaschi, L., Dottori, F., Giardino, A., Bouziotas, D., Bianchi, A., Salamon, P., and Feyen, L. (2016). Developments in large-scale coastal flood hazard mapping. *Natural Hazards and Earth System Sciences*, 16(8):1841–1853.

Winter, G., Storlazzi, C., Vitousek, S., van Dongeren, A., McCall, R., Hoeke, R., Skirving, W., Marra, J., Reyns, J., Aucan, J., et al. (2020). Steps to develop early warning systems and future scenarios of storm wave-driven flooding along coral reef-lined coasts. *Frontiers in Marine Science*, 7:199.

Zijlema, M., Stelling, G., and Smit, P. (2011). Swash: An operational public domain code for simulating wave fields and rapidly varied flows in coastal waters. *Coastal Engineering*, 58(10):992–1012.

A
Model input parameters

A.1 SFINCS input parameters

Following is an example input file for SFINCS for the Profile 12, Simulation 1, boundary location at the beachtoe:

```
mmax = 1617
nmax = 1
dx = 0.5
dy = 1
x0 = -510
y0 = 0
rotation = 0
tref = 20200728 000000
tstart = 20200728 000000
tstop = 20200728 010000
dtout = 1
alpha = 0.1
theta = 0.9
huthresh = 0.005
manning = 0.03
bndtype = 1
advection = 1
depfile = sfincs.dep
mskfile = sfincs.msk
bndfile = sfincs.bnd
bzsfile = sfincs.bzs
bzifile = sfincs.bzi
inputformat = asc
outputformat = net
```

A.2   XB-NH+ input parameters

Following is an example input file for XB-NH+ as it is contained in XB-NH+ LUT for the Profile 12, Simulation 1, beach slope of 0.1:

```
bedfriction = cf
bedfricfile = fric.txt
sedtrans = 0
morphology = 0
taper = 0
nonhq3d = 1
wavemodel = nonh
swave = 0
nhbreaker = 1
maxbrsteep = 0.6000
reformsteep = 0.3000
%%%% Flow boundary condition parameters:
front = nonh1d
back = abs1d
%%%% Grid parameters
nx = 838
ny = 0
vardx = 1
depfile = profile.dep
xfile = x.grd
posdwn = -1
Model time
tstop = 6400.0
Tide boundary conditions
tideloc = 0
zs0 = 0
%%%% Wave boundary condition parameters
wbctype = reuse
bcfile = nhbcflist.bcf
%%%% Output variables
outputformat = netcdf
tintg = 800.0
tintm = 800.0
tstart = 2400.0
tintp = 0.4
npoints = 26
-506.9759 1.  offshore
-0.021585 1.  beachtoe
-247.8997 1.  -15m
-172.9162 1.  -10m
-74.2008 1.  -5m
-28.2026 1.  -2.5m
-3.5338 1.  -0.5m
-3.8022 1.  midreef
-3.8022 1.  innerreef
300 1.  discharge
-54.5345 1.  breaking
9.9784 1.  overtop1m
20 1.  overtop2m
30 1.  overtop3m
40 1.  overtop4m
50 1.  overtop5m
```

```
60 1.  overtop6m
70 1.  overtop7m
80 1.  overtop8
90 1.  overtop9m
100 1.  overtop10m
120 1.  overtop12m
160 1.  overtop16m
180 1.  overtop18m
200 1.  overtop20m
npointvar = 3
zs
uu
qx
nrugauge = 1
300 1
rugdepth = 0.005
nglobalvar = 1
zs
nmeanvar = 2
zs
```

B

Errors of runup for pre-defined boundary locations

(Included on the next page.)
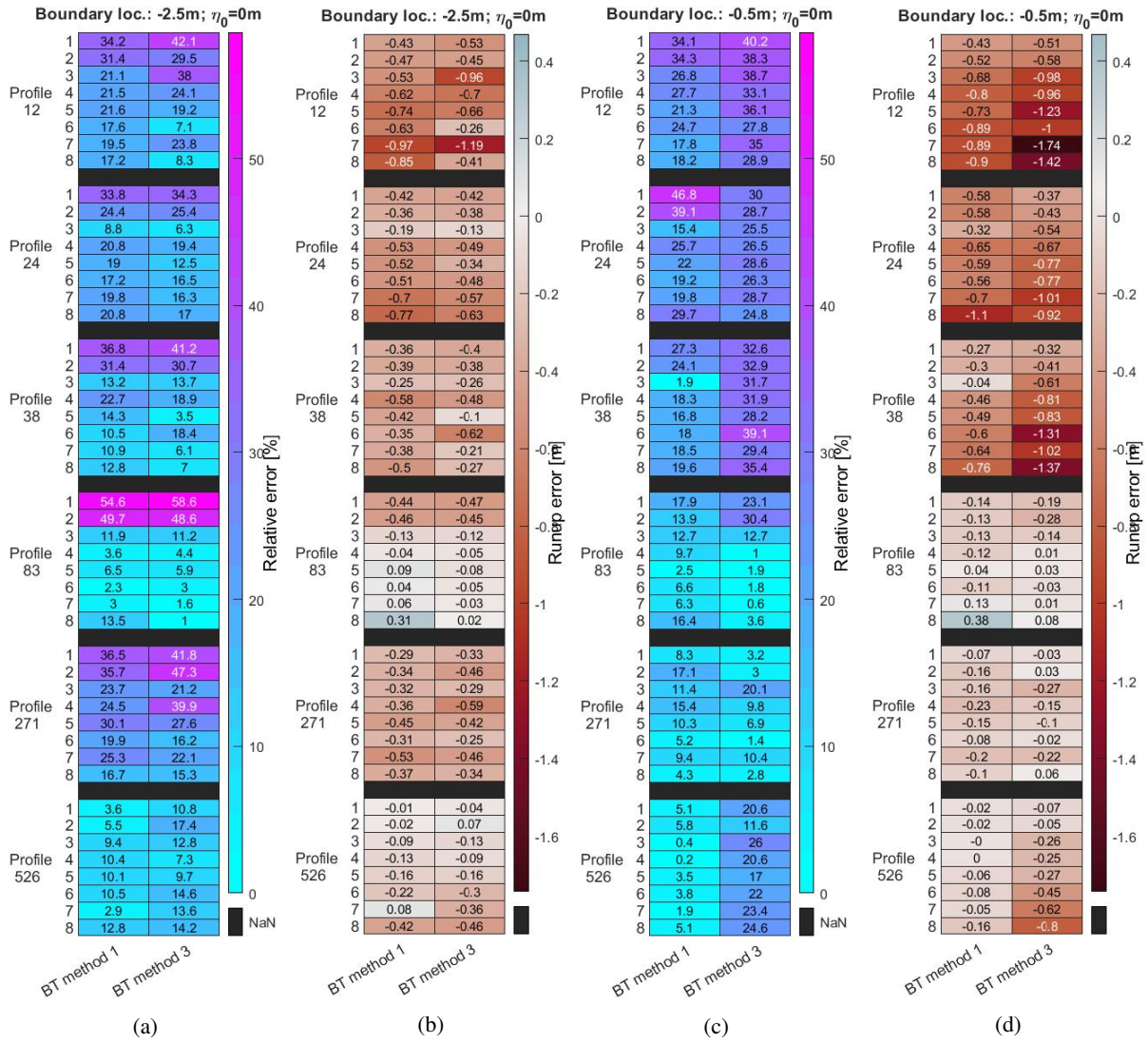
Figure B.1: Relative errors of runup (a and c) and absolute errors of runup (b and d) for pre-defined boundary locations at depths of -2.5 m (a and b) and -0.5 m (c and d). Results are depicted per profile per simulation (numbers 1 to 8) for offshore water level $\eta_0 = 0$ m.
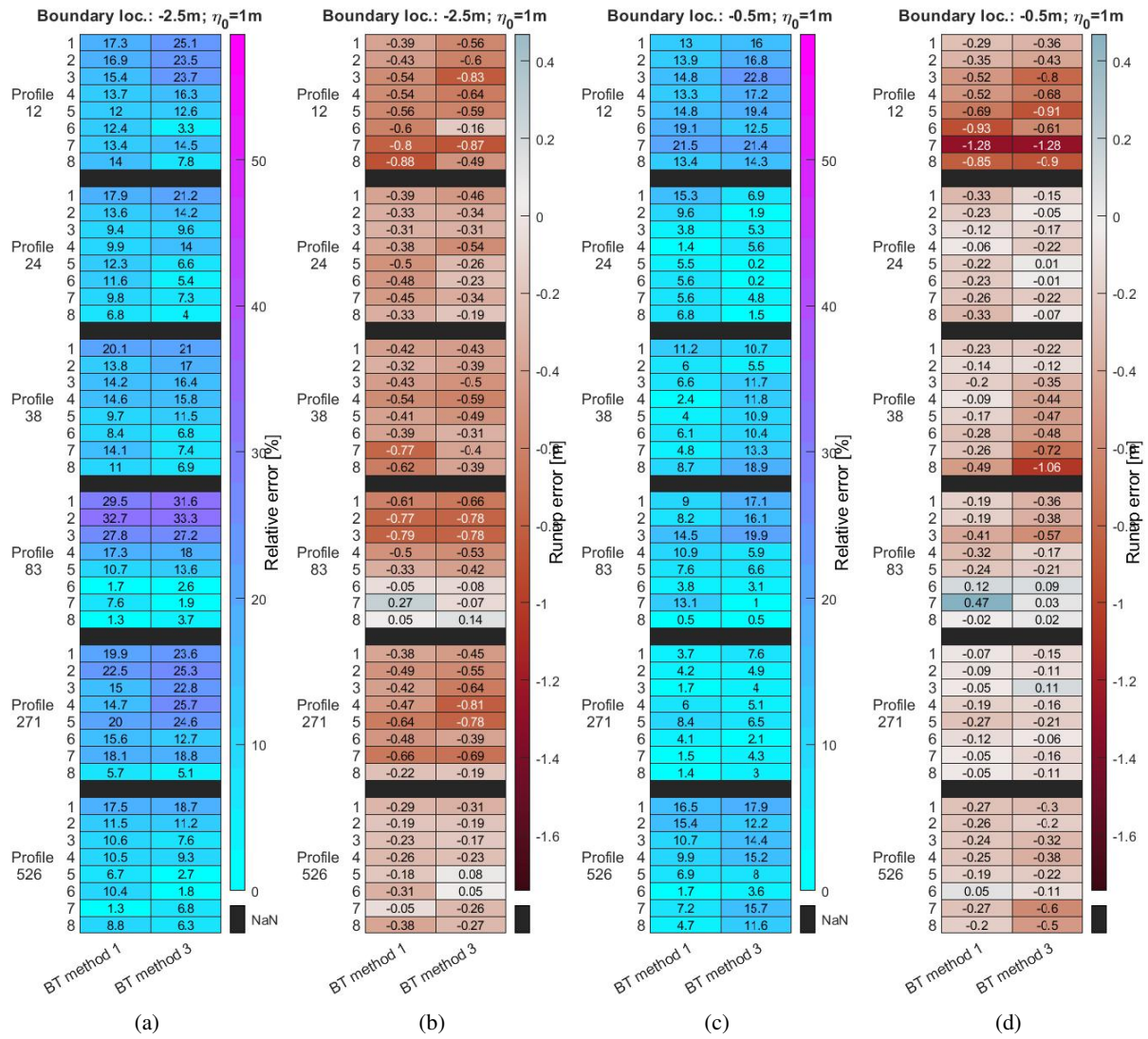
Figure B.2: Relative errors of runup (a and c) and absolute errors of runup (b and d) for pre-defined boundary locations at depths of -2.5 m (a and b) and -0.5 m (c and d). Results are depicted per profile per simulation (numbers 1 to 8) for offshore water level η_0 = 1 m.
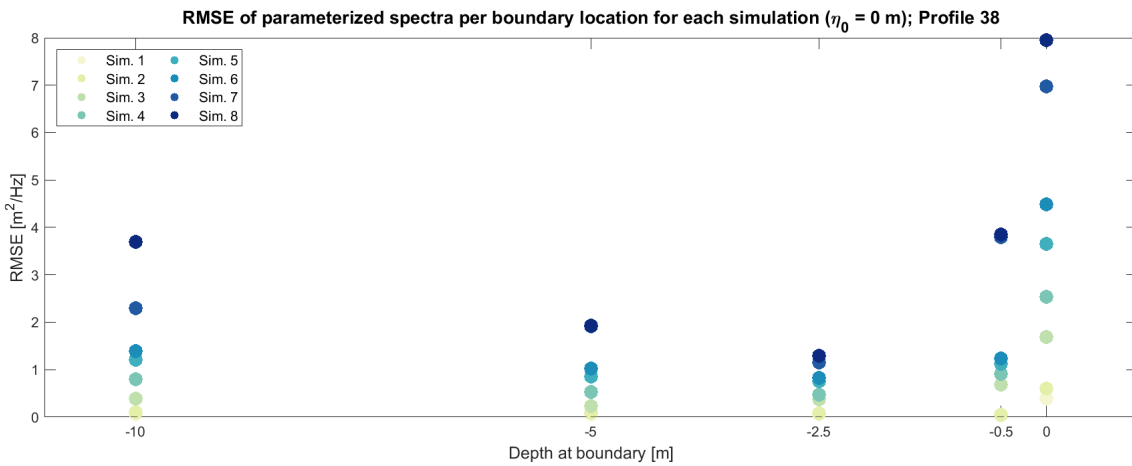
C

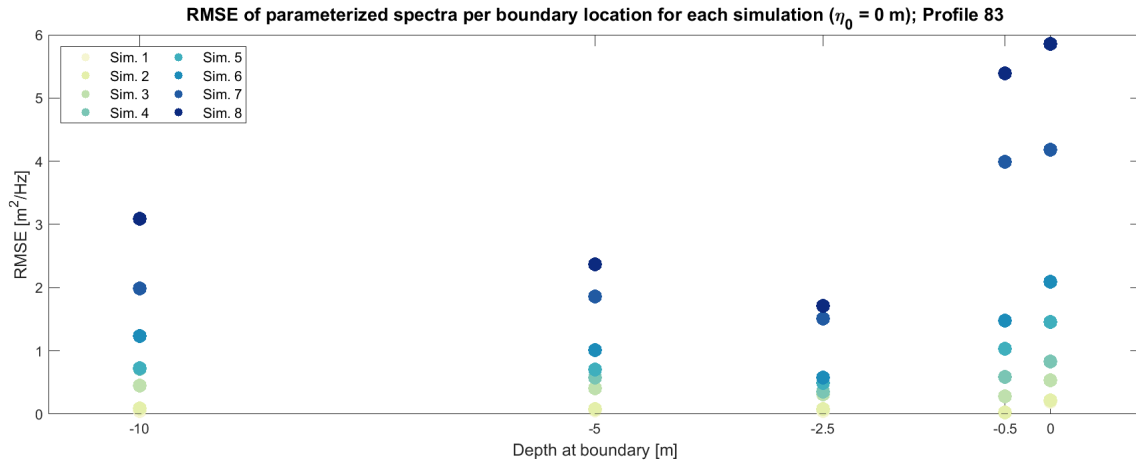## RMSE of parameterized spectra
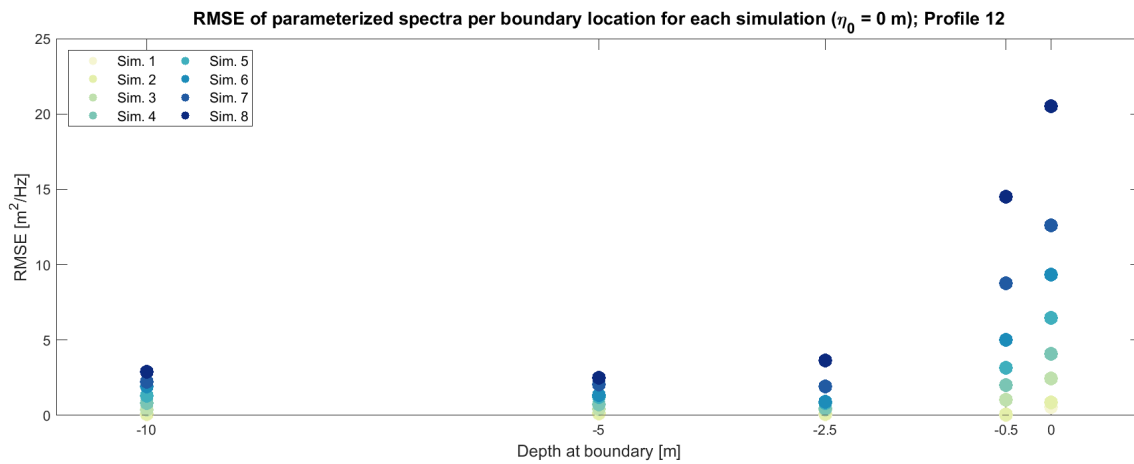
Figure C.1: Root mean square error (RMSE) between the parameterized wave spectra and the original wave spectra per each boundary location (depth at the boundary on x-axis) and for each simulation separately (coloured dots, see Table 3.3 for the list of simulations with offshore water level $\eta_0 = 0$ m), for Profile 12.
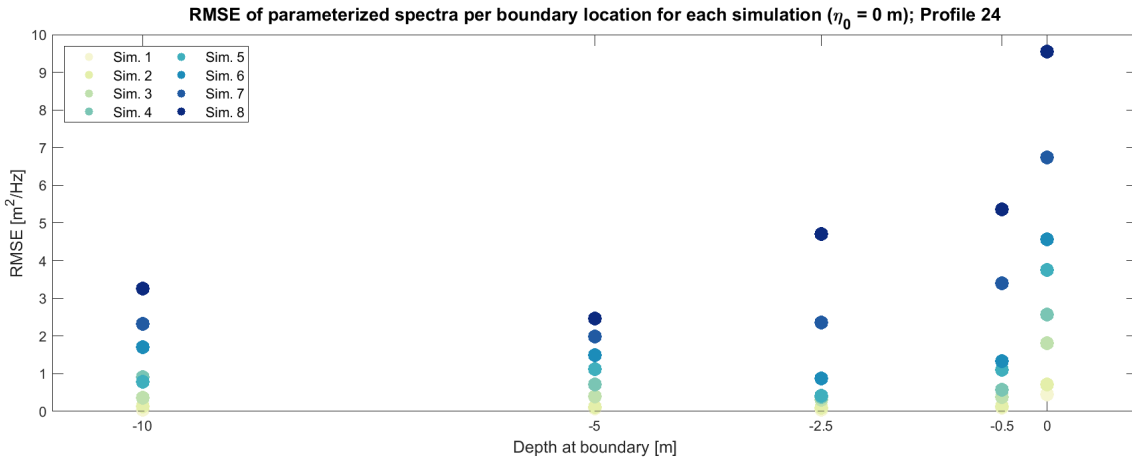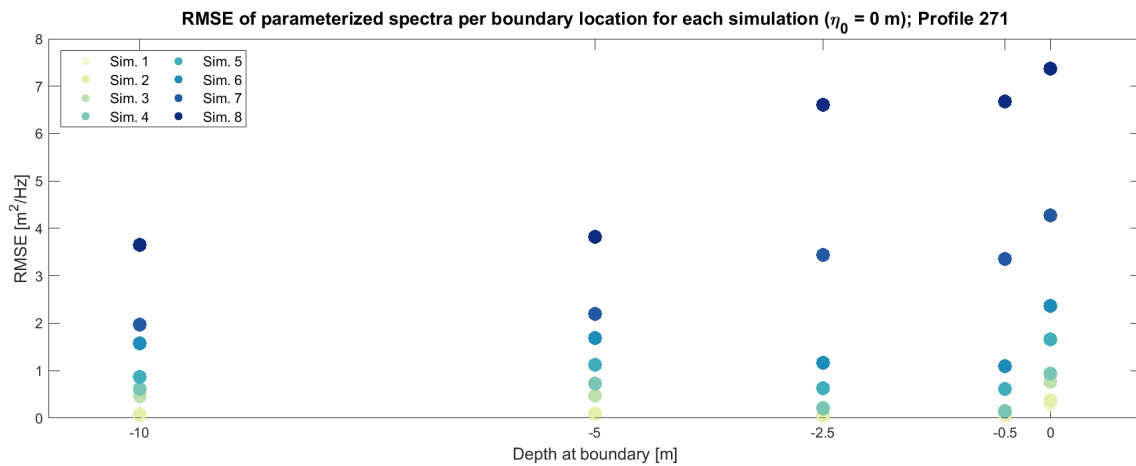
Figure C.2: Root mean square error (RMSE) between the parameterized wave spectra and the original wave spectra per each boundary location (depth at the boundary on x-axis) and for each simulation separately (coloured dots, see Table 3.3 for the list of simulations with offshore water level $\eta_0 = 0$ m), for Profile 24.

Figure C.3: Root mean square error (RMSE) between the parameterized wave spectra and the original wave spectra per each boundary location (depth at the boundary on x-axis) and for each simulation separately (coloured dots, see Table 3.3 for the list of simulations with offshore water level $\eta_0 = 0$ m), for Profile 38.
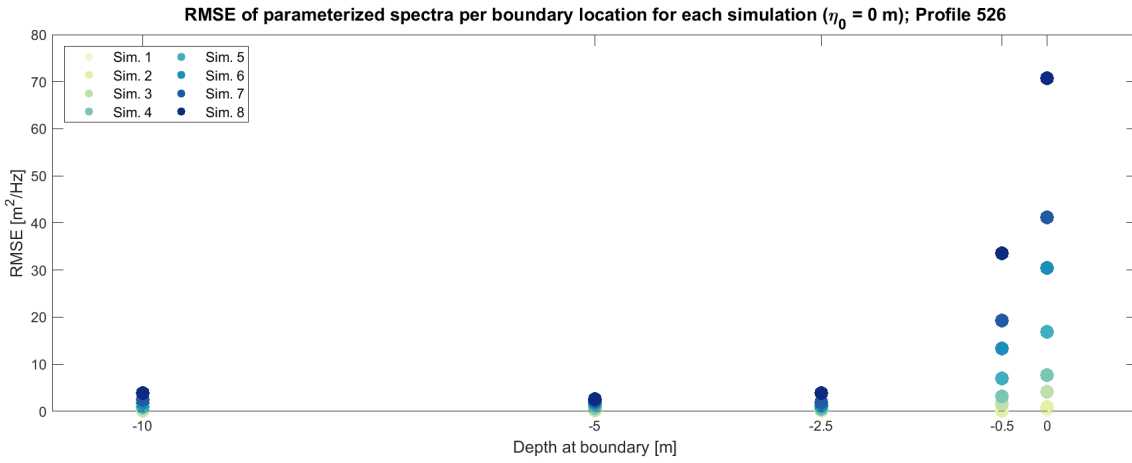
Figure C.4: Root mean square error (RMSE) between the parameterized wave spectra and the original wave spectra per each boundary location (depth at the boundary on x-axis) and for each simulation separately (coloured dots, see Table 3.3 for the list of simulations with offshore water level $\eta_0 = 0$ m), for Profile 83.
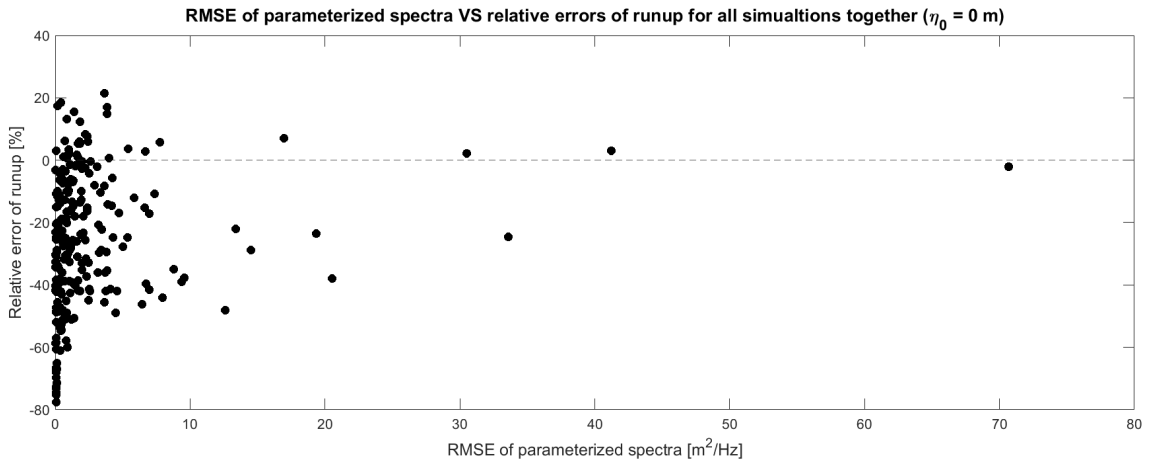

Figure C.5: Root mean square error (RMSE) between the parameterized wave spectra and the original wave spectra per each boundary location (depth at the boundary on x-axis) and for each simulation separately (coloured dots, see Table 3.3 for the list of simulations with offshore water level $\eta_0 = 0$ m), for Profile 271.

Figure C.6: Root mean square error (RMSE) between the parameterized wave spectra and the original wave spectra per each boundary location (depth at the boundary on x-axis) and for each simulation separately (coloured dots, see Table 3.3 for the list of simulations with offshore water level $\eta_0 = 0$ m), for Profile 526.

Figure C.7: Root mean square error (RMSE) between the parameterized wave spectra and the original wave spectra in relation to the relative errors of runup for all simulations together for offshore water level of 0 m.

D

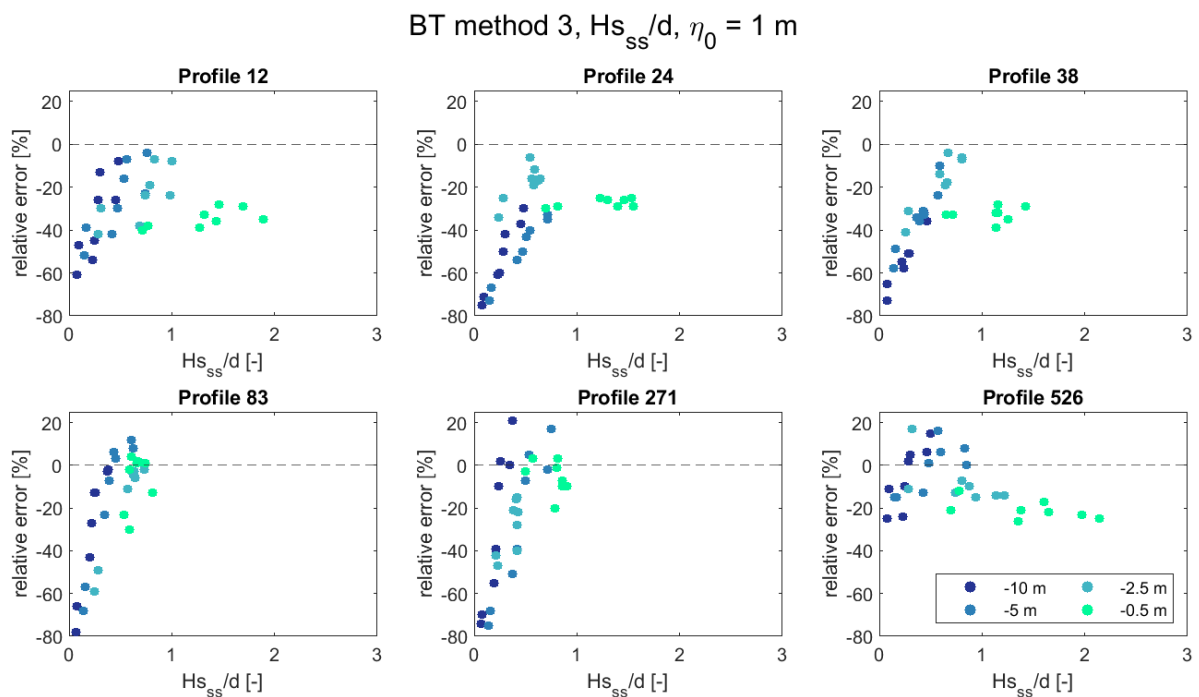# Sea-swell nonlinearities at the boundary

Figure D.1: The ratio between the significant wave height of HF waves (sea-swell) and the depth (H_{ss}/d) at the boundary locations in relation with the associated relative errors of runup. Results are depicted for each reef profile separately for all simulations (8 different cases, based on different offshore wave conditions). Offshore water level is $\eta_0 = 1$ m and parameterized boundary conditions are applied (BT method 3, see Section 3.4.1). Different colours depict 4 different boundary locations that SFINCS is forced at. Boundary location at the beachtoe is not depicted..
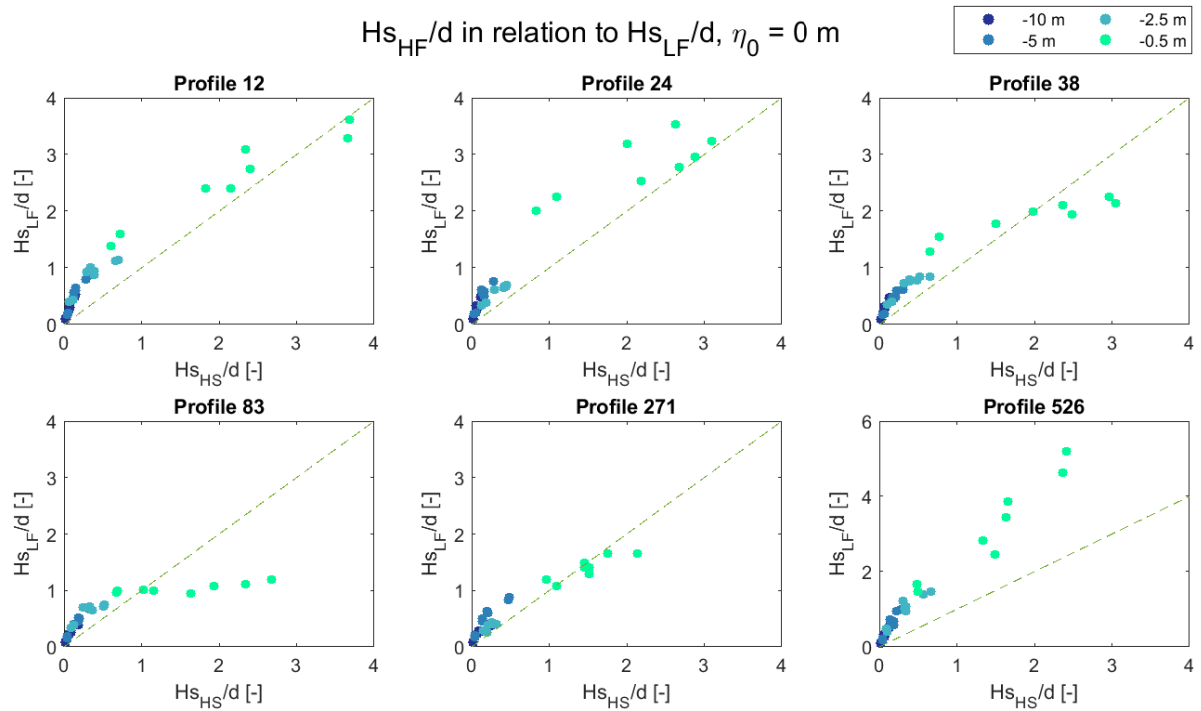
Figure D.2: The ratio between the significant wave height of HF waves (sea-swell) and the depth (H_{ss}/d) at the boundary locations in relation with he ratio between the significant wave height of LF waves (IG and VLF together) and the depth (H_{LF}/d) at the boundary locations. Results are depicted for each reef profile separately for all simulations (8 different cases, based on different offshore wave conditions). Offshore water level is $\eta_0 = 0$ m. Different colours depict 4 different boundary locations.
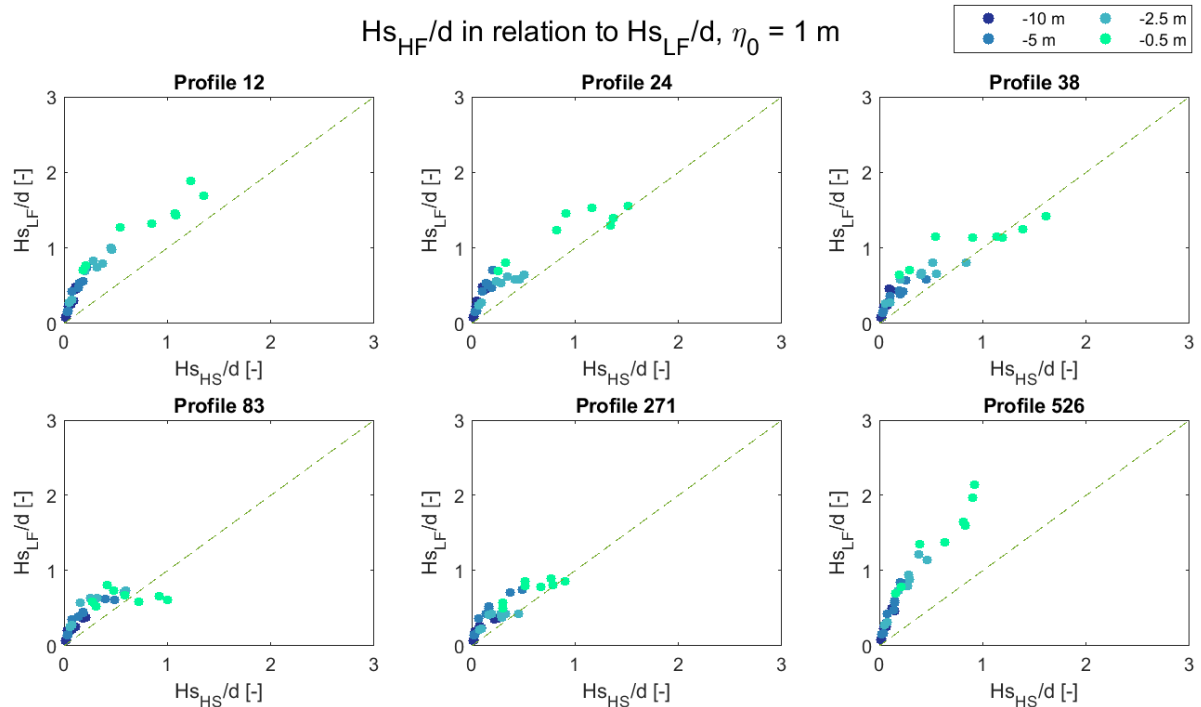

Figure D.3: The ratio between the significant wave height of HF waves (sea-swell) and the depth (H_{ss}/d) at the boundary locations in relation with he ratio between the significant wave height of LF waves (IG and VLF together) and the depth (H_{LF}/d) at the boundary locations. Results are depicted for each reef profile separately for all simulations (8 different cases, based on different offshore wave conditions). Offshore water level is $\eta_0 = 1$ m. Different colours depict 4 different boundary locations.

E
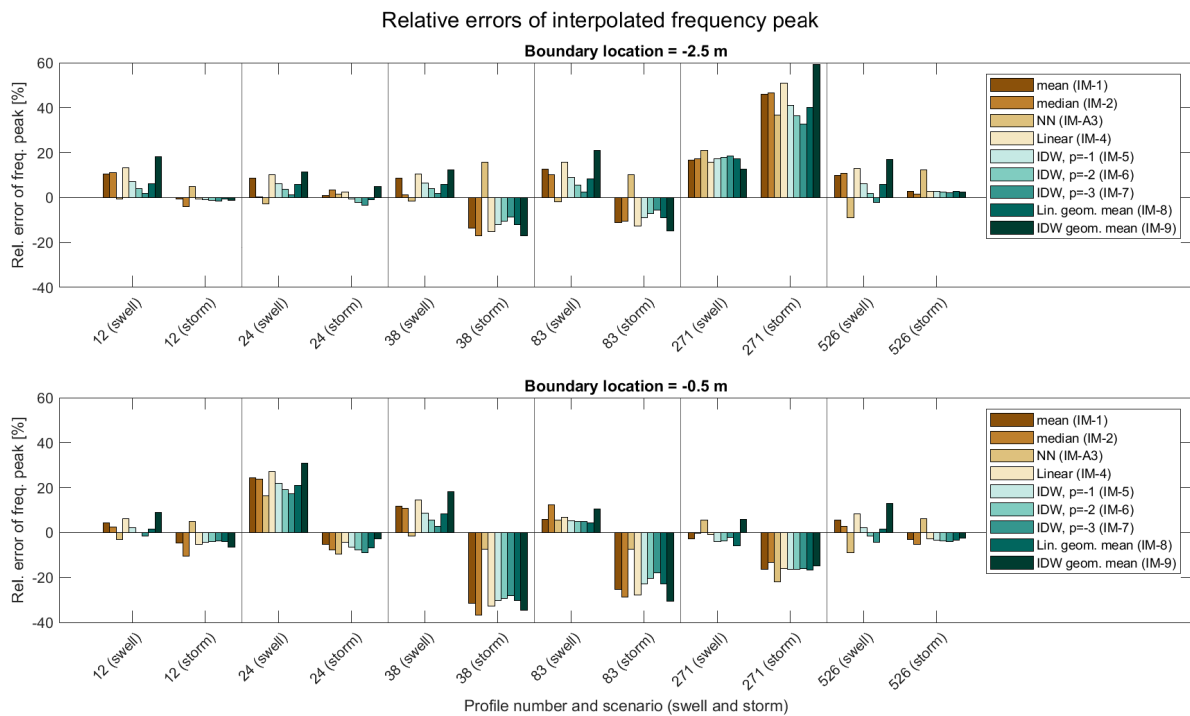# Interpolated spectral parameters: results per profile

Figure E.1: Relative errors of the interpolated frequency peak per profile, for the two forcing scenarios (swell and storm). Interpolated frequency peak values are compared to correct frequency peak values. 9 different interpolation methods are compared, each marked with different colour. Methods are applied to two boundary locations at depths of -2.5 m (top) and -0.5 m (bottom).
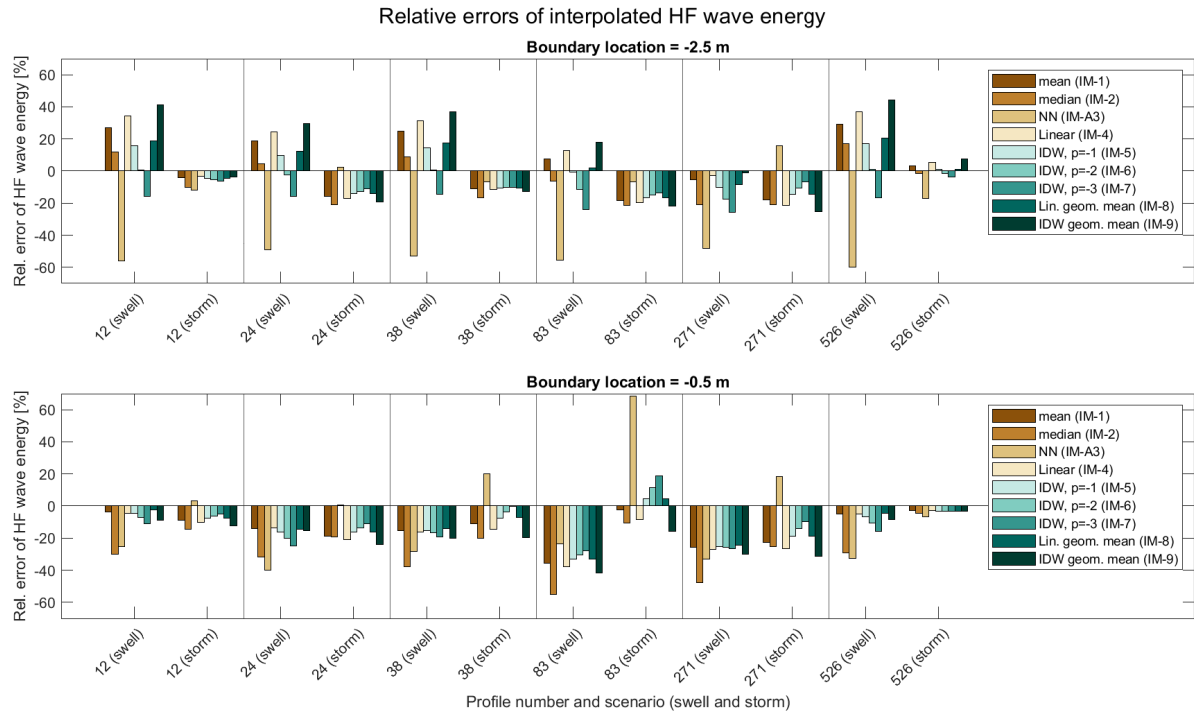
Figure E.2: Relative errors of the interpolated HF wave energy per profile, for the two forcing scenarios (swell and storm). Interpolated HF wave energy values are compared to correct HF wave energy values. 9 different interpolation methods are compared, each marked with different colour. Methods are applied to two boundary locations at depths of -2.5 m (top) and -0.5 m (bottom).
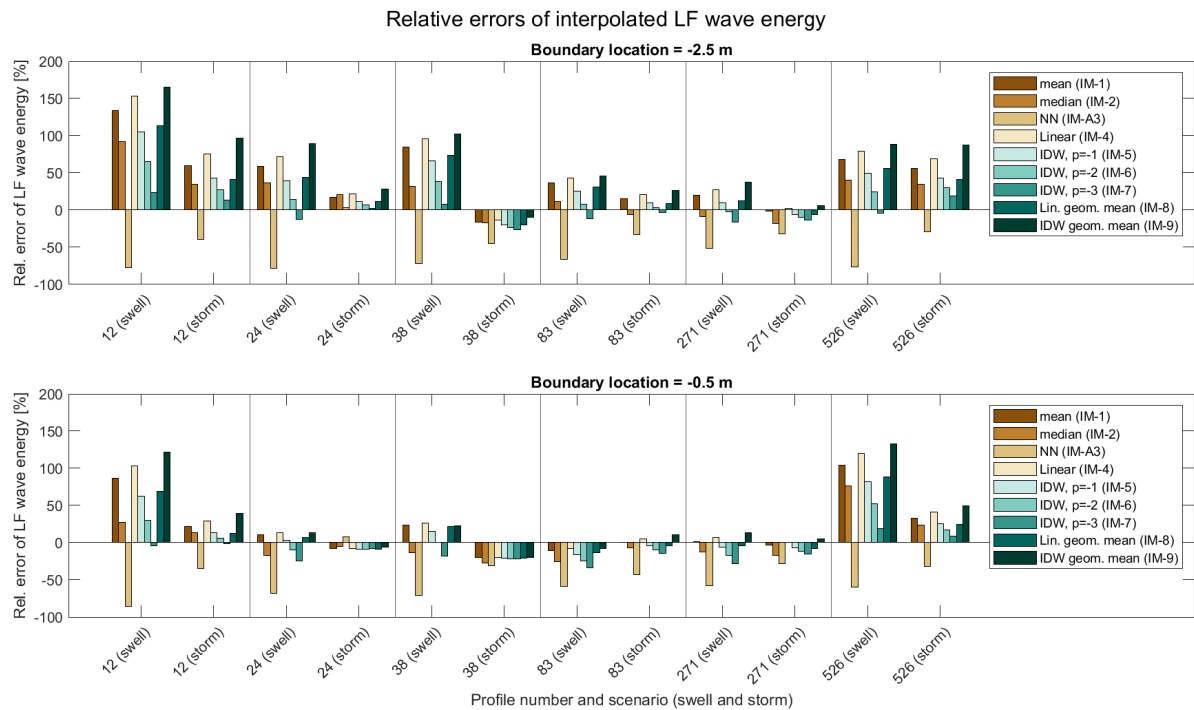

Figure E.3: Relative errors of the interpolated LF wave energy per profile, for the two forcing scenarios (swell and storm). Interpolated HF wave energy values are compared to correct LF wave energy values. 9 different interpolation methods are compared, each marked with different colour. Methods are applied to two boundary locations at depths of -2.5 m (top) and -0.5 m (bottom)